Technical Report No. 131

Computation of the Compressible Laminar Boundary-Layer Flow Including Displacement-Thickness Interaction Using Finite-Difference Methods

I. Flügge-Lotz *and*
F. G. Blottner

Division of
ENGINEERING
MECHANICS

STANFORD
UNIVERSITY

January 1962

This research was supported by the Air Force Office of Scientific Research, Office of Aerospace Research under Contract AF 49(638)-550

AFOSR 2206

Division of Engineering Mechanics
STANFORD UNIVERSITY

Technical Report No. 131

COMPUTATION OF THE COMPRESSIBLE LAMINAR BOUNDARY-LAYER FLOW INCLUDING DISPLACEMENT-THICKNESS INTERACTION USING FINITE-DIFFERENCE METHODS

by

I. FLÜGGE-LOTZ and F. G. BLOTTNER

January 1962

This research was supported by the
Air Force Office of Scientific Research,
Office of Aerospace Research
under Contract AF 49(638)-550

ACKNOWLEDGMENTS

This research was supported by the Air Force Office of Scientific Research, Air Research and Development Command, under Contract AF 49(638)-550.

Reproduction in whole or in part is permitted for any purpose of the United States Government.

TABLE OF CONTENTS

TABLE OF CONTENTS (Continued)

LIST OF ILLUSTRATIONS

LIST OF ILLUSTRATIONS (Continued)

NOMENCLATURE

$A_{1_{m,n}}$, $B_{1_{m,n}}$, $C_{1_{m,n}}$, $D_{1_{m,n}}$, $E_{1_{m,n}}$, $F_{1_{m,n}}$, $G_{1_{m,n}}$	Coefficients in the implicit finite-difference scheme for the momentum equation (3.7), and defined by equations (3.9) for the physical plane and equations (3.12) for the transformed plane
$A_{2_{m,n}}$, $B_{2_{m,n}}$, $C_{2_{m,n}}$, $D_{2_{m,n}}$, $E_{2_{m,n}}$, $F_{2_{m,n}}$, $G_{2_{m,n}}$	Coefficients in the implicit finite-difference scheme for the energy equation (3.8), and defined by equations (3.10) for the physical plane and equations (3.13) for the transformed plane
$B_{1_{m,n}}^*$, $B_{2_{m,n}}^*$, $E_{1_{m,n}}^*$, $E_{2_{m,n}}^*$, $G_{1_{m,n}}^*$, $G_{2_{m,n}}^*$	Coefficients defined by equations (3.25)
C	Constant in linear viscosity law and defined by equation (2.10)
C_1	Constant in nondimensional linear viscosity law and defined by equation (2.21)
c^*	Speed of sound, ft/sec
C_f	Local skin-friction coefficient, $C_f = 2\,\tau_w/(\rho_e u_e^2)$
C_H	Heat transfer coefficient defined by equation (2.51)
c_p	Specific heat at constant pressure
F	Viscosity factor in transformed plane and defined by equation (2.32)
$f(i)$	Nondimensional viscosity function defined by equation (2.21) for linear viscosity law and by equation (2.22) for Sutherland's viscosity law
$f^*(i^*)$	Viscosity function defined by equation (2.5)
$f(\eta_{Low})$	Function related to stream function in similar solution of boundary-layer equations by Low (Ref. 26)

$G(\eta_{Li})$	Function involved in similar solution of strong interaction boundary-layer equations by Li and Nagamatsu (Ref. 25)
$g(\eta_{Low})$	Function involved in similar solution of boundary-layer equations by Low (Ref. 26) and defined by equation (3.32a)
h^*	Local heat transfer coefficient, $h^* = \frac{q^*}{T_w^* - T_{ad}^*}$, lb/ft sec deg R
h	Nondimensional local heat transfer coefficient, $h = h^* \sqrt{Re_o^*} / (\rho_o^* c_o^* c_{p_o}^*)$
i^*	Enthalpy, $c_p T$, ft^2/sec^2
i	Nondimensional enthalpy, $i = i^*/c_o^{*2}$
$Ir(\eta_{Low})$, $Is(\eta_{Low})$	Functions involved in similar solution of boundary-layer equations by Low (Ref.26)
K	Function involved in similar solution of boundary-layer equations by Low (Ref. 26) and defined by equation (3.32c)
$K(\eta_{Li})$	Function involved in similar solution of strong interaction boundary-layer equations by Li and Nagamatsu (Ref. 25)
$K_{m,n}^{(1)}$, $K_{m,n}^{(2)}$, $K_{m,n}^{(3)}$	Coefficients in equation (3.26a) defined by equations (3.27a - 3.27b)
k^*	Thermal conductivity, lb/sec deg R
k	Nondimensional thermal conductivity, $k = k^*/(c_{p_o}^* \mu_o^*)$
L_1, L_2	Factors defined by equations (3.11a) and (3.14a), respectively
$L_{m,n}^{(1)}$, $L_{m,n}^{(2)}$, $L_{m,n}^{(3)}$	Coefficients in equation (3.26b) defined by equations (3.27d - 3.27f)
L^*	Reference length, ft
M	Mach number, u/c

NOMENCLATURE (Cont'd)

p^*	Static pressure, lb/ft^2
p	Nondimensional static pressure, $p = p^*/(\rho_o^* c_o^{*2})$
$p_{(0)}$	Constant for the zeroth-order strong interaction pressure, $p_e/p_\infty = p_{(0)}\overline{\chi} + \cdots$
Pr	Prandtl number, $Pr = \frac{\mu^* c_p^*}{k^*} = \frac{\mu c_p}{k}$
q^*	Local heat transfer rate, $q^* = -k^* \frac{\partial T^*}{\partial y^*}$, lb/ft sec
q	Nondimensional local heat transfer rate, $q = q^* \sqrt{Re_o^*}/(\rho_o^* c_o^{*3})$
Q	Factor defined by equation (3.32d), $Q = 2\sqrt{\frac{\mu_e \overline{xC}}{\rho_e u_e}}$
Q_i	Factor defined by equation (5.8e), $Q_i = \frac{2\rho_e x}{M_e^2 M_\infty}\sqrt{Re_o^* \overline{\chi}/p_{(0)}}$
R^*	Characteristic constant in equation of state, Eq. (2.4), ft^2/sec^2 deg R
R	Nondimensional characteristic constant in equation of state, $R = R^*/c_{p_o}^*$
r	Recovery factor, $r = \frac{(T_{ad}/T_\infty - 1)}{\frac{\gamma-1}{2} M_\infty^2}$
Re_o^*	Reference Reynolds number $Re_o^* = c_o^* L^* \rho_o^*/\mu_o^*$
Re_x	Local Reynolds number, $Re_x = u_e^* x^* \rho_o^*/\mu_e^*$

NOMENCLATURE (Cont'd)

Re_{x_∞}	Reynolds number based on free stream conditions, $Re_{x_\infty} = \rho_\infty^* u_\infty^* x^*/\mu_\infty^*$
S^*	Constant in Sutherland's viscosity law, equation (2.8), deg R
S	Nondimensional constant in Sutherland's viscosity law, $S = c_{p_o}^* S^*/c_o^{*2}$
St	Local Stanton number, $St = h^*/(\rho_e^* u_e^* c_p^*)$
T^*	Absolute temperature, deg R
T	Nondimensional absolute temperature, $T = c_{p_o}^* T^*/c_o^{*2}$
u^*	Velocity component in x-direction or tangent to wall, ft/sec
u	Nondimensional velocity component in x-direction or tangent to wall, $u = u^*/c_o^*$
v^*	Velocity component in y-direction or normal to wall, ft/sec
v	Nondimensional velocity component in y-direction or normal to the wall, $v = v^*\sqrt{Re_o^*}/c_o^*$
V	Transformed normal velocity component, $V = \bar{\eta}_x u + \rho v$
x^*	Coordinate along wall, ft
x	Nondimensional coordinate along wall, $x = x^*/L^*$
y^*	Coordinate normal to wall, ft
y	Nondimensional coordinate normal to wall, $y = y^*\sqrt{Re_o^*}/L^*$
γ	Ratio of specific heats
δ^*	Boundary-layer displacement thickness
$\overline{\delta^*}$	Nondimensional boundary-layer displacement thickness

NOMENCLATURE (Cont'd)

Δx	Nondimensional distance between mesh points in x-direction
Δy	Nondimensional distance between mesh points in y-direction
$\Delta \eta$	Nondimensional distance between mesh points in η-direction
$\Delta \xi$	Nondimensional distance between mesh points in ξ-direction
ϵ	Small quantity used in testing for edge of boundary layer
η	Transformed nondimensional coordinate normal to wall, $\eta = \int_0^y \rho dy$
θ	Slope of effective body, radians
ξ	Transformed nondimensional coordinate along wall, $\xi = x$
μ^*	Viscosity coefficient, lb sec/ft^2
μ	Nondimensional viscosity coefficient, $\mu = \mu^*/\mu_o^*$
ρ^*	Density, lb sec^2/ft^4
ρ	Nondimensional density, $\rho = \rho^*/\rho_o^*$
τ^*	Shear stress, $\tau^* = \mu^* \frac{\partial u^*}{\partial y^*}$, lb/ft^2
τ	Nondimensional shear stress, $\tau = \tau \sqrt{Re_o^*} / (\rho_o^* c_o^{*2})$
$\overline{\chi}$	Hypersonic interaction parameter, $\overline{\chi} = M_\infty^3 \sqrt{C/Re_{x_\infty}}$

Subscripts:

a, b, c, d, e, f, g, h, k	Points in grid page 24

ad	Adiabatic wall condition
e	Local flow outside boundary layer (external)
i	Values at initial profiles
m	Designation of mesh points in x- or ξ-direction, $x = m\Delta x$ or $\xi = m\Delta\xi$
n	Designation of mesh points in y- or η-direction, $y = (n-1)\Delta y$ or $\eta = (n-1)\Delta\eta$
N	Designation of mesh points at outer edge of boundary layer
o	Isentropic stagnation condition for the external inviscid flow
w	Wall or surface value
∞	Free-stream value

Other notations:

*	Dimensional quantities

Primes denote ordinary differentiation with respect to the appropriate independent variable.

A coordinate used as subscript represents partial differentiation with respect to the coordinate.

CHAPTER I

INTRODUCTION

The concept of the boundary layer was first introduced by Prandtl (Ref. 35) so that approximate solutions could be obtained to the Navier-Stokes equations which describe the behavior of viscous flow around moving bodies. This concept allows one to divide the flow field around a body into two parts. In the external part the effect of the viscosity of the fluid is neglected and the Navier-Stokes equations reduce to the Euler equations. In the other part of the flow field, which is near the body, the viscosity has a strong influence; but other terms in the Navier-Stokes equations can be neglected to give the classical boundary-layer equations. As a result of the simplification of the Navier-Stokes equations to the boundary-layer equations, the pressure change normal to the wall across the layer is negligibly small. Therefore the pressure in the boundary-layer equations is replaced by the pressure at the wall as determined from the external inviscid fluid problem. With the tangency boundary condition applied at the surface of the body, the solution of the Euler equations therefore gives the pressure distribution on the body, and hence the pressure gradient is known in the boundary-layer problem.

The presence of a boundary layer on a body effectively increases the thickness of the body by an amount equal to the displacement thickness as far as the external flow is concerned. Since the layer thickness is small, the pressure field of the thickened body and of the body proper are practically equal in subsonic and low supersonic flow. However, at hypersonic speeds the boundary layer cannot be neglected in solving the Euler equations for the external flow about slender bodies. Since the displacement thickness is a function of the pressure distribution along the body and the pressure distribution is a function of the effective body shape, there is an interaction between the boundary-layer problem and the external flow problem. Therefore, the Euler equations and the boundary-layer equations must be solved simultaneously.

If a formal approach is applied to approximate the Navier-Stokes equations (technique of inner and outer expansions as applied by

by Van Dyke (Ref. 41) to a blunt body) the classical boundary-layer equations are the first approximation to the Navier-Stokes equations for the boundary-layer flow. The second approximation to the Navier-Stokes equations for the boundary-layer flow introduces the effect of the displacement thickness. Also the following second-order effects are introduced: longitudinal curvature, transverse curvature, slip, temperature jump at the surface, entropy gradient, and total enthalpy gradient. In this paper only the boundary-layer flow downstream of the leading edge of a sharp flat plate will be considered. For a flat plate the longitudinal and transverse curvature effects are zero. Since slip and temperature jump at the surface are mainly important near the leading edge, the boundary-layer flow is considered only after a small distance from the leading edge. For a sharp flat plate there will be a nearly straight shock wave from the leading edge and hence the entropy gradient will be small. The stagnation enthalpy is constant across the shock wave and hence the total enthalpy gradient is zero. Therefore, the predominant second-order effect will be the displacement thickness and this will be the only effect considered in the interaction between the boundary-layer and the external flow.

Before the interaction problem can be solved it is necessary to have a satisfactory method to solve the boundary-layer equations with an arbitrary pressure distribution. Since similarity methods are only applicable for rather special pressure distributions and integral methods only give approximate results, the numerical scheme of finite-differences is employed. Several finite-difference methods for the compressible laminar boundary layer existed when this work started. Baxter and Flügge-Lotz (Ref. 1) modified the boundary-layer equations using the Crocco transformation and then used an explicit finite-difference scheme to solve the resulting equations. This method is not completely satisfactory due to the small step-sizes required for ensuring stability and convergence of the finite-difference scheme. Kramer and Lieberstein (Ref. 21) have solved essentially the same Crocco transformed equations except an implicit finite-difference scheme has been used to eliminate stability problems. Still the step-size must be sufficiently small to ensure convergence of the numerical solution to the exact solution. In their

paper there are no comparisons with known results or any indications of the validity of the method. A definite disadvantage of methods based on Crocco's equations is the fact that the methods are not applicable when the boundary-layer profiles have "overshoot." Velocity profiles with overshoot occur for certain cases of heated walls with favorable pressure gradient and this effect becomes even more important for boundary-layer flows with helium injection. Due to the above considerations, Flügge-Lotz and Yu (Ref. 11) investigated an explicit finite-difference scheme to solve the boundary-layer equations for the physical plane. However, this method did not prove completely satisfactory, especially at high Mach numbers and with a heated wall. Under these conditions the step-size requirements were so severe that it was impossible to obtain stable solutions.

Since the available numerical solutions of the boundary-layer equations were not generally adequate, a major part of this paper is concerned with developing a new method. A satisfactory method will be one which is not only stable, but one which has a grid size such that computation time is reasonable. Two main implicit finite-difference schemes are developed. Since the boundary-layer equations are analogous to the heat equation as far as stability is concerned, an implicit scheme using the boundary-layer equations in the physical plane was used initially in order to have stability as the heat equation indicates. One of the better ways to solve the heat equation is the Crank-Nicolson method (Ref. 8) which has a smaller truncation error than the implicit method. This method actually is at the dividing point between the explicit and implicit schemes, but is always stable for the heat equation. Due to the complexity of the boundary-layer equations, it is impossible to ascertain with assurance whether a Crank-Nicolson type of scheme would always be stable. In order to improve the grid size requirements, and thus have a practical method, the second difference scheme investigated is of the Crank-Nicolson type.

Especially for hypersonic flows along insulated walls, the velocity profiles vary almost linearly over a large portion of the layer except at the outer edge where there is a large change in the velocity gradient. For accurate results a particularly small grid size is required near the

outer edge. The immediate conclusion is that the grid size should vary with distance from the wall, but this is rather inconvenient. Therefore, the coordinate normal to the wall should be stretched to obtain smoother profiles across the boundary layer by using the Howarth-Dorodnitsyn transformation. This was done in the second scheme investigated.

In both of the implicit finite-difference schemes developed in this report the derivatives in the boundary-layer equations are replaced by difference quotients such that linear difference equations are obtained. If the usual procedures are followed for replacing the partial differential equations, nonlinear difference equations are obtained. Hence, one has the extremely involved problem of solving forty to sixty simultaneous nonlinear algebraic equations at each step along the wall. In order to make the implicit method feasible, the difference equations have been linearized, which then requires the solution of a large number of simultaneous linear algebraic equations. These equations are of a tridiagonal type and are well suited for solution on a digital computer. A wide variety of boundary-layer problems has been solved to indicate the usefulness and accuracy of the two methods investigated. The problems used for the verification of these methods either have exact solutions or have been solved numerically by other procedures.

Since the above finite-difference schemes have been developed, several numerical methods to solve the boundary-layer equations have appeared. Wu (Ref. 42) has used an explicit finite-difference scheme to solve the boundary-layer equations in the physical plane. The Howarth-Dorodnitsyn transformation has also been used by him to improve the stability requirements for the compressible boundary layer. However, the transformed equations as given cannot be used for a flow with a pressure gradient; this fact is not clearly indicated in the report. Another method which combines the Dorodnitsyn integration scheme with the Pohlhausen approach, has been developed by Pallone (Ref. 34). The boundary layer is divided into a number of strips (4 or 6) parallel to the wall and then the boundary-layer equations are integrated from the wall to the various strips where the velocity and enthalpy profiles have been approximated by a polynomial. This method reduces the partial differential equations of the boundary layer to a set of ordinary first-order

differential equations with the coordinate parallel to the wall as the independent variable. This method looks very attractive as the procedures to solve ordinary differential equations are highly developed. However, one would question whether this method converges to the exact solution as the number of strips is increased, since a polynomial is being fitted through a large number of points to represent the velocity and enthalpy profiles. For this situation, the polynomial can be greatly different from the exact profiles between the fitting points. An interesting numerical method for solving the incompressible boundary-layer flow has been presented by Manohar (Ref. 29) and the ideas can be extended to compressible flow. The author develops from the boundary-layer momentum equation and the continuity equation a third-order nonlinear partial differential equation and then replaces the derivatives in the direction along the wall by difference quotients. This results in a nonlinear ordinary differential equation which must be solved across the boundary layer at each step downstream. An iteration process is required for the solution since two boundary conditions are given at the wall and one at the outer edge. The problem of iteration would become even more difficult for the compressible boundary-layer equations as there would be two boundary conditions at the outer edge.

A large number of people have investigated the displacement thickness or pressure interaction between the boundary-layer and the external flow. A complete discussion of this problem with a review of previous contributors is given in Hayes and Probstein (Ref. 14). All of the previous methods of solution have either used perturbation or approximate methods to solve the Prandtl boundary-layer equations with the pressure gradient in these equations determined from the effective body shape. In this paper the same problem is investigated using the new numerical scheme developed for solving the boundary-layer equations. The tangent-wedge formula is used as the solution to the external flow field and hence the pressure distribution is known once the effective shape of the body (geometric shape plus displacement thickness) is given. Starting with the initial profiles across the boundary layer, the boundary-layer equations are solved with the pressure at the next grid line iterated until the assumed pressure equals the pressure determined from the tangent-

wedge formula. This process is repeated as one steps downstream until the desired distance has been covered. A comparison of the numerical results is made with the "strong" and "weak" interaction theories and experimental results when such are available.

CHAPTER II

MATHEMATICAL DESCRIPTION OF THE COMPRESSIBLE LAMINAR BOUNDARY LAYER

In this chapter the equations for the laminar compressible boundary layer are presented along with the necessary boundary conditions. The equations are nondimensionalized, which results in using quantities of the same order of magnitude better suited for computations. The boundary-layer equations are also modified using the Howarth-Dorodnitsyn transformation, which results in equations advantageous for numerical computation when the flow is hypersonic. Since the boundary conditions require that the enthalpy and velocity be known at the outer edge of the boundary layer, the necessary formulas are presented to calculate the exterior flow, provided the pressure distribution is known. Finally, the characteristic values of the boundary layer (shearing stress, heat transfer, and displacement thickness) are defined.

A. The System of Partial Differential Equations

1. Differential Equations. The flow of a compressible, viscous, heat-conducting fluid is mathematically described by the continuity, Navier-Stokes, and energy equations plus the equation of state, a heat-conductivity law, and a viscosity law. For flows at large Reynolds numbers, Prandtl (Ref. 35) has shown how the Navier-Stokes and energy equations can be simplified to the boundary-layer equations. If it is assumed the Prandtl number and specific heat of the fluid are constant, the classical boundary-layer equations for steady, two-dimensional, compressible flow are

Continuity
$$(\rho^* u^*)_{x^*} + (\rho^* v^*)_{y^*} = 0 \tag{2.1}$$

Momentum
$$\rho^* u^* u^*_{x^*} + \rho^* v^* u^*_{y^*} = -\frac{dp_e^*}{dx^*} + (\mu^* u^*_{y^*})_{y^*} \tag{2.2}$$

Energy

$$\rho^* u^* i^*_{x^*} + \rho^* v^* i^*_{y^*} = u^* \frac{dp_e^*}{dx^*} + \mu^* u^{*2}_{y^*} + \frac{1}{Pr} (\mu^* i^*_{y^*})_{y^*} \qquad (2.3)$$

Equation of State $\qquad p^* = \rho^* R^* T^* = \frac{\gamma - 1}{\gamma} \rho^* i^* \qquad (2.4)$

Viscosity Law $\qquad \mu^* = f^*(i^*) \qquad (2.5)$

The starred quantities have dimensions and the subscripts indicate partial differentiation. The independent variables are the space coordinates x^* and y^* which are parallel and perpendicular to the wall, respectively. The dependent variables are the density ρ^*, the velocity components u^* and v^* which are parallel and perpendicular to the wall, respectively, enthalpy i^* and viscosity μ^*. Hence, we have a system of five simultaneous equations and five unknowns.

The two original momentum equations became, after the boundary-layer simplification, equation 2.2 and the following result

$$\frac{\partial p^*}{\partial y^*} = 0 \qquad (2.6)$$

Thus the pressure in a direction normal to the boundary layer is practically constant. This result has been used in equations (2.2) and (2.3) where the pressure at any x^* has been set equal to the external pressure p_e^*. Also, from the equation of state the result is obtained that $\rho^* i^*$ is a constant, or the following relation can be written

$$\rho^* = (\rho_e^* i_e^*)/i^* \qquad (2.7)$$

The boundary-layer equations given above (2.1 - 2.5) are valid for a curved wall provided there are no large variations in curvature, and the boundary-layer thickness is small compared with the radius of curvature of the wall.

2. Boundary Conditions. In order to obtain a unique solution to the partial differential equations of the boundary layer it is necessary to satisfy the boundary conditions of the problem under consideration.

These conditions are shown schematically below.

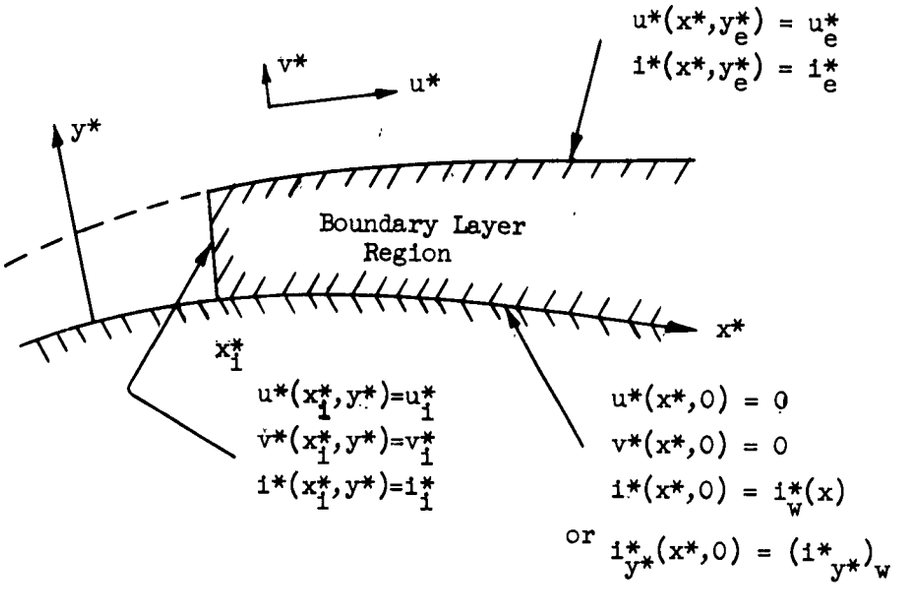

The velocity and enthalpy at the edge of the boundary layer are determined from the shape[1] of the body by using inviscid flow theory and are discussed in Section E of this chapter.

The conditions of no slip and no suction or blowing are taken as the boundary conditions at the wall. Hence, the two velocity components u^* and v^* are zero at the wall. The third boundary condition at the wall depends upon the thermal state of the wall. The temperature of the wall can be specified, which means the enthalpy along the wall is given. An alternate condition at the wall is to specify the heat transfer which determines $(\partial i^*/\partial y^*)_{wall}$. Finally, the parabolic character of the differential equations requires that initial velocity and enthalpy profiles be known at x_i^*. These initial profiles are obtained from analytical results which are applicable to the problems under consideration.

---

[1] In the classical boundary-layer theory the shape of the body is taken as the geometrical body. When interaction between the boundary-layer and inviscid flow is considered, the shape of the body is the effective body (see Chapter 5).

3. Viscosity Law. A formula for the viscosity of a gas from the standpoint of kinetic theory of gases[1] is Sutherland's law, which is

$$\mu^*/\mu_o^* = \frac{T_o^* + S^*}{T^* + S^*} (T^*/T_o^*)^{3/2} \tag{2.8}$$

The constant S* is taken as 216 or 198.6 in this work in order to compare results obtained with other reports using these values. Based on newer experiments the value of S* is 198.6.

Another viscosity law which is used in many analytical solutions to the boundary-layer equations is the linear law, which is written as

$$\mu^*/\mu_\infty^* = CT^*/T_\infty^* \tag{2.9}$$

The constant C is usually determined by matching the viscosity at the wall as given by the linear law and Sutherland's law. This results in the following value for C:

$$C = \sqrt{T_w^*/T_e^*}\, \frac{T_e^* + S^*}{T_w^* + S^*} \tag{2.10}$$

Using the relation

$$i^* = c_p^* T^* \tag{2.11}$$

gives the above viscosity laws as a function of enthalpy.

B. Nondimensional Form of the Differential Equations and Boundary Conditions

1. Nondimensional Quantities. It is advantageous to write the differential equations and other relations of interest in nondimensional form before numerical computations are performed. The following nondimensional quantities are defined so that all quantities are of the same magnitude.

---

[1] Sutherland's Hypothesis assumes that the molecules are hard spheres with a weak attraction between them and this force falls off rather rapidly with distance. The resulting viscosity law from kinetic theory has the constant S* which is a suitable empirical value. This law is valid over a certain temperature range (Ref. 19).

a. Variables appearing directly in the differential equations:

$$u = u^*/c_o^*$$

$$v = v^*\sqrt{Re_o^*}/c_o^*$$

$$i = i^*/c_o^{*2}$$

$$\rho = \rho^*/\rho_o^*$$

$$\mu = \mu^*/\mu_o^* \qquad (2.12)$$

$$p = p^*/(\rho_o^*\ c_o^{*2})$$

$$x = x^*/L^*$$

$$y = y^*\sqrt{Re_o^*}/L^*$$

with

$$i_o = 1/(\gamma-1)$$

$$\rho_o = 1$$

$$\mu_o = 1$$

b. Quantities describing the behavior of the boundary-layer flow:

$$\tau = \tau^*\sqrt{Re_o^*}/(\rho_o^*\ c_o^{*2})$$

$$q = q^*\sqrt{Re_o^*}/(\rho_o^*\ c_o^{*3})$$

$$S = c_{p_o}^*\ S^*/c_o^{*2} \qquad (2.13)$$

$$T = c_{p_o}^*\ T^*/c_o^{*2}$$

$$h = h^*\sqrt{Re_o^*}/(\rho_o^*\ c_o^*\ c_{p_o}^*)$$

(2.13 cont'd. on next page)

(2.13 cont'd)

$$k = k^*/(c_{p_o}^* \mu_o^*)$$

$$c_p = c_p^*/c_{p_o}^* = 1$$

$$Pr = c_p \mu/k = c_p^* \mu^*/k^* = Pr^*$$

$$R = R^*/c_{p_o}^*$$

In the above quantities the subscript "o" refers to the conditions at the stagnation point or reservoir of the exterior inviscid flow. The length L^* is some characteristic distance of the problem and the Reynolds number, Re_o^*, is defined by

$$Re_o^* = c_o^* L^* \rho_o^*/\mu_o^* \tag{2.14}$$

2. Boundary-Layer Equations. Since the viscosity is a function of enthalpy, the viscosity in nondimensional form can be written as

$$\mu = f(i) \tag{2.15}$$

The derivative of the viscosity can be written as

$$\mu_y = \frac{df}{di} i_y = f' i_y \tag{2.16}$$

Using the nondimensional quantities as given in (2.12), we can write the boundary-layer equations (2.1 - 2.3) as

Continuity $$(\rho u)_x + (\rho v)_y = 0 \tag{2.17}$$

Momentum $$\rho u u_x + \rho v u_y = - p_e' + f u_{yy} + f' u_y i_y \tag{2.18}$$

Energy $$\rho u i_x + \rho v i_y = u p_e' + f u_y^2 + \frac{f}{Pr} i_{yy} + \frac{f'}{Pr} i_y^2 \tag{2.19}$$

Equation of State $$\rho = \rho_e i_e/i = \frac{\gamma}{\gamma-1} p/i \tag{2.20}$$

Viscosity Law

$$\text{(Linear)} \quad \begin{cases} f = C_1 i & \text{where } C_1 = C\mu_e/i_e \\ & \quad = \dfrac{1}{i_o}\sqrt{\dfrac{i_w}{i_o}}\,\dfrac{1 + S/T_o}{i_w/i_o + S/T_o} \\ f' = C_1 & \\ & C = \sqrt{\dfrac{i_w}{i_e}}\,\dfrac{1 + S/T_e}{i_w/i_e + S/T_e} \end{cases} \tag{2.21}$$

$$\text{(Sutherland)} \quad \begin{cases} f = \dfrac{1 + S/T_o}{i/i_o + S/T_o}\,(i/i_o)^{3/2} \\ f' = f\left[\dfrac{i/i_o + 3\,S/T_o}{2i(i/i_o + S/T_o)}\right] \end{cases} \tag{2.22}$$

3. Boundary Conditions. The boundary conditions become the following when the nondimensional quantities are used:

a. Outer Edge of Boundary Layer

$$y = y_e \;,\; x \geq x_i \;:\quad \begin{aligned} u(x,y_e) &= u_e(x) \\ i(x,y_e) &= i_e(x) \end{aligned} \tag{2.23}$$

b. Wall

$$y = 0 \;,\; x \geq x_i \;:\quad \begin{aligned} u(x,o) &= 0 \\ v(x,o) &= 0 \\ i(x,o) &= i_w \\ \text{or}\quad i_y(x,o) &= (i_y)_w \end{aligned} \tag{2.24}$$

c. Initial Profiles

$$x = x_i \;,\; y_e \leq y \leq 0 \;:\quad \begin{aligned} u(x_i,y) &= u_i(y) \\ v(x_i,y) &= v_i(y) \\ i(x_i,y) &= i_i(y) \end{aligned} \tag{2.25}$$

C. Howarth - Dorodnitsyn Transformed Boundary-Layer Equations

For some numerical calculations it is advantageous to stretch the coordinate normal to the wall. The appropriate stretching is accomplished by using the Howarth - Dorodnitsyn transformation

$$\xi = x$$

$$\eta = \int_0^y \rho dy \tag{2.26}$$

In order to transform the boundary-layer equations (2.17 - 2.19) the following relations between the differential operators in the old and new coordinates are used:

$$\frac{\partial}{\partial x} = \frac{\partial}{\partial \xi} + \eta_x \frac{\partial}{\partial \eta} \tag{2.27}$$

$$\frac{\partial}{\partial y} = \rho \frac{\partial}{\partial \eta}$$

Also, a new velocity is introduced and is defined as

$$V = \eta_x u + \rho v \tag{2.28}$$

The boundary-layer equations (2.17 - 2.19) become the following in the transformed plane:

$$u_\xi + V_\eta = 0 \tag{2.29}$$

$$uu_\xi + V u_\eta = - p_e'/\rho + F u_{\eta\eta} + F' i_\eta u_\eta \tag{2.30}$$

$$ui_\xi + V i_\eta = up_e'/\rho + F u_\eta^2 + \frac{F}{Pr} i_{\eta\eta} + \frac{F'}{Pr} i_\eta^2 \tag{2.31}$$

where

$$F = \rho u = \rho_e i_e (\mu/i)$$

$$F' = \frac{dF}{di} = \rho_e i_e \frac{d}{di} (\mu/i) \tag{2.32}$$

Of course, the equation of state remains the same, but the viscosity law gives the following relations:

$$\text{(Linear Law)} \qquad \begin{cases} F = \rho_e i_e C_1 \\ F' = 0 \end{cases} \tag{2.33}$$

$$\text{(Sutherland Law)} \qquad \begin{cases} F = \dfrac{\rho_e i_e}{i_o}\left(\dfrac{1 + S/T_o}{i/i_o + S/T_o}\right)(i/i_o)^{1/2} \\ F' = \dfrac{F}{2i}\left(\dfrac{S/T_o - i/i_o}{S/T_o + i/i_o}\right) \end{cases} \tag{2.34}$$

In order to determine the physical distance normal to the wall, y, the transformation (2.26) is used to obtain the following:

$$y = \int_0^\eta (1/\rho)d\eta = (1/\rho_e) \int_0^\eta (i/i_e)\, d\eta \tag{2.35}$$

D. Exterior Flow

The following quantities will be given to describe the exterior flow and fluid properties:

$$M_\infty,\ T_\infty,\ \gamma,\ \text{Pr},\ \text{and}\ S.$$

Since we know the above quantities, the following formulas for an isentropic, perfect gas can be evaluated independent of the shape of the wall on which the boundary layer is located.

$$u_\infty = M_\infty / \sqrt{1 + \frac{\gamma-1}{2} M_\infty^2} \tag{2.36}$$

$$p_\infty = (1/\gamma)\left(1 + \frac{\gamma-1}{2} M_\infty^2\right)^{-\frac{\gamma}{\gamma-1}} \tag{2.37}$$

$$i_o = 1/(\gamma-1) \tag{2.38}$$

$$T_o = T_\infty \left(1 + \frac{\gamma-1}{2} M_\infty^2\right) \tag{2.39}$$

The next exterior flow quantity that must be determined is the pressure and pressure gradient along the boundary layer. The method to be used to determine this pressure depends upon the problem under consideration; hence, it will be discussed along with the problems considered in later sections.

Now the following formula for an isentropic, perfect gas can be evaluated using the previously obtained results above.

$$u_e = u_\infty \left[1 + \frac{1 - (p_e/p_\infty)^{\frac{\gamma-1}{\gamma}}}{\frac{\gamma-1}{2} M_\infty^2} \right]^{1/2} \tag{2.40}$$

$$i_e = i_o - 1/2\, u_e^2 \tag{2.41}$$

$$\rho_e = (i_e/i_o)^{\frac{1}{\gamma-1}} \tag{2.42}$$

$$T_e = \frac{T_o}{1 + \frac{\gamma-1}{2} M_e^2} \tag{2.43}$$

$$\mu_e = \frac{1 + S/T_o}{i_e/i_o + S/T_o} (i_e/i_o)^{3/2} \tag{2.44}$$

It should be noticed that the contribution of v_e in equation (2.41) has been neglected, which is consistent with the boundary-layer equations.

E. Boundary-Layer Parameters

1. Shearing Stress. Since the viscous drag of a body moving through a fluid is dependent upon the shearing stress at the wall, this is one of the boundary-layer characteristics of interest. The shearing stress at the wall in the physical plane is

$$\tau = \mu_w \left(\frac{\partial u}{\partial y}\right)_w \tag{2.45}$$

and in the transformed plane is

$$\tau_w = \rho_w \mu_w \left(\frac{\partial u}{\partial \eta}\right)_w \tag{2.46}$$

Rather than the above parameter, usually the skin friction and Reynolds number are combined to give one of the following characteristics to describe the boundary-layer shear stress at the wall:

$$C_f \sqrt{Re_x} = \frac{2\tau_w}{u_e} \sqrt{\frac{x}{\rho_e \mu_e \mu_e}} \tag{2.47}$$

where

$$C_f = \frac{2\tau_w^*}{\rho_e^* u_e^{*2}} \qquad \text{(local skin-friction coefficient)}$$

$$Re_x = \frac{u_e^* x^* \rho_e^*}{\mu_e^*} \qquad \text{(local Reynolds number)}$$

In the case of interaction between the boundary-layer and the external flow, the following parameter is used to describe the skin friction and is used for analytical results in Ref. 14.

$$C_f M_\infty^3 = \frac{2 M_\infty^3 \tau_w}{\rho_\infty u_\infty^2 \sqrt{Re_o^*}} \tag{2.48}$$

2. Heat Transfer. In aerodynamic heating analysis it is necessary to know the heat transfer between the boundary layer and wall. The heat transfer at the wall is related to the enthalpy by the following formula:

$$q_w = -\frac{k}{c_p} \left(\frac{\partial i}{\partial y}\right)_w = -\frac{\mu}{Pr} \left(\frac{\partial i}{\partial y}\right)_w \tag{2.49}$$

Again, there are more conventional parameters to describe the heat transfer at the wall and one is

$$St \sqrt{Re_x} = h \sqrt{\frac{x}{\rho_e \mu_e u_e}} \tag{2.50}$$

where

$$St = \frac{h^*}{\rho_e^* u_e^* c_p^*} \qquad \text{(the Stanton number)}$$

$$h^* = \frac{q^*}{T_w^* - T_{ad}^*} \qquad \text{(local heat transfer coefficient)}$$

or

$$h = \frac{q}{i_w - i_{ad}}$$

$$i_{ad} = i_e \left(1 + \frac{\gamma-1}{2} r M_e^2\right)$$

The adiabatic enthalpy, i_{ad}, is the value of the enthalpy at the wall when there is no heat transfer (insulated wall). In order to obtain the adiabatic enthalpy, it is necessary to know the recovery factor r. For the laminar flow along a flat plate at constant temperature the recovery factor is taken as 0.845 when Pr = 0.72. For some other types of flow the recovery factor is unknown. In these cases the Stanton number can be based upon the temperature at the edge of the boundary layer, T_e, and then all the adiabatic enthalpies, i_{ad}, are replaced by i_e in the above relations.

For the problem of interaction between the boundary-layer and the external flow, the following parameter is used to describe the heat transfer and is used for experimental results in Ref. (13).

$$C_H M_\infty^3 = - \frac{M_\infty^3 q}{\rho_\infty u_\infty (i_o - i_w)\sqrt{Re_o^*}} \qquad (2.51)$$

3. Displacement Thickness. For problems in which interaction between the boundary-layer and inviscid flow is important, it is necessary to have the displacement thickness to determine the effective body. The boundary-layer displacement thickness is defined as

$$\delta^* = \int_0^{y_e^*} \left(1 - \frac{\rho^* u^*}{\rho_e^* u_e^*}\right) dy^* \qquad (2.52)$$

A nondimensional displacement thickness is used in calculations as defined below:

$$\overline{\delta^*} = \int_0^{y_e} \left(1 - \frac{i_e u}{i u_e}\right) dy = \frac{\sqrt{Re^*_o}}{L^*} \delta^* \tag{2.53}$$

In the transformed plane the nondimensional displacement thickness becomes

$$\overline{\delta^*} = \int_0^{\eta_e} \frac{1}{\rho_e} (i/i_e - u/u_e)\, d\eta \tag{2.54}$$

CHAPTER III

NUMERICAL SOLUTION OF THE BOUNDARY-LAYER EQUATIONS WITHOUT INTERACTION

Since the partial differential equations governing the flow in the boundary layer are of parabolic type, they can be solved stepwise downstream starting with initial velocity and enthalpy profiles and using the boundary conditions. When the finite-difference scheme is employed, the derivatives in the partial differential equations are replaced by difference quotients, and this results in difference equations. To construct the difference quotients and equations it is necessary to divide the flow field into a grid or mesh. First, the velocities and enthaply across the boundary layer at the grid points which are a small distance downstream from the initial profiles are computed using the velocities and enthalpy given by the initial profiles. When the difference equations are solved in succeeding small steps downstream, the flow in a region of the boundary layer can be determined.

There are numerous ways of constructing difference quotients, but there are two general classifications: explicit and implicit. When the explicit scheme is used, the resulting finite-difference equations can be solved for the unknown quantities at one grid point at a time. However, to obtain stable numerical solutions, the step-size downstream must be less than some critical value. With the implicit scheme the difference equations for the unknown quantities at a row of grid points are solved simultaneously. The downstream step-size for the implicit method requires no restrictions to ensure stability; however, the step-size must be sufficiently small for the numerical solution to closely approximate the exact solution. Obviously, the implicit scheme is mathematically more complicated; however, when the difference equations are linear, a direct method of solution (an algorithm) can be evolved. Due to the repetitious form of the explicit and implicit finite-difference calculations, the solution is well suited for digital computers. The best method for a computer is determined from the consideration of computation time needed rather than the mathematical complication involved or the step-size required. The implicit methods usually require more computation time per

step, but allow larger step-sizes downstream than the explicit methods; therefore, total computation time by either method can be a minimum for a particular problem.

The essential points of the explicit method of Wu (Ref. 42) are presented in this chapter for convenience of comparison with the implicit methods. Also the equations are presented in a slightly different form which is valid for boundary-layer flow with a pressure gradient. The equations given by Wu are only valid for zero pressure gradient since the density at the edge of the boundary layer has been assumed a constant while applying the Howarth-Dorodnitsyn transformation. The explicit method is presented only for the solution of the boundary-layer equations in the transformed plane (after the Howarth-Dorodnitsyn transformation has been used). In the explicit scheme the derivatives normal to the wall are replaced using quantities from the known profiles. Therefore, the momentum equation gives the velocity, u, and the energy equation gives the enthalpy, i, directly at each grid point (except at the edges) one step downstream from the known profiles. The quantities at the edges of the boundary layer are known from the boundary conditions. The velocity, V, is determined from the continuity equation and then the above procedure is repeated at succeeding steps downstream. Wu has indicated that the continuity equation in his method is treated in a particular manner. The derivative u_ξ is replaced with a backward difference quotient and the resulting equation is integrated using the trapezoidal rule.

Two implicit finite-difference schemes are presented in this chapter for the solution of the nonlinear boundary-layer equations. The first scheme is the usual implicit one which uses backward difference quotients for the derivatives parallel to the wall and is called Method I. The second scheme is of the Crank-Nicolson type which uses difference quotients of a type to reduce the truncation error and is called Method II. Both Methods I and II replace the derivatives normal to the wall in such a manner that unknown quantities are introduced. Also, the products of the derivatives are replaced with linear difference quotients to give the possibility of linear difference equations. However, to obtain linear difference equations, it is necessary to linearize certain terms

obtained from the partial differential equations. In the process of linearizing the momentum and energy equations, only the velocity, u, and enthalpy, i, appear as unknowns in the resulting difference equations. In both methods these difference equations are of the same form with only the coefficients depending on which method is being used. Therefore, the manner of solution is identical in both cases with the appropriate coefficients used for the two methods. Since at the first grid point away from the wall the two difference equations have six unknowns and the boundary conditions at the wall can eliminate two unknowns, there are more unknowns than equations. If the two difference equations are introduced for the next grid point, there will still be more unknowns than equations. There will always be more unknowns than equations as all the difference equations are added for the grid points across the boundary layer until the outer edge is reached. Using the boundary conditions at the outer edge with those at the wall, one obtains a set of difference equations with the same number of unknowns as equations. This set of difference equations is actually a rather special system of simultaneous linear algebraic equations. Due to this special form an efficient method of solution for computers is available; and using this method, the difference equations are replaced by suitable relations useful for computation in this chapter. This method essentially introduces six new quantities which can be determined directly by using the boundary conditions at the wall and then stepping across the layer. Then, using the boundary conditions at the outer edge and these six new quantities, one determines the velocity, u, and enthalpy, i, directly by starting from the outer edge and proceeding to the wall.

As in the explicit method the continuity equation is now used to determine the velocity, v, or V, across the boundary layer. Two methods are used to write the continuity equation as a difference equation. The first one is the same as that used in the explicit method and is called Method A. The second one replaces the derivatives with difference quotients such that the truncation error is of higher order and is called Method B. By repeated use of the procedures outlined above and presented in this chapter the boundary-layer flow at succeeding steps downstream can be determined.

In the methods of solution of the boundary-layer equations discussed above it has been assumed that the boundary conditions are well defined. Of course, at the wall they are well defined if we assume no slip as the velocity u will be zero. The velocity v or V is usually taken as zero, except when there is fluid injection and in either case no difficulties are introduced. Also, either the temperature or heat transfer distribution at the wall can be easily handled. However, at the outer edge the velocity and enthalpy are known from the inviscid flow pressure distribution, but there is no definite location of the outer edge. For the boundary-layer equations in the physical plane or after the Howarth-Dorodnitsyn transformation the velocities and enthalpy approach the inviscid flow values asymptotically. There are two methods that can be used in applying the outer edge boundary conditions. One way is to pick a line which is parallel to the wall and is sufficiently far away from the wall that the outer edge boundary conditions are valid there. Since the boundary layer is normally thickest at the downstream limit of the computation, an estimate must be made of this thickness. This method is inefficient as too many steps are taken across the boundary layer where the layer is thinner than the maximum thickness. The second method, which is used in this paper, determines the edge of the boundary layer by finding out when the quantities determined across the layer become nearly a constant. By testing successive values of the quantities calculated across the layer, it is assumed that the edge is reached when the two quantities are the same to a certain number of decimal places. The number of decimal places required is easily obtained after some experience, and this question is illustrated in Chapter 4 with numerical solutions. With this method the number of steps across the boundary layer will vary as the thickness varies.

It has been assumed that initial profiles of velocity u and v or V and enthalpy i are known. Obtaining these profiles is a serious problem connected with all the numerical schemes for solving the boundary-layer equations. Since only a local solution is required, the problem is considerably simpler than solving the boundary-layer equations for an arbitrary body. Some of the profiles available and the ones used in this paper are discussed later in this chapter (Section D).

Also discussed in this chapter is the stability of the difference equations with respect to round-off error and the convergence of the numerical solution toward the exact solution. The numerical formulas used to determine the boundary-layer characteristics of shearing stress, heat transfer and displacement thickness are also presented. Finally, the chapter is concluded with the computer program used to solve the boundary-layer problem.

A. Difference Quotients

In constructing the difference quotients, the sketch below is useful for reference.

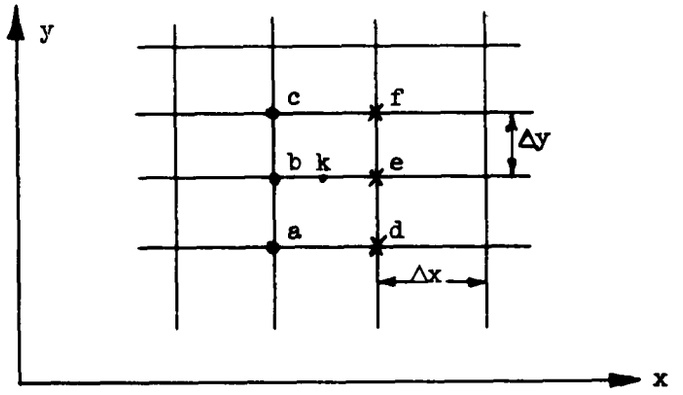

It is assumed that the functions $H(x,y)$ and $T(x,y)$ are known at a, b, c, but unknown at d, e, f. In the following sections the difference quotients that replace the partial derivatives are given as are the higher-order terms. The higher order terms are obtained using a Taylor series expansion and are shown to indicate the truncation error introduced when the first terms are used to replace the derivatives.

1. Explicit. In the explicit method the partial derivatives are evaluated at the grid point "b" and the following difference quotients are used:

$$\frac{\partial H}{\partial x} = \frac{H_e - H_b}{\Delta x} - \frac{1}{2}\Delta x\, H_{xx} + \ldots \qquad (3.1a)$$

$$\frac{\partial H}{\partial y} = \frac{H_c - H_a}{2\Delta y} - \frac{1}{6}\Delta y^2 H_{yyy} + \cdots \qquad (3.1b)$$

$$\frac{\partial^2 H}{\partial y^2} = \frac{H_c - 2H_b + H_a}{\Delta y^2} - \frac{1}{12}\Delta y^2 H_{yyyy} + \cdots \qquad (3.1c)$$

All the quantities are evaluated at point "b" unless indicated otherwise, and the truncation error is of order Δx or Δy^2.

2. Implicit.

a. Method I. This method evaluates the partial derivatives at the grid point "e" since an implicit scheme is desired. The partial derivatives are replaced by the difference quotients as indicated and all quantities are evaluated at point "e" unless denoted otherwise.

$$\frac{\partial H}{\partial x} = \frac{H_e - H_b}{\Delta x} + \frac{1}{2}\Delta x H_{xx} + \cdots \qquad (3.2a)$$

$$\frac{\partial H}{\partial y} = \frac{H_f - H_d}{2\Delta y} - \frac{1}{6}\Delta y^2 H_{yyy} + \cdots \qquad (3.2b)$$

$$\frac{\partial^2 H}{\partial y^2} = \frac{H_f - 2H_e + H_d}{\Delta y^2} - \frac{1}{12}\Delta y^2 H_{yyyy} + \cdots \qquad (3.2c)$$

In the following, difference expressions for products of derivatives are given. They are chosen such that in the products the unknown quantities appear linearly and their use can lead to linear difference equations.

$$\left(\frac{\partial H}{\partial y}\right)^2 = \left(\frac{H_c - H_a}{4\Delta y^2}\right)[(H_a - H_c) + 2(H_f - H_d)]$$

$$+ \Delta x^2 H_{xy}^2 - \frac{1}{3}\Delta y^2 H_y H_{yyy} + \cdots \qquad (3.2d)$$

$$\frac{\partial H}{\partial y}\frac{\partial T}{\partial y} = \frac{1}{4\Delta y^2}\left[(T_c-T_a)(H_f-H_d) + (H_c-H_a)(T_a-T_c) + (H_c-H_a)(T_f-T_d)\right]$$

$$+ \Delta x^2 H_{xy} T_{xy} - \Delta y^2 \frac{1}{6}\left(T_y H_{yyy} + H_y T_{yyy}\right) + \cdots \qquad (3.2e)$$

The truncation error in the above difference quotients is of the order of Δx or Δy^2 and is the same as the explicit method.

b. Method II. This method evaluates the partial derivatives at the grid point "k" since the Crank-Nicolson type of difference equations are desired. The partial derivatives are replaced by the following difference quotients:

$$\frac{\partial H}{\partial x} = \frac{H_e - H_b}{\Delta x} - \frac{1}{24}\Delta x^2 H_{xxx} + \cdots \qquad (3.3a)$$

$$\frac{\partial H}{\partial y} = \frac{1}{4\Delta y}\left(H_c-H_a + H_f-H_d\right) - \frac{1}{8}\Delta x^2 H_{xxy} - \frac{1}{6}\Delta y^2 H_{yyy} + \cdots \qquad (3.3b)$$

$$\frac{\partial^2 H}{\partial y^2} = \frac{1}{2\Delta y^2}\left(H_a-2H_b + H_c + H_d-2H_e + H_f\right) - \frac{1}{8}\Delta x^2 H_{xxyy} - \frac{1}{12}\Delta y^2 H_{yyyy} + \cdots$$

(3.3c)

$$\left(\frac{\partial H}{\partial y}\right)^2 = \frac{1}{4\Delta y^2}(H_a-H_c)(H_d-H_f) + \frac{\Delta x^2}{4}(H_{xy}^2-H_y H_{xxy}) - \frac{1}{3}\Delta y^2 H_y H_{yyy} + \cdots$$

(3.3d)

$$\frac{\partial H}{\partial y}\frac{\partial T}{\partial y} = \frac{1}{8\Delta y^2}\left[(H_a-H_c)(T_d-T_f) + (H_d-H_f)(T_a-T_c)\right]$$

$$- \frac{1}{8}\Delta x^2 \left(H_y T_{xxy} - 2H_{xy} T_{xy} + H_{xxy} T_y\right)$$

$$- \frac{1}{6}\Delta y^2 \left(H_y T_{yyy} + T_y H_{yyy}\right) + \cdots \qquad (3.3e)$$

The above difference quotients are chosen because the unknown quantities appear linearly and can result in linear difference equations. All the quantities are evaluated at point "k" unless indicated otherwise. The truncation error in this case is of order Δx^2 and Δy^2 and is of higher order in Δx than in the previous cases.

B. Difference Equations

The following sketch shows the designation of mesh points[1] in the physical plane.

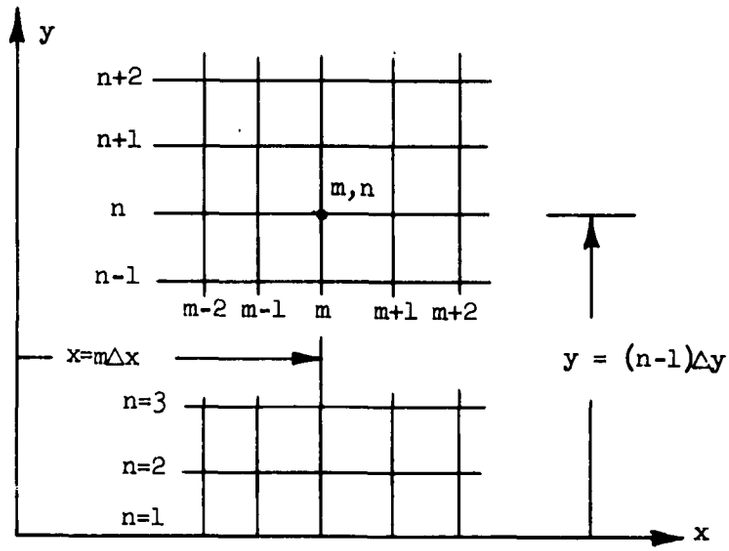

If the Howarth-Dorodnitsyn transformation is used, one has a similar grid in the transformed plane; but x and y are replaced by ξ and η, respectively. It is assumed that the velocities, u and v or V, and enthalpy, i, are known at the grid points in the m^{th} column and unknown at the grid points in the $(m+1)^{th}$ column.

[1] This notation is different from that which has been used in previous reports (Ref. 1 and 11) on finite-difference solutions of the boundary-layer equations. This change in designation of mesh points was instituted in order to be consistent with the subscript notation used in the Burroughs 220 Computer program.

1. Explicit. The transformed boundary-layer equations are used for the explicit method since the stability requirements are less severe than when the physical-plane equations are employed. The boundary-layer equations (2.29 - 2.31) become the following when equations 3.1 are used:

$$u_{m+1,n} = u_{m,n} + \frac{\Delta\xi}{u_{m,n}} \left(- V u_\eta - p_e'/\rho + F' i_\eta u_\eta + F u_{\eta\eta} \right)_{m,n} \tag{3.4}$$

$$i_{m+1,n} = i_{m,n} + \frac{\Delta\xi}{u_{m,n}} \left(-V i_\eta + u p_e'/\rho + F u_\eta^2 + \frac{F}{Pr} i_{\eta\eta} + \frac{F'}{Pr} i_\eta^2 \right)_{m,n} \tag{3.5}$$

$$V_{m+1,n} = V_{m+1,n-1} - \frac{\Delta\eta}{2\Delta\xi} \left(u_{m+1,n} - u_{m,n} + u_{m+1,n-1} - u_{m,n-1} \right) \tag{3.6}$$

The partial derivatives at (m,n) have not been actually replaced in order to keep the notation as simple as possible. However, they are readily determined from equations 3.1 since they do not involve any unknowns.

2. Implicit. The two implicit Methods I and II are quite similar and will be discussed together. As indicated previously, the derivatives in the boundary-layer equations are evaluated at the points "e" and "k" in the two methods and correspondingly the partial differential equations must be evaluated at the same place. Notice in equations 2.18 and 2.30 that there are terms of the following form:

$$T_i \left(\frac{\partial H}{\partial x} \right)_i$$

where "i" is "e" or "k", depending on the method. If the derivative is replaced by the difference quotients as given by (3.2a) or (3.3a), the above expression becomes

$$T_i \left(\frac{H_i - H_b}{\Delta x} \right)$$

Expressions of this type will be nonlinear in the unknowns and, of course, the difference equations will be nonlinear also. Using a Taylor's expansion, we can write T_i as

$$T_i = T_b + \Delta x \left(\frac{\partial T}{\partial x}\right)_b + \ldots \qquad (i = e)$$

$$T_i = T_b + \frac{1}{2} \Delta x \left(\frac{\partial T}{\partial x}\right)_b + \ldots \qquad (i = o)$$

Therefore, in order to have linear difference equations, the original expression is written as

$$T_i \left(\frac{H_i - H_b}{\Delta x}\right) \approx T_b \left(\frac{H_i - H_b}{\Delta x}\right)$$

where terms of order Δx have been neglected as indicated in the above expansions.

Using the above linearization technique and the difference quotients (3.2) and (3.3), we can write the momentum and energy equations (2.18 - 2.19) or (2.30 - 2.31) of the boundary layer as the following difference equations:

$(2 \leq n \leq N-1 \quad \text{and} \quad m \geq 1)$

$$A_{1_{m,n}} u_{m+1,n-1} + B_{1_{m,n}} u_{m+1,n} + C_{1_{m,n}} u_{m+1,n+1} + D_{1_{m,n}} i_{m+1,n-1} + E_{1_{m,n}} i_{m+1,n} + F_{1_{m,n}} i_{m+1,n+1} = G_{1_{m,n}} \qquad (3.7)$$

$$A_{2_{m,n}} u_{m+1,n-1} + B_{2_{m,n}} u_{m+1,n} + C_{2_{m,n}} u_{m+1,n+1} + D_{2_{m,n}} i_{m+1,n-1} + E_{2_{m,n}} i_{m+1,n-1} + F_{2_{m,n}} i_{m+1,n+1} = G_{2_{m,n}} \qquad (3.8)$$

where the coefficients vary, depending on whether Method I or II is being used. The coefficients for Method I, which result from equations (2.18 and 2.19) with equations 3.2, are the following:

Method I (Physical Plane)

$$A_{1_{m,n}} = L_1 \left(-\rho v + f' i_y - \frac{2f}{\Delta y}\right) \tag{3.9a}$$

$$B_{1_{m,n}} = \rho u + \frac{4fL_1}{\Delta y} \tag{3.9b}$$

$$C_{1_{m,n}} = L_1 \left(\rho v - f' i_y - \frac{2f}{\Delta y}\right) \tag{3.9c}$$

$$D_{1_{m,n}} = f' L_1 u_y \tag{3.9d}$$

$$E_{1_{m,n}} = 0 \tag{3.9e}$$

$$F_{1_{m,n}} = - f' L_1 u_y \tag{3.9f}$$

$$G_{1_{m,n}} = \rho u^2 - \Delta x \left(p'_e + f' u_y i_y\right) \tag{3.9g}$$

and

$$A_{2_{m,n}} = 2f L_1 u_y \tag{3.10a}$$

$$B_{2_{m,n}} = 0 \tag{3.10b}$$

$$C_{2_{m,n}} = - 2f L_1 u_y \tag{3.10c}$$

$$D_{2_{m,n}} = L_1 \left(-\rho v + \frac{2f'}{Pr} i_y - \frac{2f}{Pr\Delta y}\right) \tag{3.10d}$$

$$E_{2_{m,n}} = \rho u + \frac{4fL_1}{Pr\Delta y} \tag{3.10e}$$

$$F_{2_{m,n}} = L_1 \left(\rho v - \frac{2f'}{Pr} i_y - \frac{2f}{Pr\Delta y}\right) \tag{3.10f}$$

$$G_{2_{m,n}} = \rho u i + \Delta x \left(u p'_e - f u_y^2 - \frac{f'}{Pr} i_y^2\right) \tag{3.10g}$$

where

$$L_1 = \Delta x/(2\Delta y) \tag{3.11a}$$

$$i_y = (i_{m,n+1} - i_{m,n-1})/(2\Delta y) \tag{3.11b}$$

$$u_y = (u_{m,n+1} - u_{m,n-1})/(2\Delta y) \tag{3.11c}$$

In the above relations all the quantities are evaluated at the grid point (m,n) due to the linearization. Without the linearization all the unsubscripted quantities would be evaluated at the grid point (m+1,n).

The coefficients for Method II, which results from equations (2.30 and 2.31) with equations 3.3 are the following:

Method II (Transformed Plane)

$$A_{1_{m,n}} = L_2 \left(- V - \frac{2F}{\Delta\eta} + F' i_\eta\right) \tag{3.12a}$$

$$B_{1_{m,n}} = 2u + \frac{4 FL_2}{\Delta\eta} \tag{3.12b}$$

$$C_{1_{m,n}} = L_2 \left(V - \frac{2F}{\Delta\eta} - F' i_\eta\right) \tag{3.12c}$$

$$D_{1_{m,n}} = F' L_2 u_\eta \tag{3.12d}$$

$$E_{1_{m,n}} = 0 \tag{3.12e}$$

$$F_{1_{m,n}} = - F' L_2 u_\eta \tag{3.12f}$$

$$G_{1_{m,n}} = 2u u_{m,n} + \Delta\xi \left(-2p_e'/\rho - V u_\eta + F u_{\eta\eta}\right) \tag{3.12g}$$

and

$$A_{2_{m,n}} = 2L_2 F u_\eta \tag{3.13a}$$

$$B_{2_{m,n}} = 0 \tag{3.13b}$$

$$C_{2_{m,n}} = -\,2\,L_2\,F\,u_\eta \tag{3.13c}$$

$$D_{2_{m,n}} = L_2\left(-\,V - \frac{2F}{Pr\Delta\eta} + \frac{2F'}{Pr}\,i_\eta\right) \tag{3.13d}$$

$$E_{2_{m,n}} = 2u + \frac{4FL_2}{Pr\Delta\eta} \tag{3.13e}$$

$$F_{2_{m,n}} = L_2\left(\,V - \frac{2F}{Pr\Delta\eta} - \frac{2F'}{Pr}\,i_\eta\,\right) \tag{3.13f}$$

$$G_{2_{m,n}} = 2u\,i_{m,n} + \Delta\xi\,\left(2up'_e/\rho - V\,i_\eta + \frac{F}{Pr}\,i_{\eta\eta}\right) \tag{3.13g}$$

where

$$L_2 = \Delta\xi/(2\,\Delta\eta) \tag{3.14a}$$

$$i_\eta = (i_{m,n+1} - i_{m,n-1})/(2\Delta\eta) \tag{3.14b}$$

$$u_\eta = (u_{m,n+1} - u_{m,n-1})/(2\Delta\eta) \tag{3.14c}$$

$$i_{\eta\eta} = (i_{m,n+1} - 2i_{m,n} + i_{m,n-1})/\Delta\eta^2 \tag{3.14d}$$

$$u_{\eta\eta} = (u_{m,n+1} - 2u_{m,n} + u_{m,n-1})/\Delta\eta^2 \tag{3.14e}$$

In the above relations all the quantities are evaluated at the grid point (m,n) due to the linearization. Without the linearization all the unsubscripted quantities would be evaluated at the grid point (m+1/2,n).

Two methods are used to replace the continuity equation and will be called Methods A and B. The following sketch of the grid will be useful in the description of these methods of writing the difference equations.

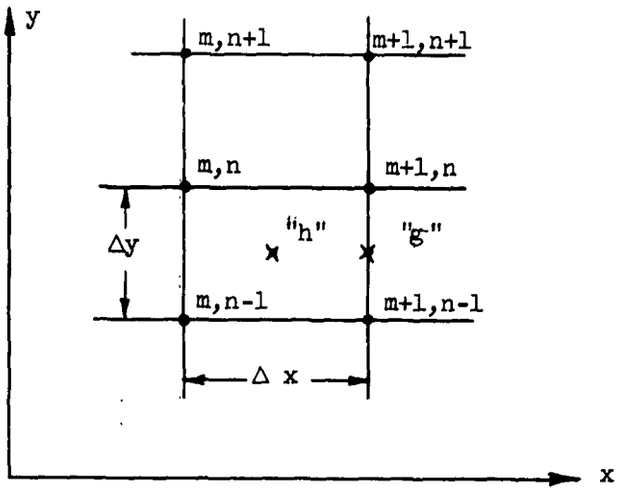

Method A evaluates the derivatives in the continuity equations at point "g" and uses the backward difference scheme for x-derivatives. The difference quotients are

$$(\rho v)_y = \frac{(\rho v)_{m+1,n} - (\rho v)_{m+1,n-1}}{\Delta y} + \frac{1}{24}\Delta y^2 (\rho v)_{yyy} + \ldots$$

$$(\rho u)_x = \frac{1}{2\Delta x}\left[(\rho u)_{m+1,n} - (\rho u)_{m,n} + (\rho u)_{m+1,n-1} - (\rho u)_{m,n-1}\right]$$

$$- \frac{1}{2}\Delta x (\rho u)_{xx} + \ldots \qquad (3.15)$$

The continuity equation (2.17) becomes the following when the above difference quotients are used.

(Physical Plane - Method A)

$$(\rho v)_{m+1,n} = (\rho v)_{m+1,n-1} - \frac{\Delta y}{2\Delta x}\left[(\rho u)_{m+1,n} - (\rho u)_{m,n} + (\rho u)_{m+1,n-1} - (\rho u)_{m,n-1}\right]$$

(3.16)

For Method B the derivatives are evaluated at point "h" as shown in the preceding sketch. The difference quotients used in this method are

$$(\rho u)_x = \frac{1}{2\Delta x}\left[(\rho u)_{m+1,n} - (\rho u)_{m,n} + (\rho u)_{m+1,n-1} - (\rho u)_{m,n-1}\right]$$

$$+ \frac{1}{24}\Delta x^2 (\rho u)_{xxx} + \frac{1}{8}\Delta y^2 (\rho u)_{xyy} + \ldots \qquad (3.17)$$

$$(\rho v)_y = \frac{1}{2\Delta y}\left[(\rho v)_{m,n} - (\rho v)_{m,n-1} + (\rho v)_{m+1,n} - (\rho v)_{m+1,n-1}\right]$$

$$+ \frac{1}{8}\Delta x^2 (\rho v)_{xxy} + \frac{1}{24}\Delta y^2 (\rho v)_{yyy} + \ldots$$

It should be noticed that the truncation error in these difference quotients is of higher order in the x-direction than in Method A. Using the above difference quotients gives for the continuity equation (2.17) the following:

(Physical Plane - Method B)

$$(\rho v)_{m+1,n} = (\rho v)_{m+1,n-1} - (\rho v)_{m,n} + (\rho v)_{m,n-1} \qquad (3.18)$$

$$- \frac{\Delta y}{\Delta x}\left[(\rho u)_{m+1,n} - (\rho u)_{m,n} + (\rho u)_{m+1,n-1} - (\rho u)_{m,n-1}\right]$$

The continuity equation (2.29) in the transformed plane becomes the following for the two methods discussed above.

(Transformed Plane - Method A)

$$V_{m+1,n} = V_{m+1,n-1} - \frac{\Delta\eta}{2\Delta\xi}\left(u_{m+1,n} - u_{m,n} + u_{m+1,n-1} - u_{m,n-1}\right) \qquad (3.19)$$

(Transformed Plane - Method B)

$$V_{m+1,n} = V_{m+1,n-1} - V_{m,n} + V_{m,n-1}$$

$$- \frac{\Delta\eta}{\Delta\xi} \left(u_{m+1,n} - u_{m,n} + u_{m+1,n-1} - u_{m,n-1}\right) \tag{3.20}$$

C. Method of Solution

In order to solve the difference equations either in the explicit or implicit form, it is necessary to have the boundary conditions in a form suitable for numerical computation. The velocity and enthalpy at the outer edge of the boundary layer are known in the case where there is no interaction and from (2.23) become

$$u_{m,N} = u_e(x) \tag{3.21a}$$

$$i_{m,N} = i_e(x) \tag{3.21b}$$

where N is the number of grid points across the boundary layer. At the wall the velocity is zero and the other boundary condition depends upon whether the temperature of the wall or the heat transfer is specified. These boundary conditions are written as

$$v_{m,1} = 0 \tag{3.22a}$$

$$u_{m,1} = 0 \tag{3.22b}$$

$$i_{m,1} = i_w(x) \tag{3.22c}$$

or

$$q_w = \frac{\mu}{Pr} \left(\frac{\partial i}{\partial y}\right)_w \approx \frac{\mu}{\Delta y\, Pr} \left(i_{m,2} - i_{m,1}\right) \tag{3.22d}$$

The approximation for the above derivative in (3.22d) is rather crude and this point will be discussed later when an insulated wall is considered. The other condition that must be given is the velocity and

enthalpy profiles across the boundary layer at the start. The determination of initial profiles is considered in Section D.

1. Explicit Difference Equations. The method of solving the explicit difference equations (3.4 - 3.6) is apparent. Since all the quantities on the right side of the equations are known from the initial profiles, the velocities and enthalpy are calculated directly at each grid point across the boundary layer. After starting at the wall the calculations proceed until the velocity $u_{m+1,n}$ and enthalpy $i_{m+1,n}$ are sufficiently close to the velocity u_e and enthalpy i_e determined from the external flow. Then the profiles across the boundary layer are calculated at succeeding steps downstream until the desired distance is obtained.

2. Implicit Difference Equations. The method of solving the implicit difference equations (3.7) and (3.8) is the same for both implicit difference Methods I and II. Of course, the coefficients in the difference equations will depend upon the method being used. Obviously, the difference equations cannot be solved directly as in the explicit case, but one has the problem of solving a large number of linear algebraic equations. The system of algebraic equations is of a special type since a large number of the coefficients in the complete system are zero. Because of the special form of the equations, the following relations exist (see Appendix B, especially equations 14b):

$$u_{m+1,n-1} = K^{(1)}_{m+1,n-1} + K^{(2)}_{m+1,n-1}\, u_{m+1,n} + K^{(3)}_{m+1,n-1}\, i_{m+1,n} \qquad (3.23a)$$

$$i_{m+1,n-1} = L^{(1)}_{m+1,n-1} + L^{(2)}_{m+1,n-1}\, u_{m+1,n} + L^{(3)}_{m+1,n-1}\, i_{m+1,n} \qquad (3.23b)$$

When the above are substituted into the difference equations (3.7) and (3.8), the following is obtained:

$$B^*_{1_{m,n}}\, u_{m+1,n} + E^*_{1_{m,n}}\, i_{m+1,n} = G^*_{1_{m,n}} - C_{1_{m,n}}\, u_{m+1,n+1} - F_{1_{m,n}}\, i_{m+1,n+1} \qquad (3.24a)$$

$$B^*_{2_{m,n}}\, u_{m+1,n} + E^*_{2_{m,n}}\, i_{m+1,n} = G^*_{2_{m,n}} - C_{2_{m,n}}\, u_{m+1,n+1} - F_{2_{m,n}}\, i_{m+1,n+1}$$

(3.24b)

where

$$B^*_{1_{m,n}} = B_{1_{m,n}} + A_{1_{m,n}}\, K^{(2)}_{m+1,n-1} + D_{1_{m,n}}\, L^{(2)}_{m+1,n-1} \qquad (3.25a)$$

$$B^*_{2_{m,n}} = B_{2_{m,n}} + A_{2_{m,n}}\, K^{(2)}_{m+1,n-1} + D_{2_{m,n}}\, L^{(2)}_{m+1,n-1} \qquad (3.25b)$$

$$E^*_{1_{m,n}} = E_{1_{m,n}} + A_{1_{m,n}}\, K^{(3)}_{m+1,n-1} + D_{1_{m,n}}\, L^{(3)}_{m+1,n-1} \qquad (3.25c)$$

$$E^*_{2_{m,n}} = E_{2_{m,n}} + A_{2_{m,n}}\, K^{(3)}_{m+1,n-1} + D_{2_{m,n}}\, L^{(3)}_{m+1,n-1} \qquad (3.25d)$$

$$G^*_1 = G_{1_{m,n}} - A_{1_{m,n}}\, K^{(1)}_{m+n,n-1} - D_{1_{m,n}}\, L^{(1)}_{m+1,n-1} \qquad (3.25e)$$

$$G^*_2 = G_{2_{m,n}} - A_{2_{m,n}}\, K^{(1)}_{m+1,n-1} - D_{2_{m,n}}\, L^{(1)}_{m+1,n-1} \qquad (3.25f)$$

Solving equation (3.24a) and (3.24b) for $u_{m+1,n}$ and $i_{m+1,n}$ gives

$$u_{m+1,n} = K^{(1)}_{m+1,n} + K^{(2)}_{m+1,n}\, u_{m+1,n+1} + K^{(3)}_{m+1,n}\, i_{m+1,n+1} \qquad (3.26a)$$

$$i_{m+1,n} = L^{(1)}_{m+1,n} + L^{(2)}_{m+1,n}\, u_{m+1,n+1} + L^{(3)}_{m+1,n}\, i_{m+1,n+1} \qquad (3.26b)$$

where

$$K^{(1)}_{m+1,n} = \Delta\, (G^*_1\, E^*_2 - G^*_2\, E^*_1)_{m,n} \qquad (3.27a)$$

$$K^{(2)}_{m+1,n} = \Delta\, (E^*_1\, C_2 - C_1\, E^*_2)_{m,n} \qquad (3.27b)$$

$$K^{(3)}_{m+1,n} = \Delta\,(E^*_1 F_2 - F_1 E^*_2)_{m,n} \qquad (3.27c)$$

$$L^{(1)}_{m+1,n} = \Delta\,(B^*_1 G^*_2 - B^*_2 G^*_1)_{m,n} \qquad (3.27d)$$

$$L^{(2)}_{m+1,n} = \Delta\,(C_1 B^*_2 - B^*_1 C_2)_{m,n} \qquad (3.27e)$$

$$L^{(3)}_{m+1,n} = \Delta\,(F_1 B^*_2 - B^*_1 F_2)_{m,n} \qquad (3.27f)$$

where

$$\Delta = 1/(B^*_1 E^*_2 - E^*_1 B^*_2)_{m,n}$$

After we apply the boundary condition at the wall (3.22b), equations (15B) in Appendix B require the following:

$$K^{(1)}_{m,1} = K^{(2)}_{m,1} = K^{(3)}_{m,1} = 0 \qquad (3.28)$$

Similarly, the boundary condition (3.22c) and equations (15B) give

$$L^{(1)}_{m,1} = i_w$$

Specified wall temperature (3.29)

$$L^{(2)}_{m,1} = L^{(3)}_{m,1} = 0$$

while boundary condition (3.22d) gives

$$L^{(1)}_{m,1} = -\frac{\Delta y\,\mu_w}{Pr}\,q_w$$

$$L^{(2)}_{m,1} = 0 \qquad \text{Specified heat transfer} \qquad (3.30)$$

$$L^{(3)}_{m,1} = 1$$

Now the necessary relations exist to solve the implicit finite-difference equations, but the method needs to be clarified.

The quantities $K^{(1)}_{m,n}$, $K^{(2)}_{m,n}$, $K^{(3)}_{m,n}$, $L^{(1)}_{m,n}$, $L^{(2)}_{m,n}$, and $L^{(3)}_{m,n}$ can be determined across the boundary layer by using the following procedure:

(a) Perform the following steps at the first point away from the wall:

(1) Calculate A_1, B_1, C_1, D_1, E_1, F_1, and G_1 from equations (3.9a -3.9g) or (3.12a - 3.12g).

(2) Calculate A_2, B_2, C_2, D_2, E_2, F_2, and G_2 from equations (3.10a - 3.10g) or (3.13a - 3.13g).

(3) Using the results from the previous steps and the boundary conditions (3.28) and (3.29) or (3.30), calculate B_1^*, B_2^*, E_1^*, E_2^*, G_1^*, and G_2^* as given by equations (3.25a - 3.25f).

(4) Using previous results, calculate $K^{(1)}$, $K^{(2)}$, $K^{(3)}$, $L^{(1)}$, $L^{(2)}$, and $L^{(3)}$ with equations (3.27a - 3.27f).

(b) Now the procedure outlined in step (a) can be repeated at the second point away from the wall using results obtained at the first point. The above procedure is repeated until the boundary layer is traversed and all values of $K^{(1)}$, $K^{(2)}$, $K^{(3)}$, $L^{(1)}$, $L^{(2)}$, and $L^{(3)}$ are determined.

Now the velocity, u, and enthalpy, i, are determined across the boundary layer, starting at the outer edge. Knowing the K's and L's across the boundary layer, we can use equations (3.26a) and (3.26b) to solve for the velocity and enthalpy utilizing the boundary conditions (3.21a) and (3.21b) at the outer edge.

As yet the continuity equation has not been required in order to calculate the velocity, v or V, due to the linearization of the difference equations. Before the computations can proceed downstream, the velocity, v or V, must be determined across the boundary layer. Starting at the wall calculate the velocities v or V from equation (3.16) or (3.18) for the physical plane and equation (3.14) or (3.20) for the transformed plane, respectively. Now the velocity and enthalpy profiles can be determined at succeeding steps downstream.

D. Initial Profiles

In most of the problems solved using numerical schemes, initial profiles are obtained from similarity solutions of the boundary-layer equations. However, Wu (Ref. 42) has proposed the following type of initial profiles for leading edges or stagnation flow:

(1) The velocity u and enthalpy i are freestream values at all the grid points across the layer except at the wall.

(2) At the wall the velocity u is zero and the enthalpy corresponds to the wall temperature.

(3) The velocity V is assumed zero at all the grid points across the boundary layer.

Since this method would be very advantageous for starting numerical computations, it has been investigated further.[1]

To study the possibility of using the Wu type initial profiles, the boundary-layer flow from the leading edge of a flat plate at Mach number 9.6 was solved using the explicit method. A linear viscosity law was used so that the results could be compared to similarity solutions which were obtained from Low (Ref. 26). The displacement thickness of the boundary layer has been used to show the influence of using Wu type initial profiles on the numerical solutions. The displacement thickness along a flat plate for two sizes of mesh normal to the wall, $\Delta\eta$, and two sizes of mesh parallel to the wall, $\Delta\xi$, is shown in Fig. 1a. It seems that the numerical solutions can be close to the exact solution at a sufficient distance downstream if the proper step-sizes are chosen. However, simply reducing the step-sizes does not always improve the results.

In the Wu type initial profiles it has been assumed that V is zero at the leading edge, but the similar solution gives V equal to infinity. From physical consideration the assumption $V = 0$ is reasonable; but from the mathematical point of view, the similar solution

[1] It should be mentioned that such profiles are not correct for stagnation flow, e.g., as the mesh size approaches zero. For incompressible flow at a stagnation point the displacement thickness is finite, while the Wu profiles would give zero for this quantity.

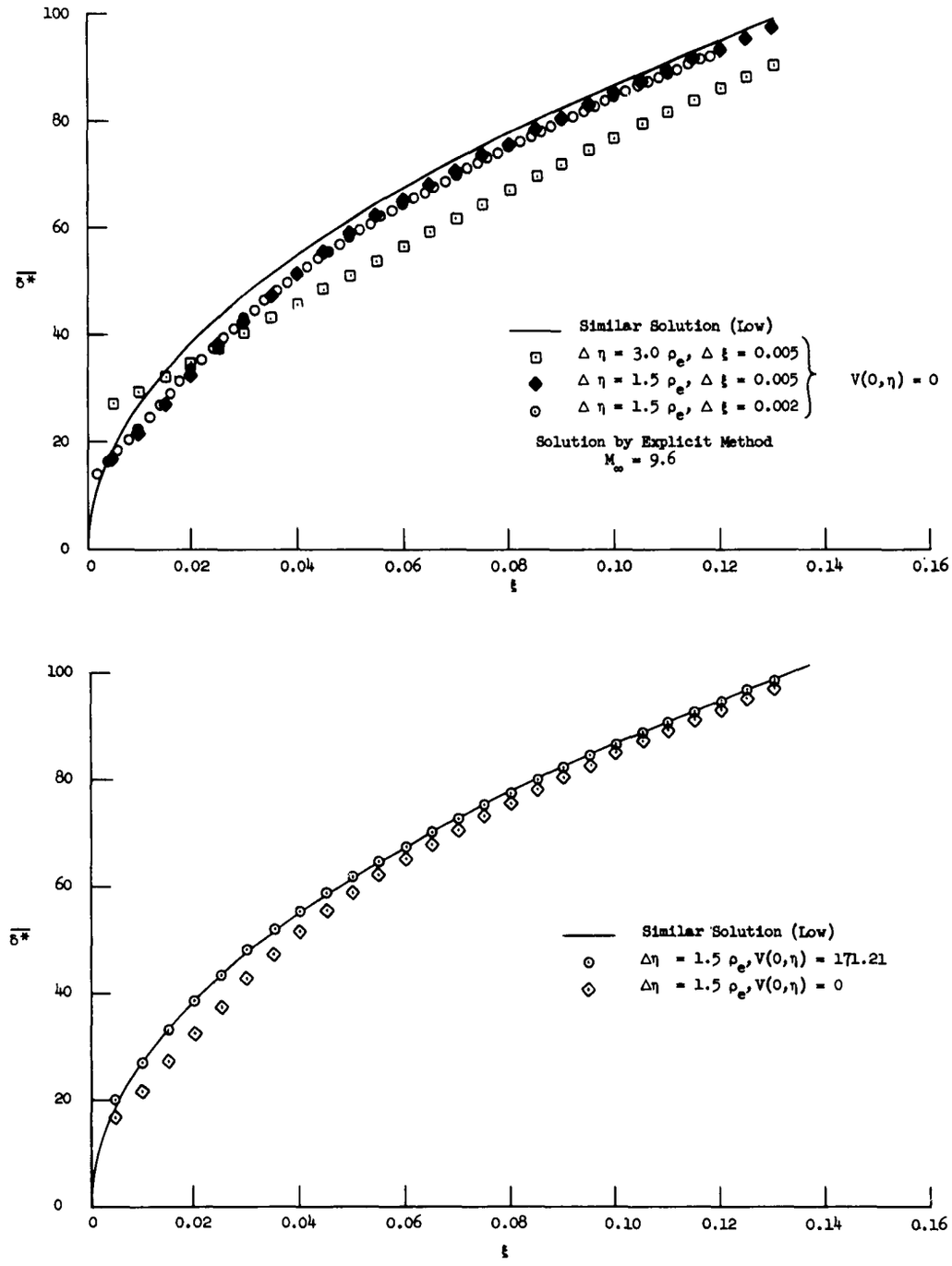

Figure 1. Flat Plate Flow with Wu Type Initial Profiles at the Leading Edge

is correct. In other words, the boundary-layer equations are not valid near the leading edge, which is well known. Therefore, in the next test the velocity, V, for the initial profile was assumed at all grid points across the boundary layer equal to the value given by the similarity solutions at the outer edge and at the first step from the leading edge. At the wall the velocity V was assumed zero as usual. The influence on the displacement thickness by assuming V finite at the leading edge is shown in Fig. 1b. In this case the numerical solution agrees closely with the similar solution.

From the above discussion it is concluded that Wu type initial profiles can give reasonable results if the proper mesh sizes are chosen. Even better results are obtained when the velocity V is given the appropriate value rather than zero. Since it is difficult to ascertain the required mesh sizes and velocity V, the Wu type initial profiles must be used with extreme care.

To obtain initial profiles it seems better to use similar solutions rather than the Wu type of initial profiles. There are three types of initial boundary-layer profiles which should be sufficient for most practical problems. The three types are flat plate, wedge, and stagnation flow. For a complete discussion of similar solutions of the boundary-layer equations, see Chapter 8 of Hayes and Probstein (Ref. 14). For supersonic speeds with an attached shock wave, the flat plate and wedge profiles are the same (i.e., constant-pressure profiles). For the case of Prandtl number 0.72 and the linear viscosity law, the initial profiles are easily obtained from Low (Ref. 26). When the Sutherland viscosity law is used, the initial profiles can be obtained using Crocco's method of solution as applied by Van Driest (Ref. 40).

For two-dimensional stagnation-point flow the profiles that are available are based on the assumption that Prandtl number is one or a linear viscosity law is used. Since the boundary-layer equations for the stagnation point reduce to two simultaneous nonlinear ordinary differential equations, it is possible to solve these equations numerically. Because these equations are of a "two-point boundary-value problem" type, they are tedious to solve, but the Sutherland viscosity law and $Pr = 0.7$ can be used.

In the verification of the implicit finite-difference scheme, initial profiles for the flow along a flat plate are used. A linear viscosity law is assumed since the profiles are easily obtained from Low for this case. In order to obtain the profiles in the notation of this paper, certain relations must be established with Low's results. Where the derivation of these relations become involved, the procedure is presented in Appendix A. The necessary relations to obtain the initial profiles in the physical plane are the following:

$$y = Q\, g(\eta_{Low}) \tag{3.31a}$$

$$u = \frac{1}{2}\, u_e\, f'(\eta_{Low}) \tag{3.31b}$$

$$i = i_e\, g'(\eta_{Low}) \tag{3.31c}$$

$$v = \frac{u_e Q}{4x} \left[f'(\eta_{Low})\, g(\eta_{Low}) - f(\eta_{Low})\, g'(\eta_{Low}) \right] \tag{3.31d}$$

where

$$g(\eta_{Low}) = \eta_{Low} + \frac{\gamma-1}{2} M_e^2\, Ir(\eta_{Low}) + K\, Is(\eta_{Low}) \tag{3.32a}$$

$$g'(\eta_{Low}) = 1 + \frac{\gamma-1}{2} M_e^2\, r(\eta_{Low}) + K\, s(\eta_{Low}) \tag{3.32b}$$

$$K = \frac{1}{2.0748} \left[\left(\frac{T_w}{T_e} - 1 \right) - \frac{\gamma-1}{2} M_e^2\, (0.8477) \right] \tag{3.32c}$$

$$Q = 2\sqrt{\frac{\mu_e\, xC}{\rho_e\, u_e}} \tag{3.32d}$$

The relations used to obtain the initial profiles in the transformed plane are the following:

$$\eta = \rho_e\, Q\, \eta_{Low} \tag{3.33a}$$

$$u = \frac{1}{2}\, u_e\, f'(\eta_{Low}) \tag{3.33b}$$

$$i = i_e\, g'(\eta_{Low}) \tag{3.33c}$$

$$V = \frac{\rho_e u_e Q}{4\xi} [\eta_{low} f'(\eta_{low}) - f(\eta_{low})] \qquad (3.33d)$$

Some of the initial profiles are given in Chapter 4 along with the numerical problems solved.

E. Stability and Convergence of the Difference Schemes

All of the difference schemes presented in this paper are consistent or are a formal approximation to the partial differential equations. A scheme is consistent if the difference between the partial differential equation and difference equation goes to zero as the mesh size approaches zero. In other words, the truncation error goes to zero as the step-sizes go to zero, which is easily seen from the difference quotients used in the various schemes. The faster the truncation error goes to zero, the more accurate is the difference approximation and more likely is the numerical solution to be a good approximation to the exact solution. However, consistency does not imply that the solution of the difference equations tends to the solution of the partial differential equations as the step-sizes go to zero. For this to be true the difference equations must be convergent. For equations of the boundary-layer type, there is no completely satisfactory mathematical analysis to show the convergences of the difference schemes. Flügge-Lotz and Yu (Ref. 11) have made the most significant investigation of the convergence of the explicit difference scheme. The convergence of the difference equations can be studied numerically by varying the mesh sizes. This type of verification of the convergence of the difference schemes is presented in Chapter IV, along with the numerical examples solved.

Since there are round-off errors in the computations, the numerical error between the exact and numerical solutions of the difference equations must be investigated. This problem is referred to as the stability of the numerical scheme. By making several assumptions and using the von Neumann method of stability analysis, we can obtain an approximate estimation of step-size for stability. Previous experience (Ref. 1) indicates that the momentum equation dominates in determining the stability of the boundary-layer equations. Therefore, only the

momentum equation will be considered for the stability of the boundary-layer equations. If the pressure gradient term is assumed zero and a linear viscosity law is used, the momentum equation (2.30) in the transformed plane becomes

$$u u_{\xi} + V u_{\eta} = F u_{\eta\eta} \tag{3.34}$$

Next it is assumed that the mesh is sufficiently small so that the coefficients in the above equation vary slightly and are considered constants. The above equation then can be written as

$$\bar{u} u_{\xi} + \bar{V} u_{\eta} = \bar{F} u_{\eta\eta} \tag{3.35}$$

where the bars indicate the quantities are to be considered constants. If the derivatives are replaced with the explicit difference quotients (3.1) and the von Neumann analysis is applied, the usual stability requirement is obtained

$$\text{Stability Parameter} = \frac{2 F \Delta\xi}{u \Delta\eta^2} \leq 1 \tag{3.36}$$

The bars have been omitted because the local values of the quantities will be used. Since the velocity is smallest near the wall, the first grid point away from the wall will give the largest value for the left-hand side of the inequality (3.36).

The flow along a flat plate at Mach number 9.6 has been solved using the explicit method with a grid size large enough to cause instability. The calculated displacement thickness is given in Fig. 2 where the instability occurs at approximately $\xi = 0.05$. Also shown in this figure is the stability parameter (3.36) at the first grid point away from the wall. The value of the stability parameter is approximately two when the instability occurs, rather than one as relation (3.36) requires. Besides the assumptions mentioned previously, some of this difference can be attributed to the fact that the known boundary conditions at the wall improve stability (see Ref. 15).

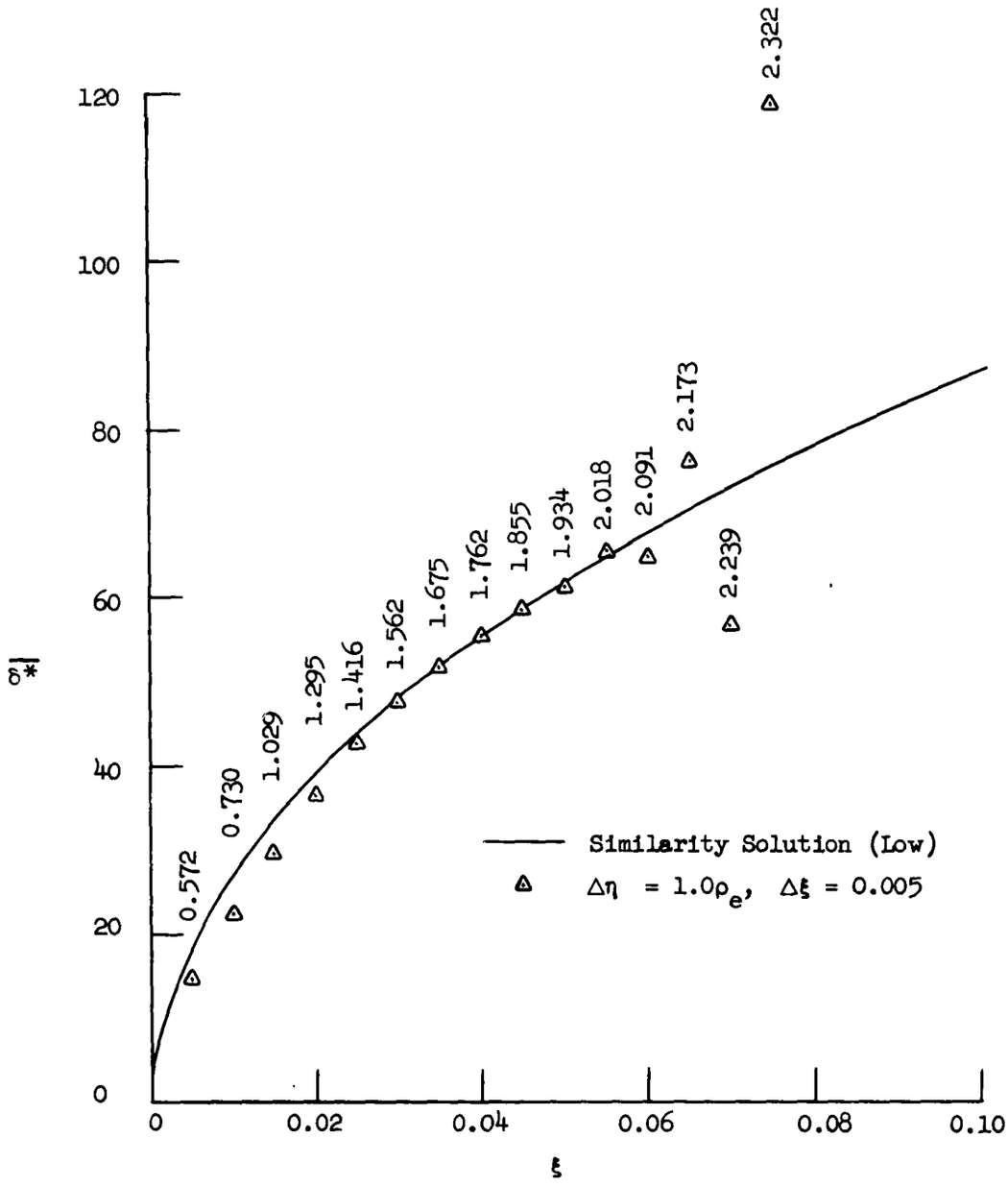

Figure 2. Displacement Thickness for Unstable Explicit Difference Scheme Solution with Variation of Stability Parameter Shown

Since the simple analysis above gives a reasonable estimate of stability requirements, the same type of analysis is now applied to the second implicit difference scheme. Substituting the difference quotients (3.3) into the momentum equation (3.35) gives the following difference equation:

$$a_1 u_{m+1,n-1} + b_1 u_{m+1,n} + c_1 u_{m+1,n+1} + d_1 u_{m,n-1} + e_1 u_{m,n} + f_1 u_{m,n+1} = 0 \tag{3.36}$$

where

$$a_1 = d_1 = -r - s \tag{3.37a}$$

$$b_1 = 1 + 2s \tag{3.37b}$$

$$c_1 = f_1 = r - s \tag{3.37c}$$

$$e_1 = -1 + 2s \tag{3.37d}$$

and

$$r = \frac{\bar{V}\,\Delta\xi}{4\bar{u}\,\Delta\eta} \tag{3.38a}$$

$$s = \frac{\bar{F}\,\Delta\xi}{2\bar{u}\,\Delta\eta^2} \tag{3.38b}$$

Applying the von Neumann method of stability analysis, we substitute $u = e^{\alpha x} e^{i\beta y} = e^{\alpha m \Delta x} e^{i\beta(n-1)\Delta y}$ into equation (3.36), and letting $\xi = e^{\alpha \Delta x}$, gives

$$\xi = -\frac{d_1 e^{-i\beta\Delta y} + e_1 + f_1 e^{i\beta\Delta y}}{a_1 e^{-i\beta\Delta y} + b_1 + c_1 e^{i\beta\Delta y}}$$

$$= -\frac{e_1 + (d_1+f_1)\cos\beta\Delta y - i(d_1-f_1)\sin\beta\Delta y}{b_1 + (a_1+c_1)\cos\beta\Delta y - i(a_1-c_1)\sin\beta\Delta y} \tag{3.39}$$

Using relations (3.37), we can write the above as

$$\xi = \frac{1 - 2s(1 - \cos \beta\Delta y) - i\, 2r \sin \beta\Delta y}{1 + 2s(1 - \cos \beta\Delta y) + i\, 2r \sin \beta\Delta y} \tag{3.40}$$

The above can be written in the following form:

$$\xi = \frac{(1 - \phi)(1 + \phi) - \theta^2 - i2\theta}{(1 + \phi)^2 + \theta^2} \tag{3.41}$$

where

$$\phi = 2s(1 - \cos \beta\Delta y) \tag{3.42a}$$

$$\theta = 2r \sin \beta\Delta y \tag{3.42b}$$

The condition for stability is

$$|\xi| \leq 1 \tag{3.43a}$$

or

$$|\xi|^2 \leq 1 \tag{3.43b}$$

From equation (3.41) the following is obtained:

$$|\xi|^2 = \frac{(1-\phi)^2 (1+\phi)^2 + 2\theta^2 (1+\phi^2) + \theta^4}{(1+\phi)^2 (1+\phi)^2 + 2\theta^2 (1+\phi)^2 + \theta^4} \tag{3.44}$$

If we consider the case when $\bar{u} \geq 0$, then $\phi \geq 0$. If $\phi = 0$, then equation (3.44) becomes

$$|\xi|^2 = 1$$

for all θ. If $\phi > 0$, then the following relations exist:

$$(1+\phi)^2 > (1-\phi)^2 \tag{3.45a}$$

$$(1+\phi)^2 > 1+\phi^2 \tag{3.45b}$$

Using these relations with (3.44), it is easy to see that

$$|\xi|^2 < 1$$

for all θ when $\phi > 0$. Therefore, the implicit Method II with $\bar{u} > 0$ is stable regardless of the mesh size as shown in the above analysis. The numerical examples investigated in Chapter IV corroborate this result.

F. Formulas for Shear Stress, Heat Transfer, and Displacement Thickness

The formula for the shear stress in the physical plane at the wall has been presented in equation (2.45), but now it is necessary to express the derivative in this expression numerically. The velocity u near the wall may be expressed with sufficient accuracy as

$$u = \gamma_1 y + \gamma_2 y^2 + \gamma_3 y^3 \tag{3.46}$$

Taking the derivative of the above with respect to y and setting $y = 0$, we can write the formula for shear stress at the wall (2.45) as

$$\tau_w = \mu_w \gamma_1 \tag{3.47}$$

The value of γ_1 can be determined by evaluating equation (3.46) at the three grid points nearest the wall and solving the three resulting equations for γ_1. When the result for γ_1 is substituted into equation (3.47), the following is obtained for the shear stress at the wall in the physical plane:

$$\tau_w = \frac{\mu_w}{6\Delta y} (18 u_2 - 9 u_3 + 2 u_4) \tag{3.48a}$$

An expression for the shear stress at the wall in the transformed plane is obtained in a similar manner from equation (2.46) and is

$$\tau_w = \frac{F_w}{6\Delta \eta} (18 u_2 - 9 u_3 + 2 u_4) \tag{3.48b}$$

The formula for the heat transfer at the wall has been presented in equation (2.49) and again it is necessary to replace the derivative. If the same procedure is followed as above, except the velocity is replaced by the enthalpy in all the expressions, the following formula is obtained for evaluation of the heat transfer at the wall in the physical plane:

$$q_w = \frac{\mu_w}{6\Delta y \, Pr} (11\, i_1 - 18\, i_2 + 9\, i_3 - 2\, i_4) \qquad (3.49a)$$

The corresponding expression for the transformed plane is

$$q_w = \frac{F_w}{6\Delta\eta \, Pr} (11\, i_1 - 18\, i_2 + 9\, i_3 - 2\, i_4) \qquad (3.49b)$$

In order to determine the displacement thickness as given by equation (2.53) a trapezoidal rule of integration is used. Since u is zero at the wall, the dimensionless displacement thickness in the physical plane can be written as

$$\overline{\delta^*} = \Delta y \left[\frac{1}{2} + \sum_{j=2}^{N} \left(1 - \frac{i_e u}{i u_e} \right)_j \right] \qquad (3.50a)$$

Using the trapezoidal rule again, we write the displacement thickness in the transformed plane as given by equation (2.54) as

$$\overline{\delta^*} = \Delta\eta \left[i_w/(2 i_e \rho_e) + \frac{1}{\rho_e} \sum_{j=2}^{N} \left(\frac{i}{i_e} - \frac{u}{u_e} \right)_j \right] \qquad (3.50b)$$

To determine the displacement thickness, a better integration method is Simpson's rule which gives the following relation in the transformed plane:

$$\overline{\delta^*} = \frac{1}{3} \Delta\eta \left[\frac{i_w}{\rho_e i_e} + \frac{4}{\rho_e} \sum_{j=1} \left(\frac{i}{i_e} - \frac{u}{u_e} \right)_{2j} + \frac{2}{\rho_e} \sum_{j=2} \left(\frac{i}{i_e} - \frac{u}{u_e} \right)_{2j-1} \right] \qquad (3.50c)$$

G. Computer Program

Due to the lengthy and repetitious nature of the implicit finite-difference schemes for solving the boundary-layer equations, the problem was programmed for the IBM 650 and Burroughs 220 digital computers. The flow diagram for the basic computer program for the explicit difference

scheme without interaction is given in Fig. 3a. For the implicit finite-difference schemes the explicit subroutine for $u_{m+1,n}$ and $i_{m+1,n}$, as indicated in Figure 3a, is replaced by the subroutine for computing $u_{m+1,n}$ and $i_{m+1,n}$ using the implicit scheme (see Figure 3b). The flow diagram can be divided into many subroutines, as shown in the diagram; however, some operations are not as clearly separated as indicated.

Given below is the computation procedure which will relate previous formulas with the flow diagram.

1. Program Constants. This consists of computing various parameters which are used frequently but do not change. Also computed are u_∞, p_∞, i_o, and T_o from equations (2.36 - 2.39).
2. Compute $p_{e_{m+1}}$ and $p'_{e_{m+1}}$. The pressure and pressure gradient are computed at the points m+1. The formulas or values for these quantities are given under the specific problem being solved.
3. Compute Exterior Flow Quantities. The exterior flow quantities u_e, i_e, ρ_e, T_e, and μ_e are computed using formulas (2.40 - 2.44).
4. $\tau_w < 0$. This is a check to be sure that there is no laminar separation.
5. Compute $u_{m+1,n}$ and $i_{m+1,n}$. The velocity and enthalpy across the boundary layer at mesh points m+1 are calculated. For the method of solution and equations used, see Chapter III, Section C,2.
6. Test for Edge of Boundary Layer While Computing u and i. The following test that is described is applicable only when the velocity and enthalpy of the exterior flow at any x are independent of y. In the implicit calculation procedure it is necessary to know how far to calculate the $K^{(i)}$'s and $L^{(i)}$'s (i = 1,2,3) across the boundary layer. The typical variation of $K^{(1)}$ and $L^{(1)}$ across the boundary layer is shown in Fig. 4. At the outer edge of the boundary layer these quantities become independent of the distance away from the wall. Therefore, to stop the calculation of the $K^{(i)}$'s and $L^{(i)}$'s (i = 1,2,3) after the boundary layer has been transversed, two consecutive values of $K^{(1)}$ are compared to see if the difference between them is less than some small quantity ϵ. The value of ϵ is determined by the desired accuracy of the

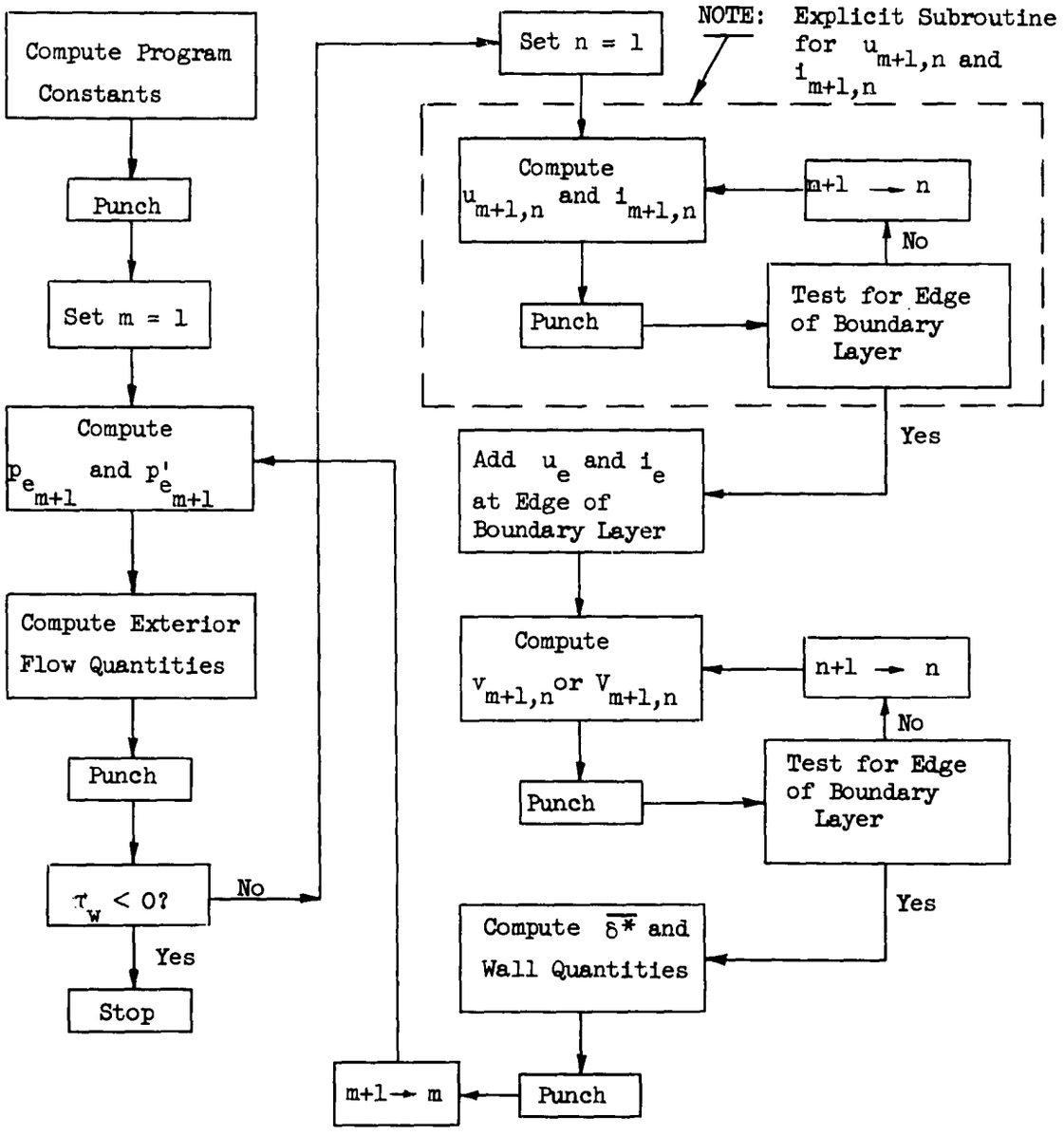

Figure 3a. Flow Diagram for Explicit Finite-Difference Schemes Without Interaction

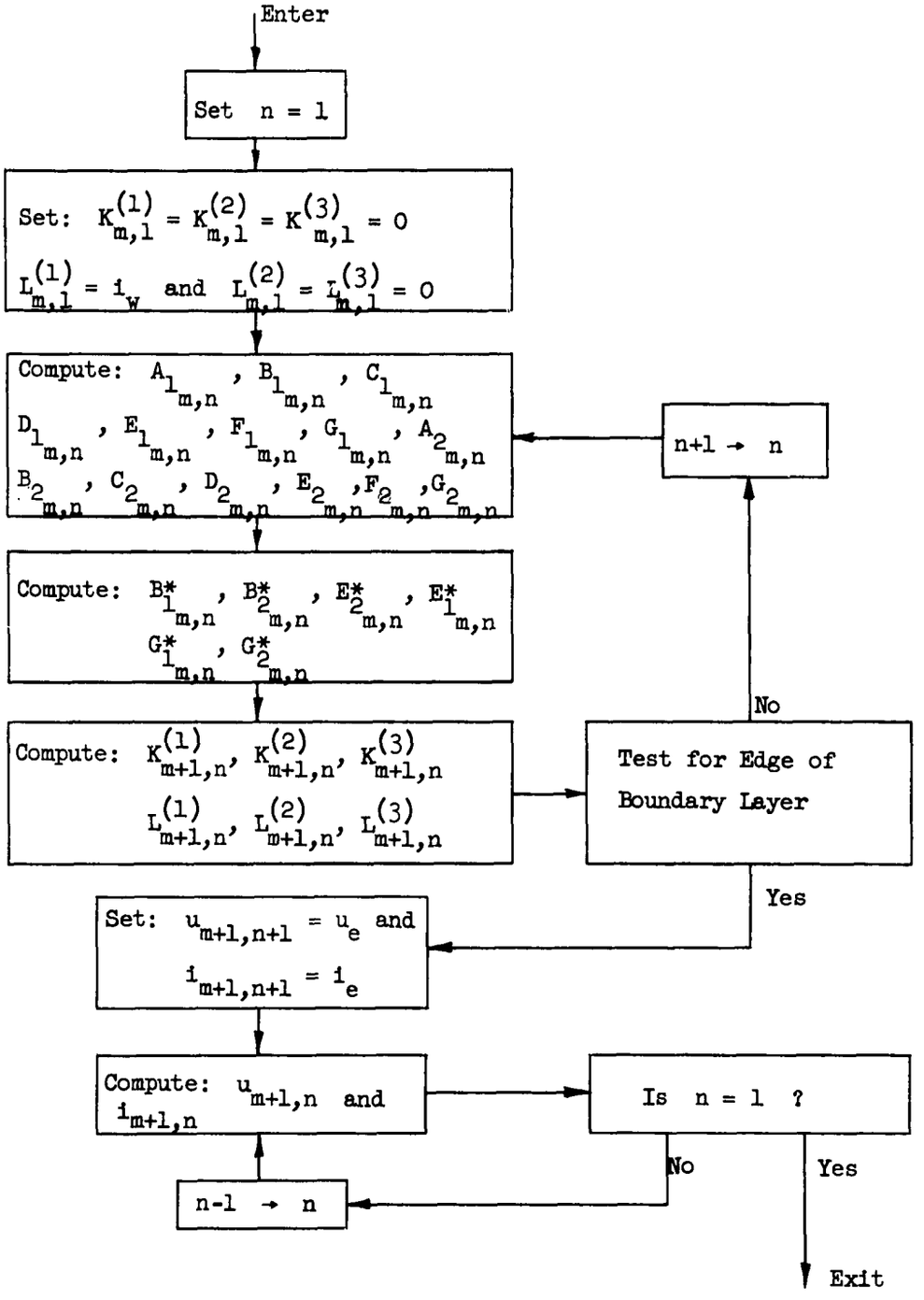

Figure 3b. Subroutine for Computing $u_{m+1,n}$ and $i_{m+1,n}$ using the Implicit Finite-Difference Scheme

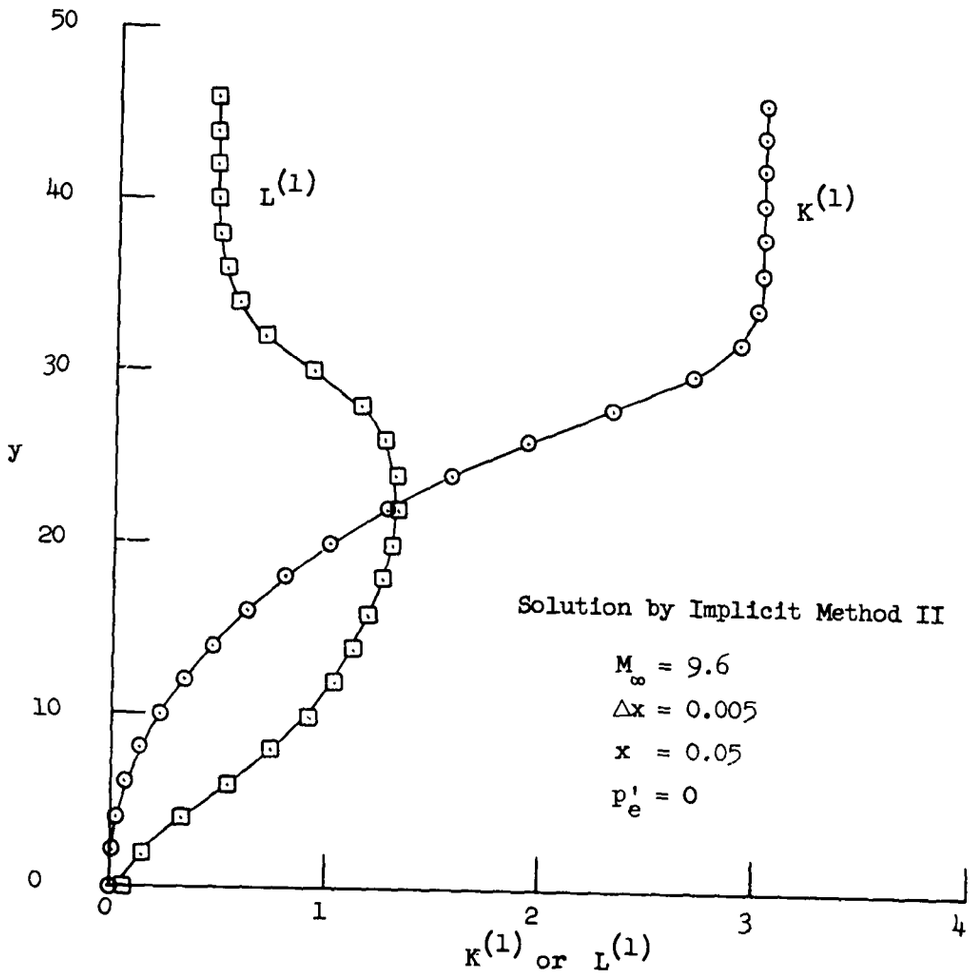

Figure 4. Typical Variation of $K^{(1)}$ and $L^{(1)}$ Across the Boundary Layer

calculations and is discussed further in Chapter IVwith the numerical examples. If the difference between the $K^{(1)}$'s is less than ϵ, the difference between two consecutive $L^{(1)}$'s is compared with ϵ. When this difference is also less than ϵ, the computations proceed to the next step. This procedure applies for computations in both the physical and transformed planes.

7. Add u_e and i_e at Edge of Boundary Layer. This portion of the program adds u_e and i_e at the mesh points beyond the last points computed. This step is required so that the number of mesh points across the boundary layer will not decrease by one at each step downstream.

8. Compute $v_{m+1,n}$ or $V_{m+1,n}$. The velocity v or V is computed across the boundary layer using equations (3.16 or 3.18) and equations (3.19 or 3.20), respectively.

9. Test for Edge of Boundary Layer While Computing v or V. This time the test for the edge of the boundary layer is simply to have the same number of mesh points across the boundary layer as for the u and i computations.

10. Compute $\overline{\delta^*}$ and Wall Quantities. The displacement thickness, $\overline{\delta^*}$, is computed from the appropriate equation of (3.50a) to (3.50c). The wall quantities τ_w and q_w are computed from equations (3.48) and (3.49), respectively. The shear stress parameter $C_f\sqrt{Re_x}$ and heat transfer parameter $St\sqrt{Re_x}$ are computed using equations (2.47) and (2.50).

CHAPTER IV

ILLUSTRATIONS OF THE IMPLICIT DIFFERENCE SCHEMES WITHOUT INTERACTION

The results for a variety of boundary-layer problems, using the implicit difference schemes developed in the previous chapter, will now be presented. Although Implicit Method II is superior, it has the disadvantage of using the transformed plane. Since Implicit Method I solves the boundary-layer equation in the physical plane, it is interesting to consider examples solved by this method and understand its features. Four problems are investigated using Method I, and two problems with Method II. In addition, the flow near the leading edge of a flat plate is solved by both methods.

A. Implicit Method I

Five problems were solved with an IBM 650 computer using Implicit Method I, which solves the boundary-layer equations in the physical plane. The first two problems involve the flow along a flat plate where the initial profiles are at one reference length from the leading edge ($x_i = 1.00$). In example one the wall temperature is assumed constant, but with a value such that the wall is heated. The second flat plate problem assumes the wall is insulated (zero heat transfer). In both of these examples a linear viscosity law is used so that a direct comparison can be made with similar solutions of the boundary-layer equations. Then in example three the flow along a wall with a ramp pressure gradient is investigated and is compared with numerical results of Baxter. Since Baxter uses Sutherland's viscosity law in this example, the present example uses the same viscosity law. To study the influence of the viscosity law on the boundary-layer solution, the fourth example considers the flow along a flat plate with the same conditions as example one except Sutherland's viscosity law is used. Finally, the flow near the leading edge of a flat plate ($x = 0.01$) is investigated, since this case will be considered with displacement thickness interaction in Chapter V.

1. Flat Plate Flow With Constant Wall Temperature. The boundary-layer flow along a flat plate whose surface is heated and temperature is constant has been investigated by Flügge-Lotz and Yu (Ref. 11). An explicit finite-difference scheme was used by Flügge-Lotz and Yu for solving the boundary-layer equations in the physical plane. For this example the numerical solution became unstable after a few steps from the initial profiles. Also, the solution to this problem can be obtained from similarity results and is readily obtained from Low (Ref. 26). Since the similar solution is based upon a linear viscosity law (Eq. 2.21), the same assumption is used in the numerical solution.

The following fluid properties, exterior flow, and wall quantity, are used for this example:

$$M_\infty = 3 \tag{4.1a}$$

$$T_\infty^* = 389.99^\circ R \tag{4.1b}$$

$$\gamma = 1.4 \tag{4.1c}$$

$$Pr = 0.72 \tag{4.1d}$$

$$S^* = 216^\circ R \tag{4.1e}$$

$$T_w/T_{ad} = 2 \tag{4.1f}$$

The pressure distribution has not been discussed previously. For a flat plate without interaction the following relations are used:

$$p_e = p_\infty \tag{4.2a}$$

$$p_e' = 0 \tag{4.2b}$$

As a consequence of the above relations, the exterior flow quantities at the edge of the boundary layer are the same as the corresponding quantities at the free stream conditions. The initial profiles are obtained from equations (3.31a - 3.31d) and are shown in Figure 5.

This problem has been solved with Implicit Method I and no stability difficulties are encountered. In these calculations step-sizes up to one hundred times greater than the size employed by Yu have been used.

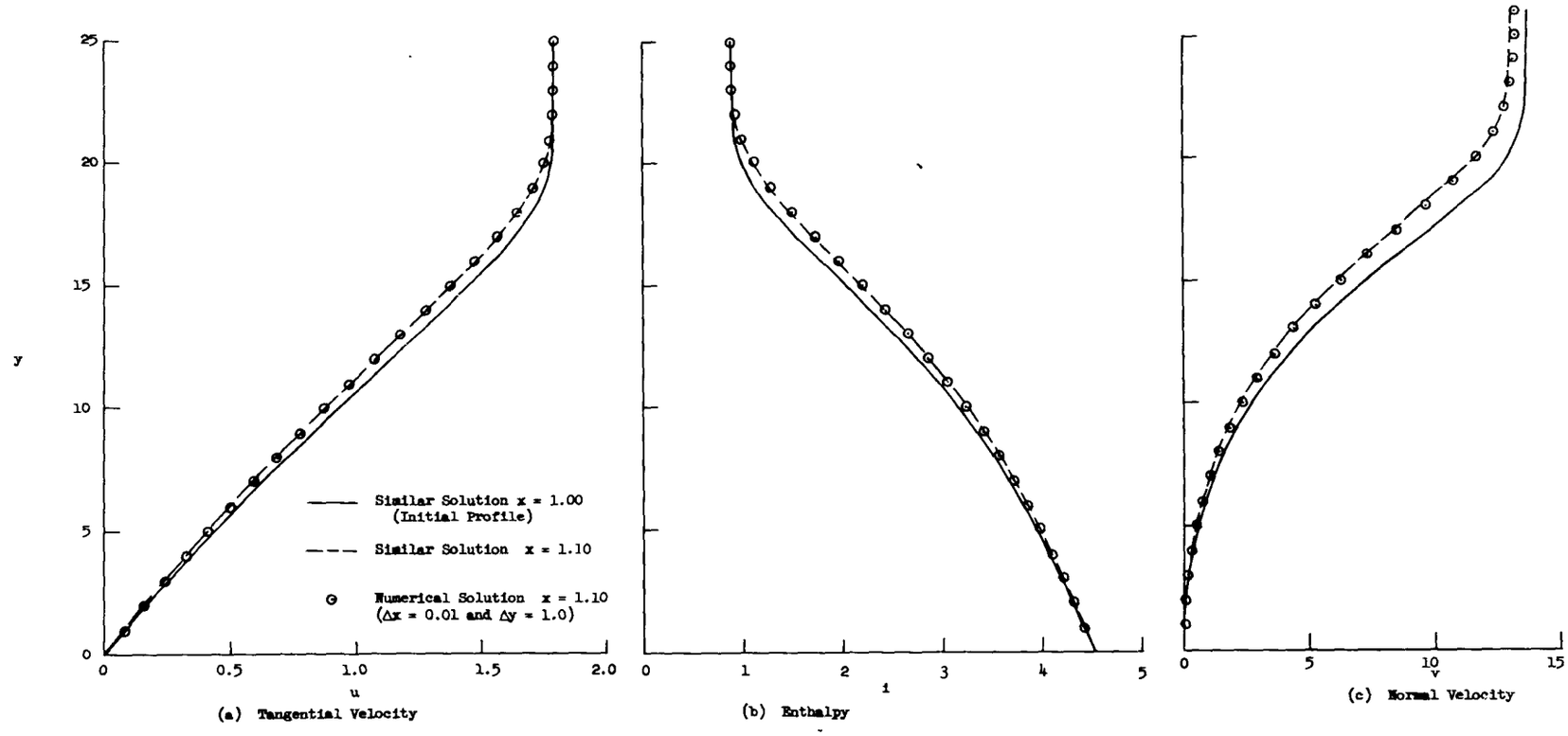

Figure 5. Flat Plate Profiles ($M_\infty = 3$ and $T_w/T_{ad} = 2$)

The velocity profiles u and v and the enthalpy profile i obtained from the numerical solution, after ten steps downstream of the initial profiles, are shown in Figure 5. The similar solution to the boundary-layer equations at the same distance downstream is also given.

In the numerical computations the parameter ϵ and the step-size must be chosen. In Chapter III, Section G.6 the computer program test for the edge of the boundary layer was discussed and certain quantities had to be less than ϵ. The value of ϵ was determined by decreasing its magnitude until there was no influence on the displacement thickness. For this problem $\epsilon = 0.00001$. Several step-sizes have been used to solve this problem. The effect of changing Δy and Δx on the boundary-layer characteristics is shown in Figures 6 and 7 respectively. These characteristics were obtained from equations (3.48a), (3.49a), and (3.50a). The boundary-layer characteristics, as given by similar solution, are also shown in these figures. For the range of step-sizes investigated there is very little influence on the convergence of the numerical solution to the exact solution. It should be noticed that the scales in these figures are greatly expanded and the differences between the numerical and similar solutions are actually very small. Since the initial profiles are only accurate to four decimal places, there are initially errors in the boundary-layer calculations and characteristics. These errors appear to decrease as the computations proceed.

2. Flat Plate Flow With Zero Heat Transfer. At the wall either the wall temperature or the heat transfer can be specified. Since the previous example considered the specified wall temperature, this example takes the case when the heat transfer is zero (insulated wall). This example is the same as the problem in the previous section except for the wall boundary condition. The fluid properties and exterior flow are given by expressions (4.1a - 4.1e), and the relations (4.2a - 4.2b) are also applicable for the pressure distribution. The initial profiles are shown in Figure 9 and were obtained from equations (3.31).

The wall boundary condition for the case of a specified heat transfer is given in equation (3.22d). The values for the coefficients

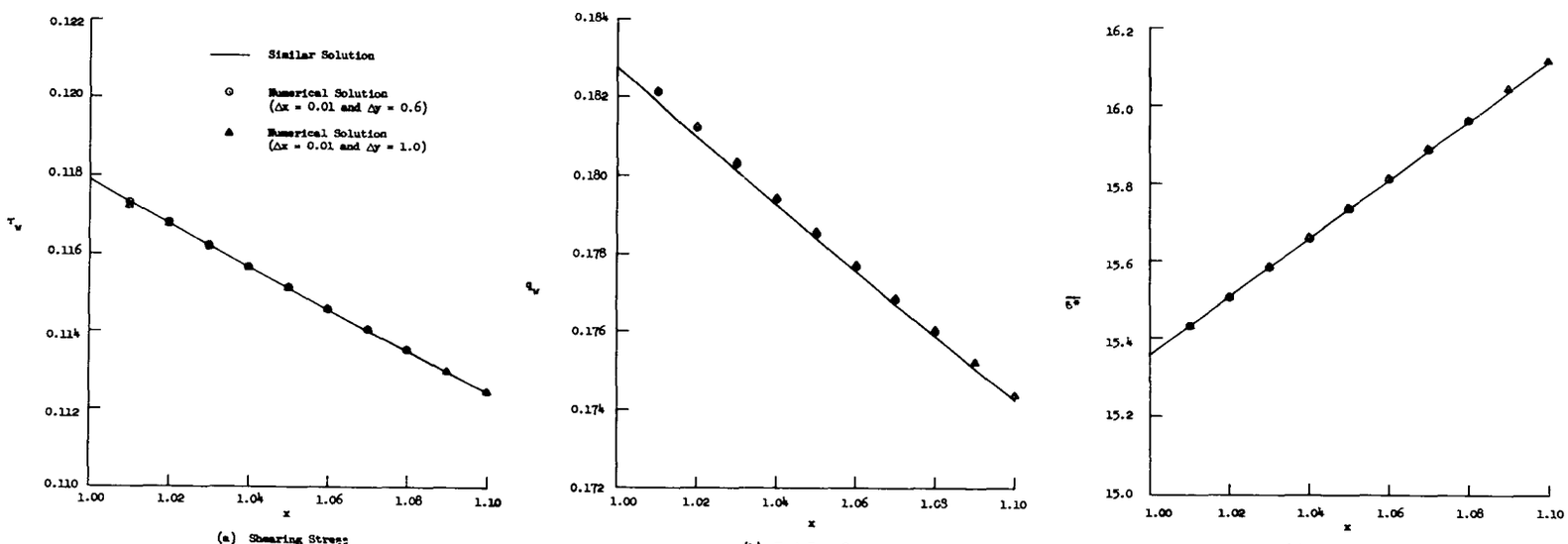

Figure 6. Influence of Δy on Flat Plate Boundary-Layer Characteristics ($M_\infty = 3$ and $T_w/T_{ad} = 2$)

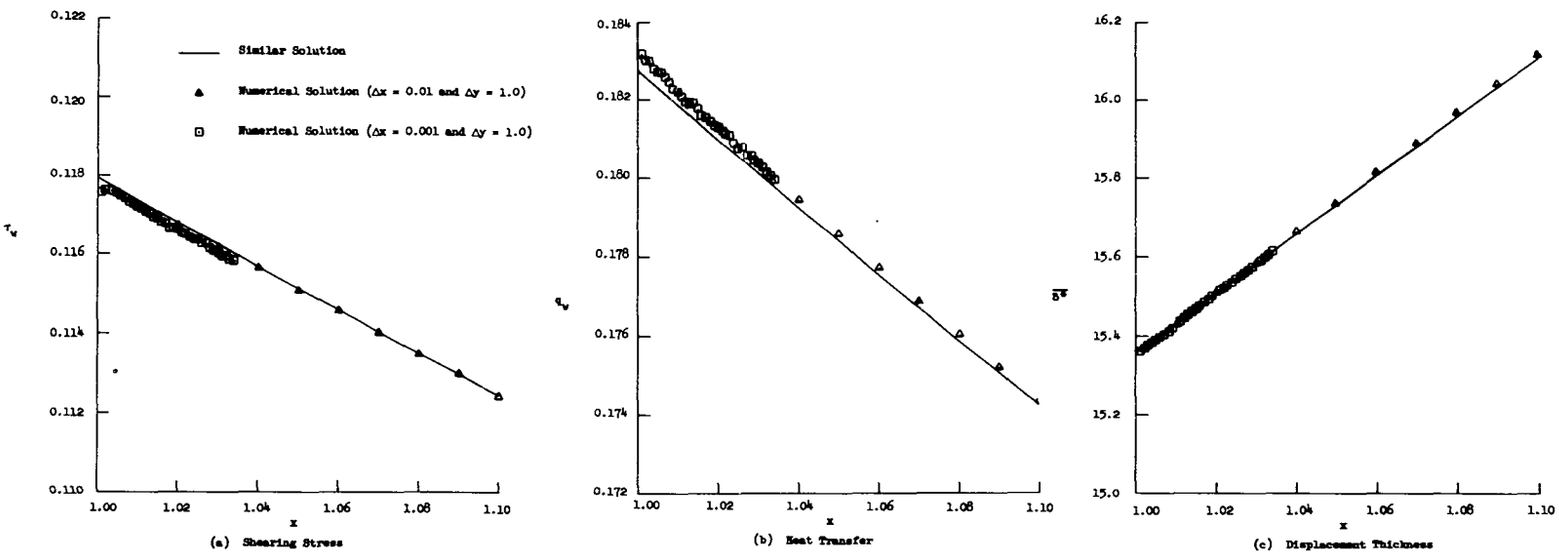

Figure 7. Influence of Δx on Flat Plate Boundary-Layer Characteristics ($M_\infty = 3$ and $T_w/T_{ad} = 2$)

$L^{(1)}_{m,1}$, $L^{(2)}_{m,1}$, $L^{(3)}_{m,1}$, due to this boundary condition, are given in equation (3.30). For the case of zero heat transfer, this boundary condition gives the following results:

$$i_{m,1} = i_{m,2} \tag{4.3a}$$

$$L^{(1)}_{m,1} = 0 \tag{4.3b}$$

$$L^{(2)}_{m,1} = 0 \tag{4.3c}$$

$$L^{(3)}_{m,1} = 1 \tag{4.3d}$$

As previously mentioned, the derivative in the boundary condition (3.22d) has been replaced by a rather crude approximation. By using two mesh points beyond the wall in writing the difference quotient, a better approximation for the derivative is obtained. For an insulated wall the following relation results:

$$i_{m,1} = \frac{4}{3} i_{m,2} - \frac{1}{3} i_{m,3} \tag{4.4}$$

If n is set equal to two and $u_{m,1}$ is set equal to zero (boundary condition 3.22b) in equations 3.7 and 3.8, then $u_{m,3}$ can be eliminated from the two resulting equations. As a result of these operations, the following equation is obtained :

$$(B_1C_2 - B_2C_1)_{m,2}\, u_{m,2} + (D_1C_2 - D_2C_1)_{m,2}\, i_{m,1} + (E_1C_2 - E_2C_1)_{m,2}\, i_{m,2} + (F_1C_2 - F_2C_1)_{m,2}\, i_{m,3} = (G_1C_2 - G_2C_1)_{m,2} \tag{4.5}$$

Substituting equation (4.4) into the above equation (4.5) and rearranging gives:

$$[3(F_1C_2 - F_2C_1) - (D_1C_2 - D_2C_1)]_{m,2}\, i_{m,1} = (G_2C_1 - G_1C_2)_{m,2} + (B_1C_2 - D_2C_1)_{m,2}\, u_{m,2} + [(E_1C_2 - E_2C_1) + 4(F_1C_2 - F_2C_1)]_{m,2}\, i_{m,2} \tag{4.6}$$

By comparing coefficients in the above equation with equation (3.26b), the following is obtained:

$$L_{m,1}^{(1)} = \Delta_1 \, (G_2C_1 - G_1C_2)_{m,2} \tag{4.7a}$$

$$L_{m,1}^{(2)} = \Delta_1 \, (B_1C_2 - B_2C_1)_{m,2} \tag{4.7b}$$

$$L_{m,1}^{(3)} = \Delta_1 \, [(E_1C_2 - E_2C_1) + 4(F_1C_2 - F_2C_1)]_{m,2} \tag{4.7c}$$

where

$$1/\Delta_1 = [3(F_1C_2 - F_2C_1) - (D_1C_2 - D_2C_1)]_{m,2}$$

The flow along an insulated flat plate has been solved using the different boundary conditions (4.3) and (4.7). In Figure 8 the wall enthalpy is shown when the two different boundary conditions are used, and the similarity result is also shown. The profiles across the boundary layer at $x = 1.10$ are shown in Figure 9. The numerical solution with boundary conditions (4.7) are compared with the similar solution in this figure. The boundary-layer characteristics for the insulated flat plate are presented in Figure 10. The numerical results with the two different boundary conditions are compared with the similar solutions in this figure. From these results it is apparent that boundary conditions 4.3 are indeed crude. Therefore, to approximate the enthalpy gradient at the wall it is necessary to use at least three grid points as was done for the boundary conditions (4.7).

3. Ramp Pressure Gradient. In order to investigate the influence of the boundary-layer pressure gradient term on the numerical solution, the flow along a wall with a constant wall temperature and a ramp pressure gradient is considered. This problem has been solved by Baxter and Flügge-Lotz (Ref. 1), using an explicit finite-difference scheme with the Crocco transformed boundary-layer equations. The fluid properties, exterior flow, and wall quantities are the same as the first example and are given in relations (4.1). Since Baxter uses Sutherland's viscosity law (Eq. 2.22), it is also used in this example. The pressure and pressure gradient are the following

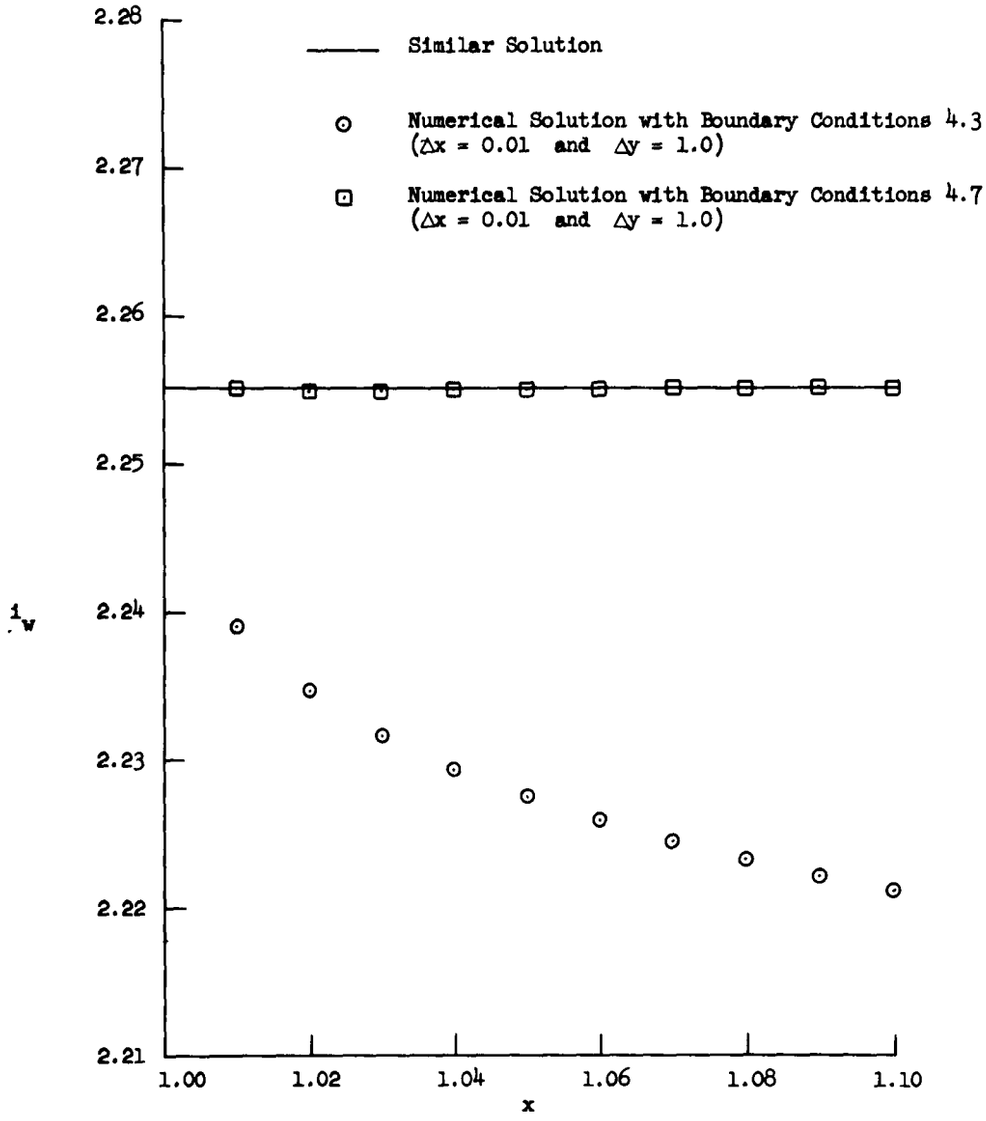

Figure 8. Wall Enthalpy for Insulated Flat Plate (M_∞ = 3.0)

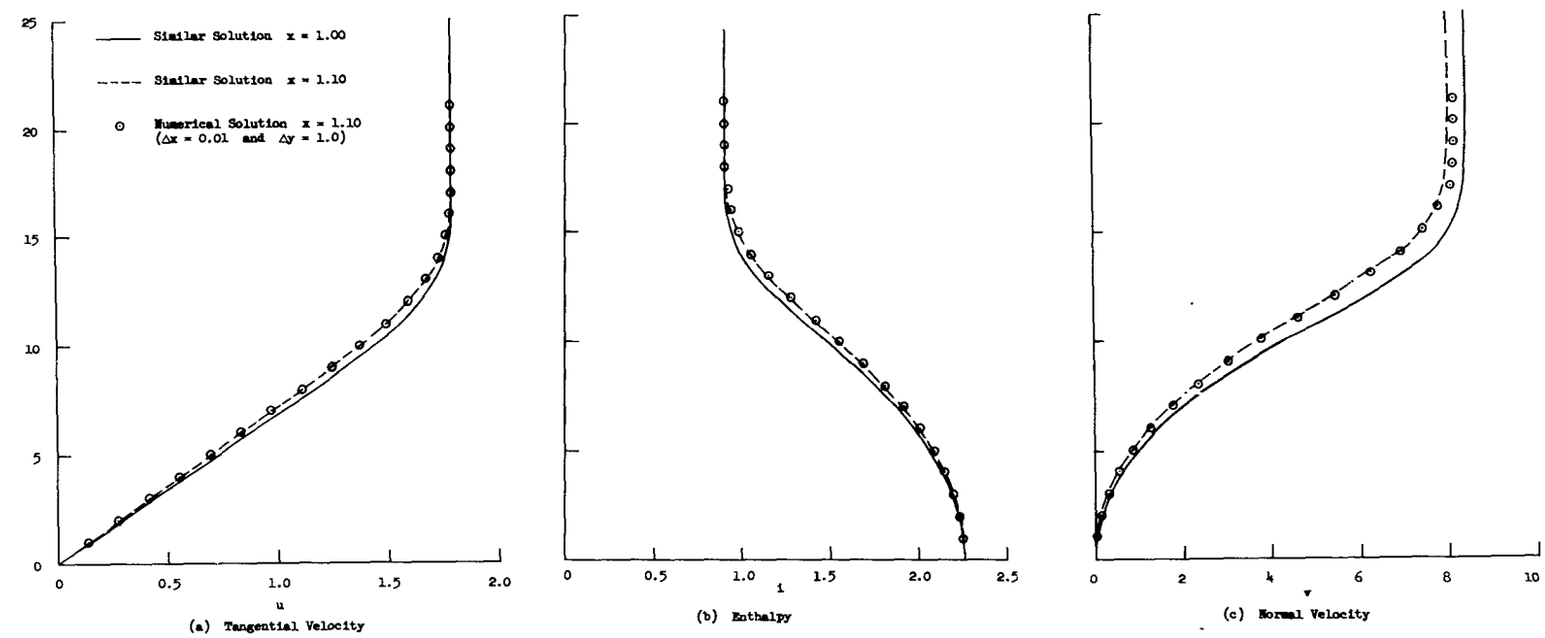

Figure 9. Insulated Flat Plate Profiles (M_∞ = 3 and Boundary Conditions 4.7)

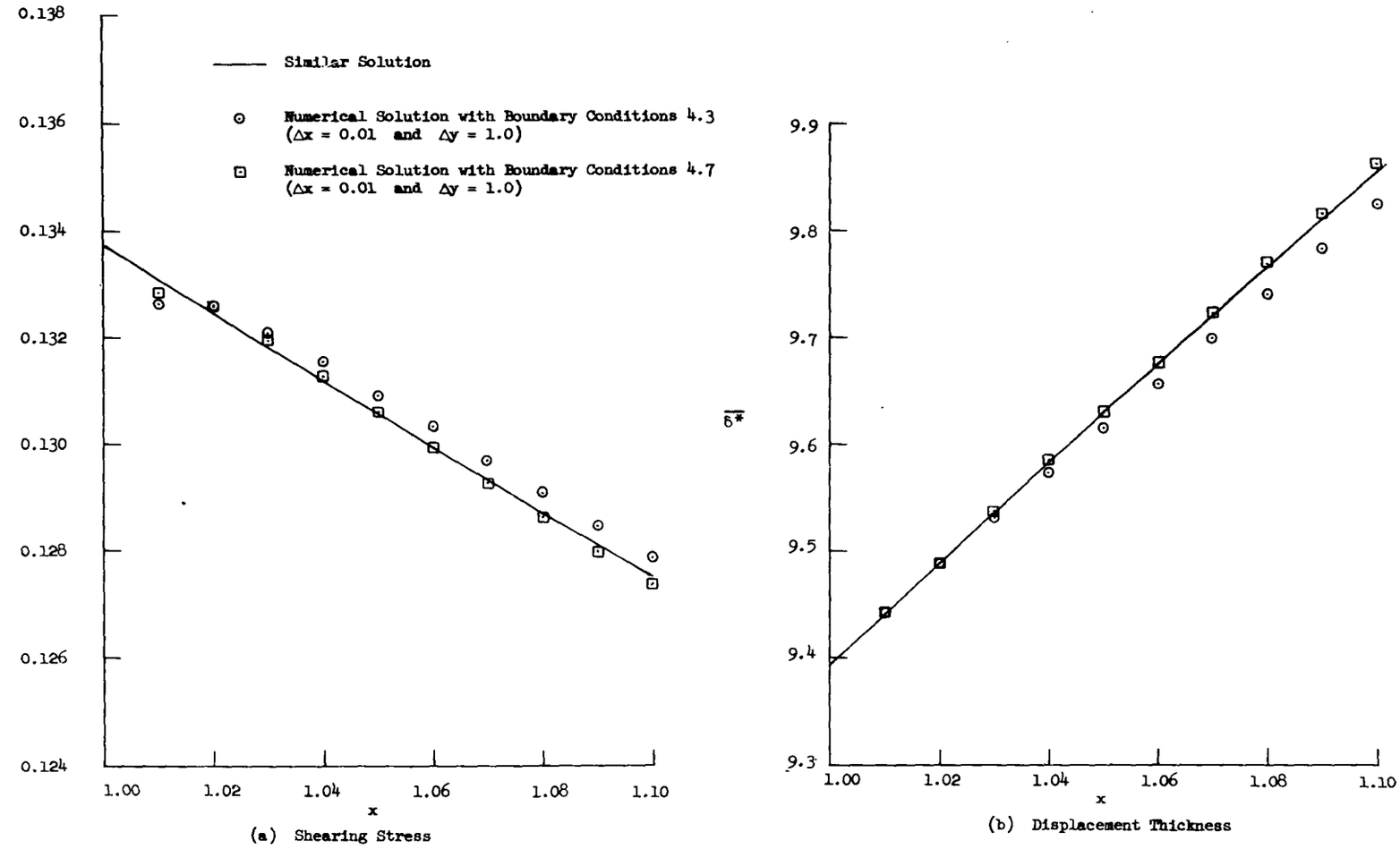

(a) Shearing Stress

(b) Displacement Thickness

Figure 10. Insulated Flat Plate Boundary-Layer Characteristics ($M_\infty = 3$)

$$p_e = p_\infty + \frac{5}{2}(x - 1)^2 \rho_\infty u_\infty^2 \qquad (x \geq 1) \qquad (4.8a)$$

$$p_e' = 5 (x - 1) \rho_\infty u_\infty^2 \qquad (x \geq 1) \qquad (4.8b)$$

for the ramp pressure gradient case. Flow along a flat plate is assumed upstream of $x = 1$, and the initial profiles given in Figure 5 are used to start the calculations. Rather than use equation (2.40), the small-disturbance form of this equation was used. The simpler equation is:

$$u_e = u_\infty \left[1 - \frac{1}{\gamma M_\infty^2} (p_e/p_\infty - 1) \right] \qquad (4.9)$$

In the finite-difference solution $\Delta y = 1.0$ and $\Delta x = 0.001$ or 0.0004. The latter value of the step-size was used by Baxter in order to have a stable numerical solution. The parameter ϵ used in testing for the edge of the boundary was increased to 10^{-4} for this example.

The boundary-layer characteristics for a ramp pressure gradient are given in Figure 11. The shearing stress parameter was obtained from equations (2.47) and (3.48a), while the heat transfer parameter was obtained from equations (2.50) and (3.49a). The displacement thickness parameter is the ratio of the dimensionless displacement thickness at any x to the value at $x = 1.0$. The displacement thickness is obtained from formula (3.50a). The step-size must be the same size ($\Delta x = 0.0004$) as used by Baxter in order to have reasonable agreement with his results. Since the boundary-layer profiles are changing very rapidly, the truncation error is more important than stability considerations in determining the step-size. As the truncation error in Baxter's and the present method are of the same order, it is not surprising that the required step-sizes are approximately the same for this example.

It should be remembered that the initial profiles are based upon a linear viscosity law, while the numerical results use Sutherland's viscosity law. Near the start of the computation of the boundary-layer characteristics, the influence of changing the viscosity law can be seen in Figure 11.

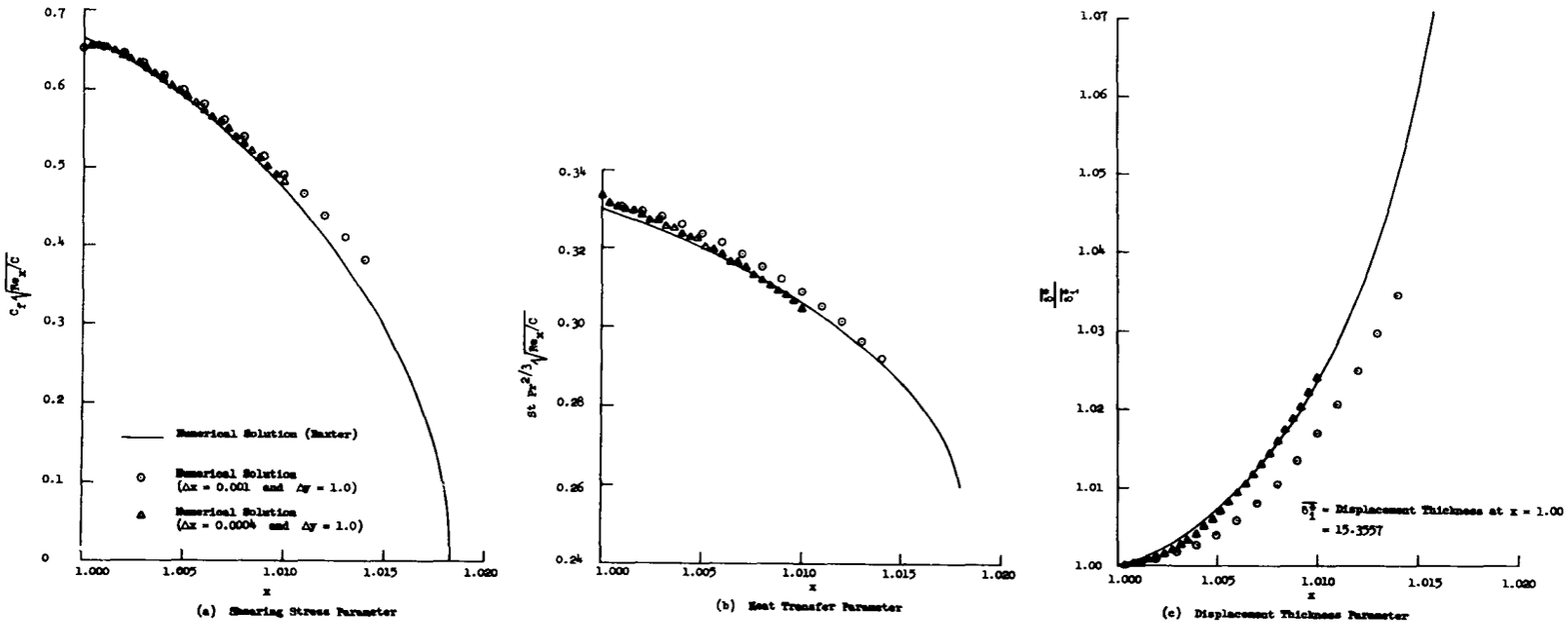

Figure 11. Ramp Pressure Gradient Boundary-Layer Characteristics ($M_\infty = 3$ and $T_w/T_{ad} = 2$)

4. Flat Plate Flow With Sutherland's Viscosity Law. In example 3 the initial profiles were based upon a linear viscosity law, while the numerical computation used Sutherland's viscosity law. In order to investigate the influence of such a procedure on the boundary-layer characteristics, example 1 is solved again using Sutherland's viscosity law.

In Figure 12 the variation of viscosity with enthalpy for the two viscosity laws is illustrated. For a heated wall and large Mach number the linear viscosity law becomes a poor approximation for the more exact Sutherland's law.

The boundary-layer characteristics for this example are given in Figure 13. The results for the similar solution with a linear viscosity law are from Low (Ref. 26), while those with Sutherland's viscosity law are from Van Driest (Ref. 40). Two step-sizes were used in the numerical computations and these results are presented in this figure. The boundary-layer characteristics which are obtained from the numerical solution with Sutherland's viscosity law tend to approach the similar solution from Van Driest. The computations with the small step-size seem to be approaching the results of Van Driest faster than the other numerical solution. As this type of problem is considered again in Section B example 1 of this chapter (See Figure 20), the computations have not been extended further downstream.

5. Flow Near the Leading Edge of a Flat Plate. This example considers the flow near the leading edge of a flat plate when the free-stream Mach number is 9.6. The linear viscosity law is used so that the results can be compared to the similar solution easily obtained from Low (Ref. 26). The following fluid properties, exterior flow, and wall quantity, are assumed:

$$M_\infty = 9.6 \tag{4.10a}$$

$$T_\infty^* = 82.34^\circ R \tag{4.10b}$$

$$\gamma = 1.4 \tag{4.10c}$$

$$Pr = 0.72 \tag{4.10d}$$

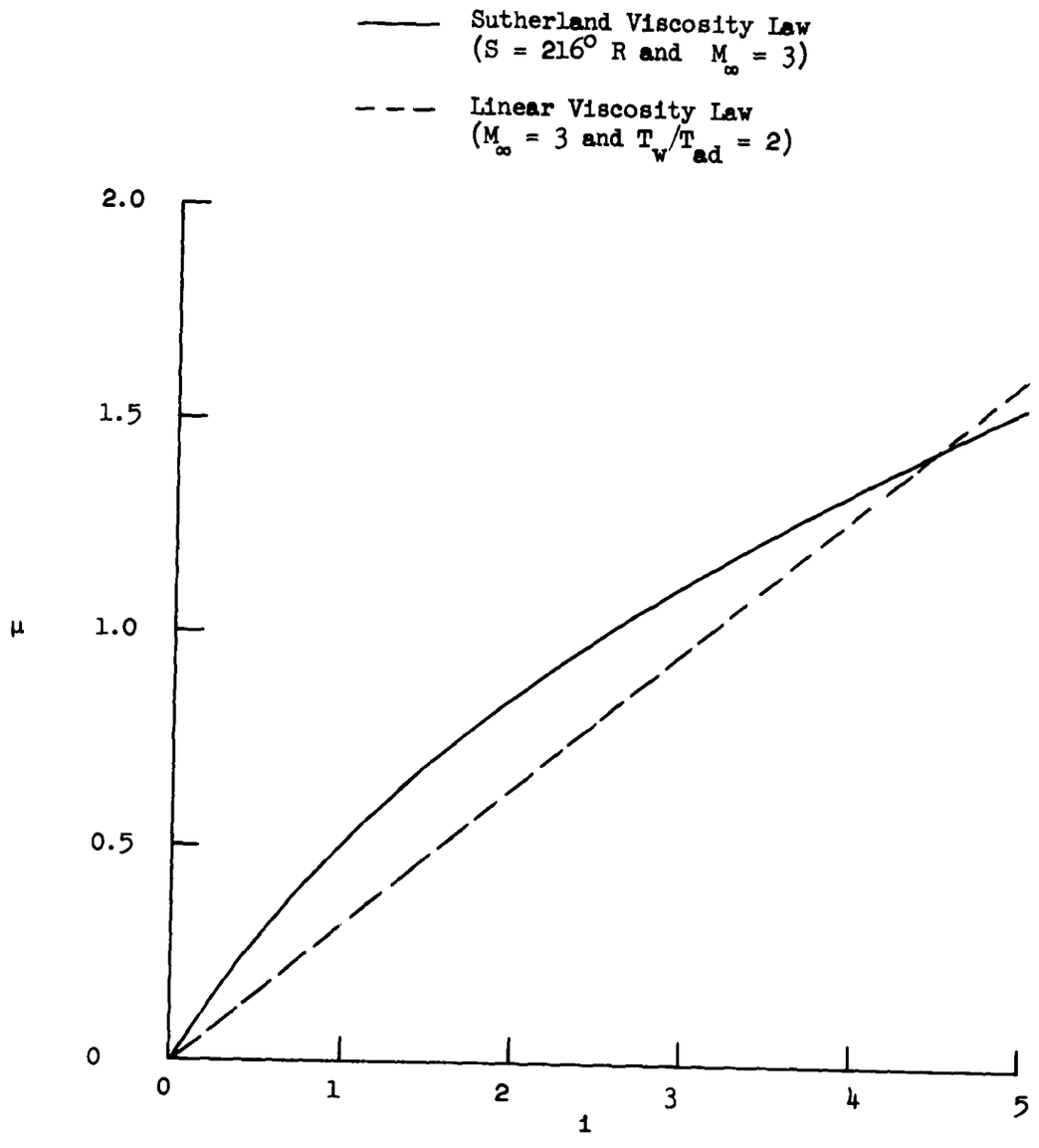

Figure 12. Viscosity Laws

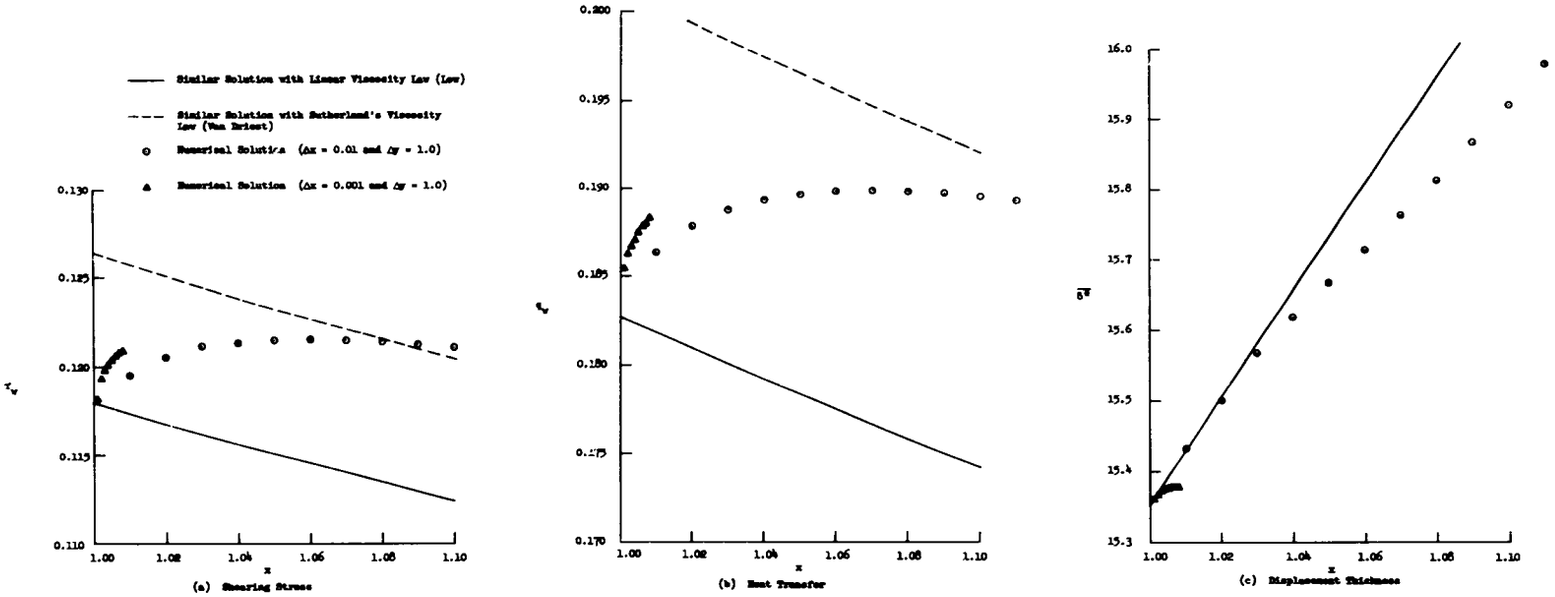

Figure 13. Influence of Viscosity Law on Boundary-Layer Characteristics

$$S^* = 198.6^\circ \text{ R} \qquad (4.10e)$$

$$T_w/T_{ad} = 1 \qquad (4.10f)$$

The wall temperature is specified by equation (4.10f) such that there is no heat transfer in this example. The pressure distribution is still given by equations (4.2) since this is flow along a flat plate. The initial profiles are obtained from equations (3.31a - 3.31d) and are shown in Figure 14. In this problem the test for the edge of the boundary layer uses $\epsilon = 10^{-4}$.

In this problem the initial profiles are taken at $x_i = 0.01$ and the calculations proceed to $x = 0.10$. This is equivalent to starting at $x_i = 1.00$ as done in example 1 (Section A.1) but continuing the computations until $x = 10.00$. Therefore a relatively large step-size is required if the finite-difference scheme is going to be of any practical value in this example.

Two step-sizes have been used to solve this problem and the boundary-layer displacement thickness is used to illustrate the resulting solutions in Figure 15. The similar solution is shown in this figure also. This figure shows that the grid size is too large and hence the truncation error has significant influence on the results. As the grid size Δx is reduced, the solution appears to be converging to the similar solution. When the numerical solution is to be sufficiently accurate, the required grid size would become prohibitively small.

Another factor has been introduced which requires the grid size to be small in this problem. In order to approximate the profiles as shown in Figure 14 with sufficient accuracy, it is necessary to have a small grid size Δy near the outer edge of the boundary layer. Shown in this figure is the numerical and similar solution at one step downstream from the initial profiles. The numerical solution is greatly different from the similar solution near the outer edge of the boundary layer.

The problem of reducing the truncation error and of increasing the step-size near the outer edge of the boundary layer requires going to Implicit Method II.

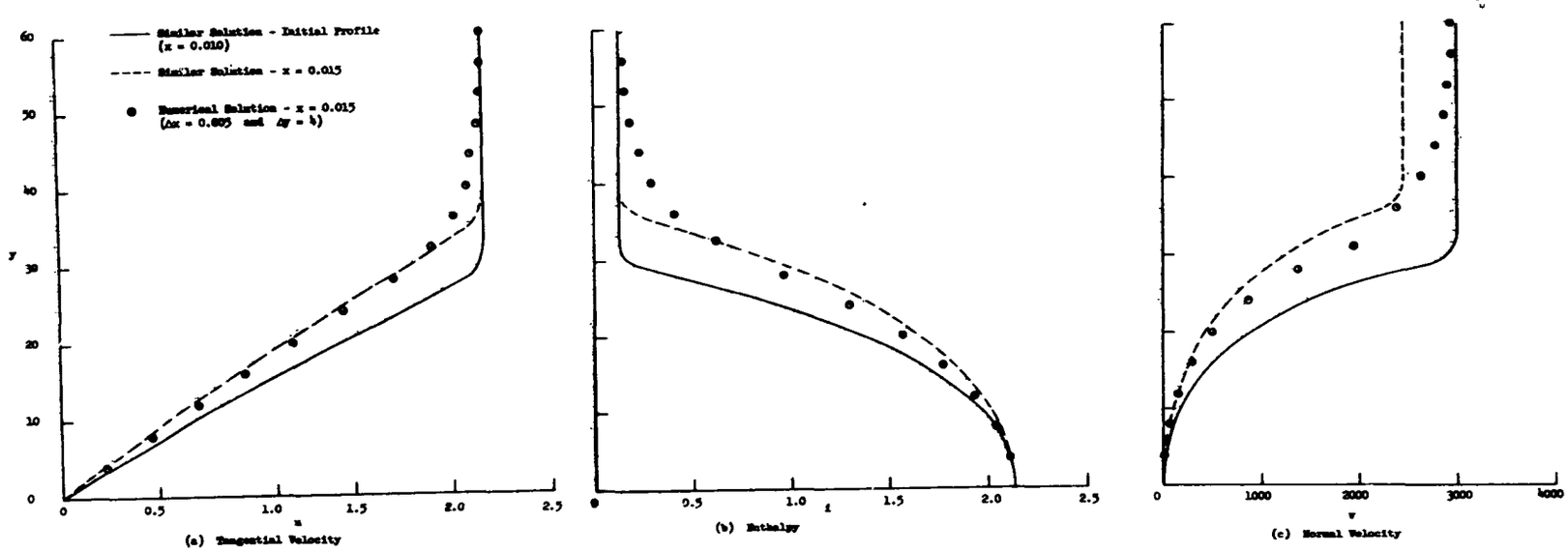

Figure 14. Profiles for the Flow Near the Leading Edge of a Flat Plate ($M_\infty = 9.6$)

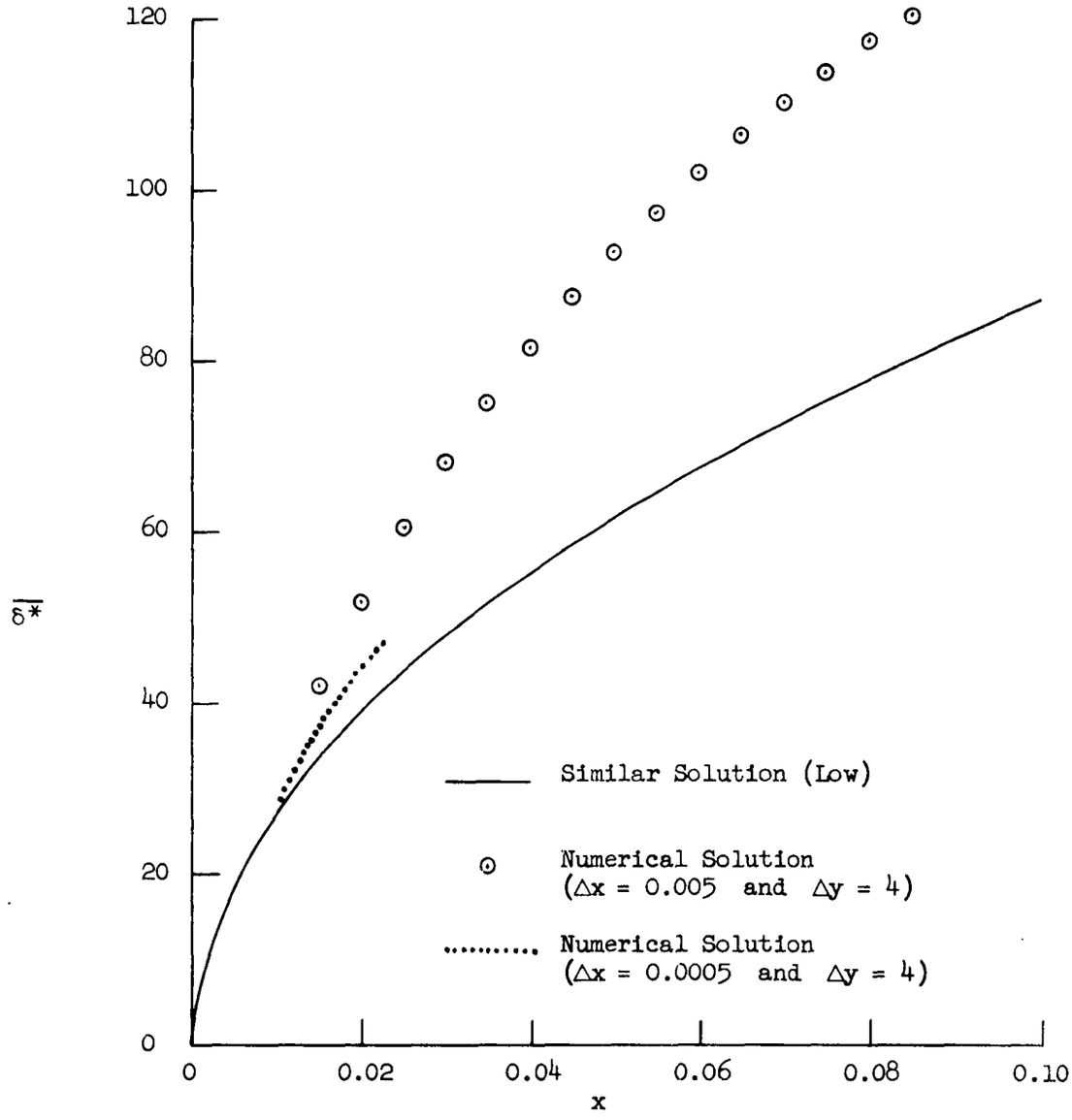

Figure 15. Displacement Thickness for the Flow Near the Leading Edge of a Flat Plate ($M_\infty = 9.6$)

B. Implicit Method II

Three examples were solved with a Burroughs 220 computer using Implicit Method II, which solves the boundary-layer equations in the transformed plane. The first example is the same as the last case considered in the previous section. This example illustrates that Method II has a much smaller truncation error than Method I. Other effects studied in this example are: the two methods of replacing the continuity equation, integration formula for the displacement thickness, value of ϵ for test at edge of boundary layer, iteration of the solution at each step downstream, and type of viscosity law. In the second example the flow downstream of a transpiration cooled region is investigated. The wall in the region of interest has $i_w/i_{ad} = 0.5$. This problem and the insulated wall case have been solved by Howe (Ref. 17) using the numerical method of Baxter and Flügge-Lotz (Ref. 1). The insulated wall case has been solved by Pallone (Ref. 34) with another numerical method. This example allows an indirect comparison between these numerical methods for solving the boundary-layer equations. The third example illustrates that the implicit method can be used to solve the boundary-layer flow along a wall with a variable temperature. The specific case considered is a wall with a "hot spot" as this problem has been solved by Baxter and Flügge-Lotz (Ref. 1).

1. Flow Near the Leading Edge of a Flat Plate. The same problem as given in Section A.5 of this chapter is now investigated. The displacement thickness of the boundary layer is used to illustrate the influences of several parameters in Figure 16. In all parts of the figure the similar solution of the boundary-layer equations is given to indicate the desired result. In part (a) the result using Implicit Method I for this problem as given in Section A.5 is presented for convenience. Also in this part of the figure the displacement thickness is shown for the case when the problem is solved in the physical plane but with the difference quotients used in Implicit Method II. By using the new difference quotients, the truncation error has been greatly reduced. However, when the profiles are examined for this solution, the numerical result still has some error near the outer edge.

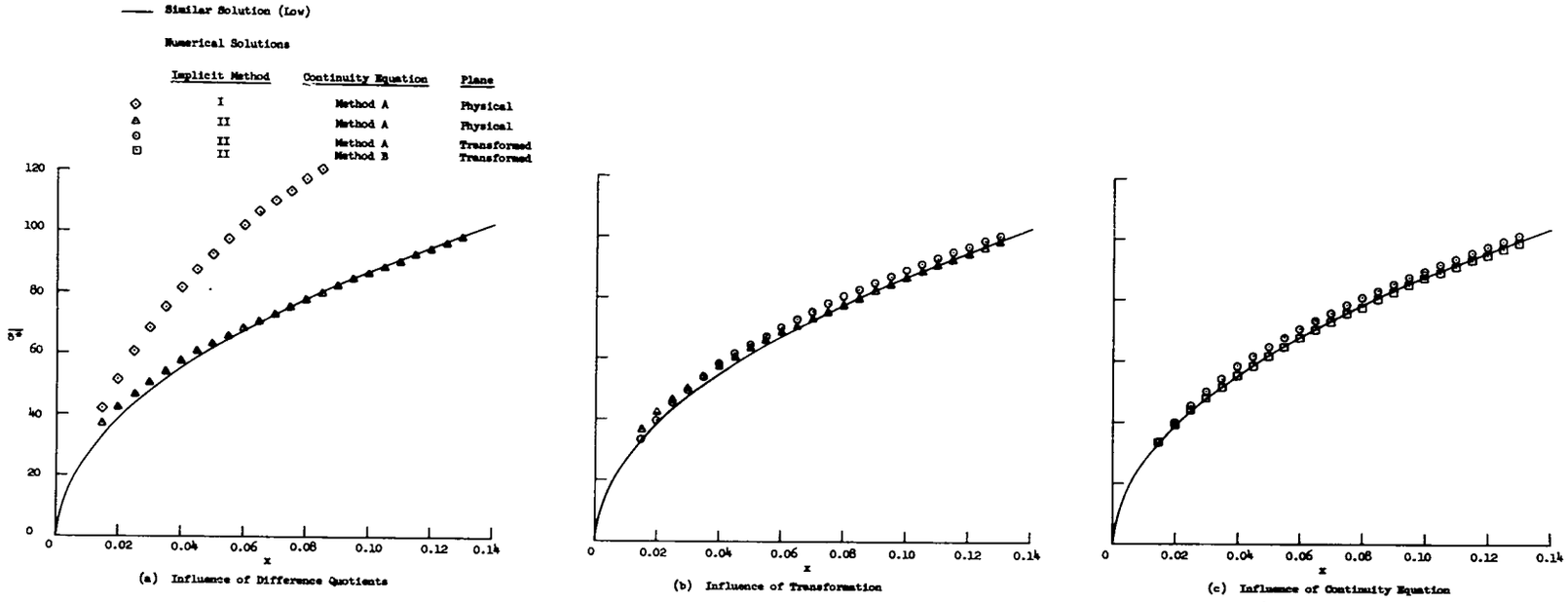

Figure 16. Displacement Thickness for the Flow Near the Leading Edge of a Flat Plate ($M_\infty = 9.6$)

In Figure 16b the influence of transforming the boundary-layer equations is illustrated. The displacement thickness, as a result of solving these transformed equations, does not seem to be improved. This numerical solution does approximate the similar solution profiles closer than the physical plane solution, especially near the outer edge. It should be remembered that all solutions have used Method A for the continuity equation. In Figure 16c the influence of using the two methods of replacing the continuity equation is shown. When Method B is used with Implicit Method II the best numerical solution of the displacement thickness is obtained. For this case the numerical profiles are a good approximation for the similar solution results.

Several other items that have a smaller influence on the solution of this problem have been investigated. In order to illustrate the influence of these items, the displacement thickness is divided by the similar solution displacement thickness at the corresponding value of x. This displacement thickness ratio is given in Figure 17 for the various cases studied. The numerical values have been connected by straight lines to clarify the figure. The first item investigated was the influence of the integration formula used in evaluating the displacement thickness. The displacement thicknesses computed, using the trapezoidal rule (Eq. 3.50b) and Simpson's rule (Eq. 3.50c), give essentially the same result for this problem. Since Simpson's rule is a better formula in general and is only slightly more complicated than the trapezoidal rule, Simpson's rule is used with Implicit Method II. The influence of ϵ on the displacement thickness ratio is shown in Figure 17. From this figure it is impossible to ascertain the better value of ϵ to use. To study the effect of ϵ further, the velocity profile near the outer edge is given in Figure 18. This figure gives the velocity profile at $x = 0.125$ for the numerical solution with two values of ϵ and the similar solution is also given. This figure shows that the smaller value of ϵ results in a velocity profile which is a better approximation to the similar solution.

Returning to Figure 17, another item that has been investigated is the effect of iterating Implicit Method II at each downstream step. In order to obtain linear difference equations certain quantities at

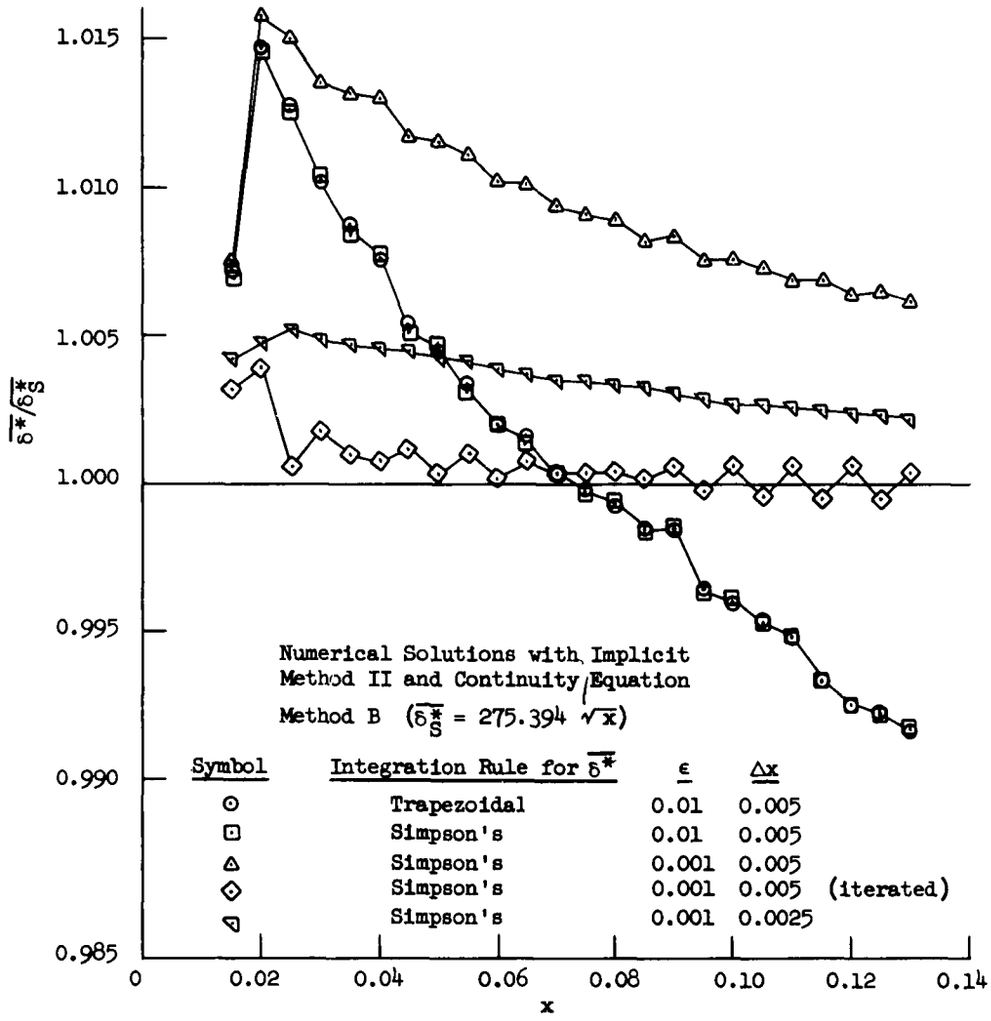

Figure 17. Displacement Thickness Ratio for the Flow Near the Leading Edge of a Flat Plate ($M_\infty = 9.6$)

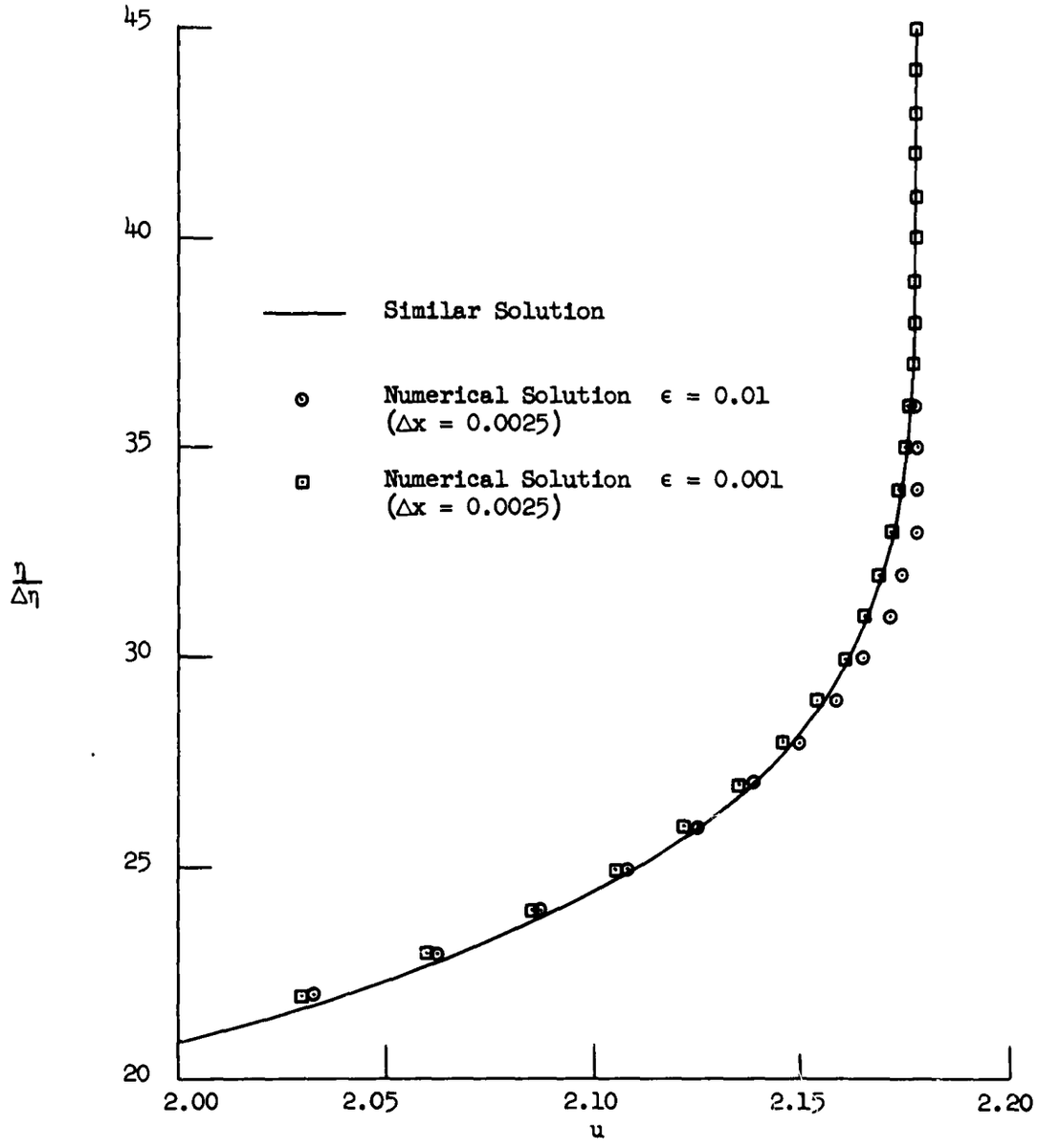

Figure 18. Velocity Profile Near Outer Edge of Boundary Layer for Two Values of ϵ (x = 0.125)

$(m + \frac{1}{2})$ were replaced by known quantities at m. (See Chapter III, Section B.2). After the boundary-layer equations are solved as usual for the unknown quantities at $(m + 1)$, the equations are resolved with the quantities at $(m + \frac{1}{2})$ replaced by the average of the corresponding quantities at (m) and $(m + 1)$. By iterating in such a manner, the truncation error should be reduced. This is the case as illustrated in Figure 17 where the solution was iterated once at each step. Since this iteration almost doubles the computation time, it would be equivalent to halving the step-size downstream. The results for the displacement thickness ratio for this smaller step-size are given in Figure 17. Although this result is closer to the similar solution than previous cases considered, it is not as close as the iterated solution. However, the iterated method has a small oscillation that does not occur when the usual method is used.

The comparison between Implicit Method II (Transformed Plane) and the similar solution is now completed by considering profiles and shearing stress at the wall. For this comparison the results are obtained by using continuity equation Method B with $\epsilon = 0.001$, $\Delta x = 0.0025$, and $\Delta\eta = 0.00023288$.[1] The initial profiles in the transformed plane are given in Figure 19 and are obtained from equations (3.33). The numerical and similar profiles at $x = 0.125$ are shown in this figure. The two velocity and enthalpy profiles obtained by both methods agree, as expected from the displacement thickness results. In Figure 20 the shearing stress at the wall from the numerical solution is given. This was obtained from equation (3.48b). The shearing stress from the similar solution with linear viscosity (Ref. 26) is presented in this figure for comparison with the numerical solution. Since the initial profiles for the numerical computation were determined with a linear viscosity law, the same law is normally used in the numerical computations. Here, however, the numerical solution has been performed with Sutherland's viscosity law and the result for the shearing stress is shown in Figure 20a. The skin-friction parameter for this example

[1] This number for $\Delta\eta$ occurs as $\Delta\eta_{Low}$ is taken as a convenient value in determining the initial profiles from equations (3.33).

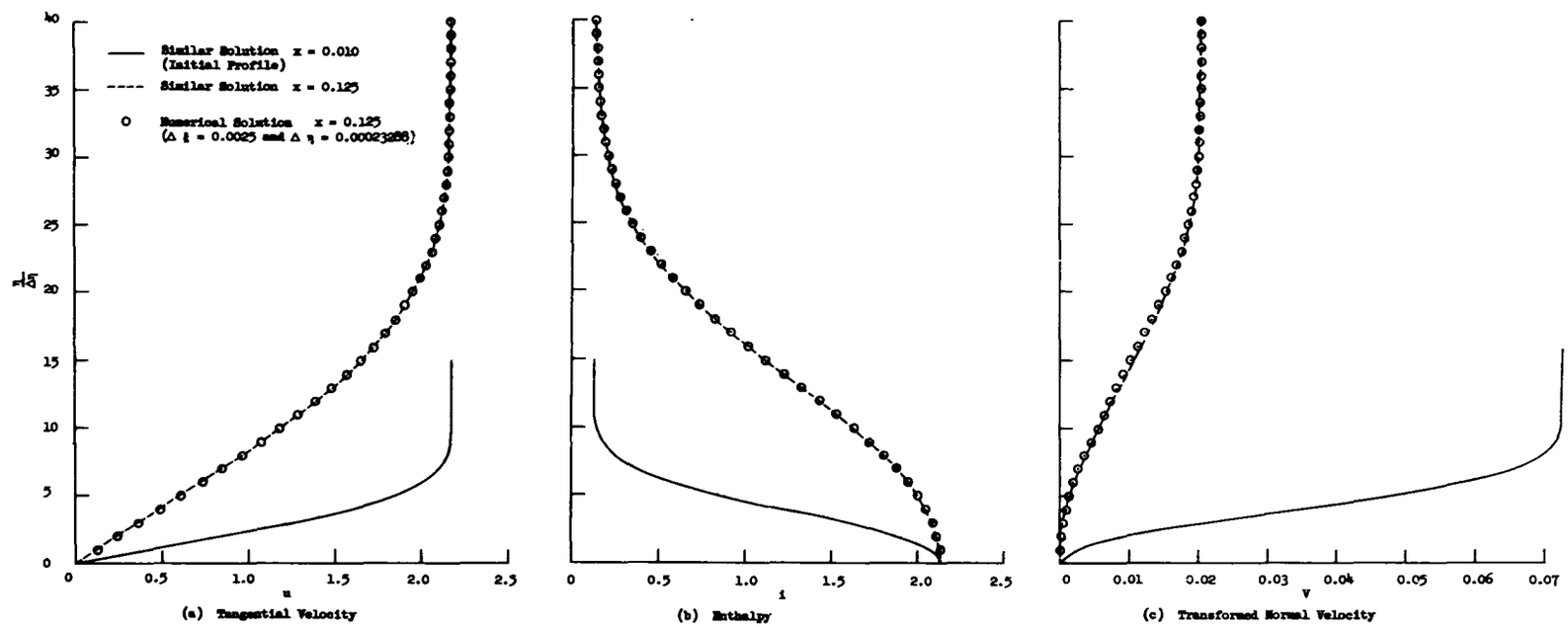

Figure 19. Boundary-Layer Profiles for the Flow Near the Leading Edge of a Flat Plate ($M_\infty = 9.6$)

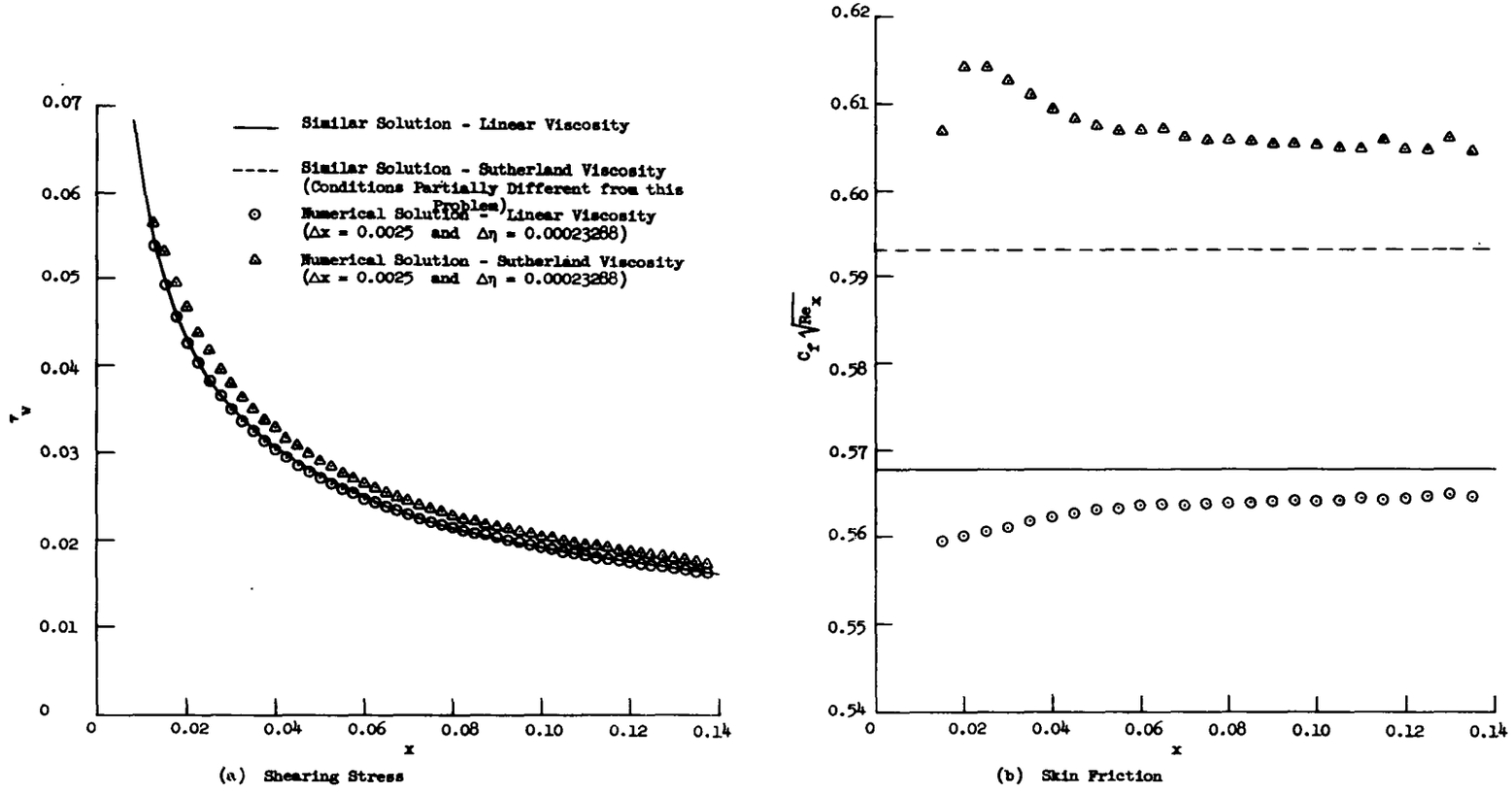

Figure 20. Shearing Stress and Skin Friction for the Flow Near the Leading Edge of a Flat Plate ($M_\infty = 9.6$)

is given in Figure 20b. The numerical solutions obtained with the linear and Sutherland's viscosity law are shown. In addition the skin-friction parameter, as obtained from similar solutions for the two viscosity laws, is given. The similar solution result with a linear viscosity law is obtained from Low (Ref. 26), while the result with Sutherland's law is obtained from Young and Janssen (Ref. 43). The latter result is not obtained using the same conditions as the numerical solution. The skin-friction parameter obtained from Young and Janssen was determined with the following different conditions: $T_\infty^* = 100^\circ R$, $M_\infty = 9.57$, and variable Prandtl number. (See equations 4.10 for conditions in present problem.) For the case with a linear viscosity law, the larger error near the start can be attributed to the relatively large grid size in this region. When Sutherland's viscosity law is employed, the skin-friction parameter near the start is over corrected as a result of the error introduced by the initial profiles. The skin-friction parameter then becomes nearly constant but at a slightly higher value than the similar solution. Some of this difference can be accounted for by the different conditions employed in the two problems. The heat transfer for this case is not presented since it is approximately zero as the wall temperature was specified to correspond to an insulated wall.

2. Flow Downstream of a Transpiration Cooled Region. This example is concerned with the flow downstream of a transpiration cooled region. The flow conditions, fluid properties, and wall condition are the following:

$$M_\infty = 3 \tag{4.11a}$$

$$T_\infty^* = 389.99^\circ \text{ R} \tag{4.11b}$$

$$\gamma = 1.4 \tag{4.11c}$$

$$Pr = 0.72 \tag{4.11d}$$

$$S^* = 216^\circ \text{ R} \tag{4.11e}$$

$$T_w/T_{ad} = 0.5 \tag{4.11f}$$

The wall for this case is taken as a flat plate; hence, the pressure gradient is zero. The injection region extends from the leading edge to $x = 1.0$ and is such that the boundary-layer flow is described by the similar solutions of Low (Ref. 27). Hence, the injection velocity at the wall, v_w, varies parabolically from the leading edge. The initial profiles are obtained from equations (3.33). The f and g functions are evaluated with $f(0) = -\frac{2}{\sqrt{C}} (\rho_w v_w / \rho_\infty u_\infty) \sqrt{\rho_\infty u_\infty x/\mu_\infty} = -1.0$ from Low (Ref. 27). The initial profiles are based upon a linear viscosity law and are presented in Figure 21. At the wall the transformed normal velocity V is not zero for the initial profile as shown in Figure 21c. Since the wall is solid downstream of $x = 1.0$, the velocity V is zero for $x > 1.0$. In the test for the edge of the boundary layer in the numerical computations, $\epsilon = 10^{-3}$. The viscosity law used in these computations is indicated when the results are presented.

In Figure 21 the boundary-layer profiles for a linear viscosity law are presented at $x = 2.00$ where the numerical computations were terminated. There is very little change in the thickness of the boundary layer in the transformed plane. However, there has been an appreciable change in the shape of the profiles. The quantity ρv is presented in Figure 21c as it has a more physical significance while V does not.

The skin-friction ratio has been employed to illustrate the solution of the boundary-layer equation for various conditions in this problem. The skin-friction ratio is obtained by dividing the local skin-friction coefficient by the following flat-plate value based upon a linear viscosity law:

$$(C_f)_{f(0) = 0} = 0.6641 \sqrt{C/Re_x} \qquad (4.12)$$

The skin-friction ratio obtained from Implicit Method II with several step-sizes of Δx is presented in Figure 22a. As the step-size Δx is decreased, the truncation error should be reduced and the numerical solution should be a closer approximation to the exact solution (see Ref. 32). When $\Delta x = 0.004$, the results indicate that the truncation

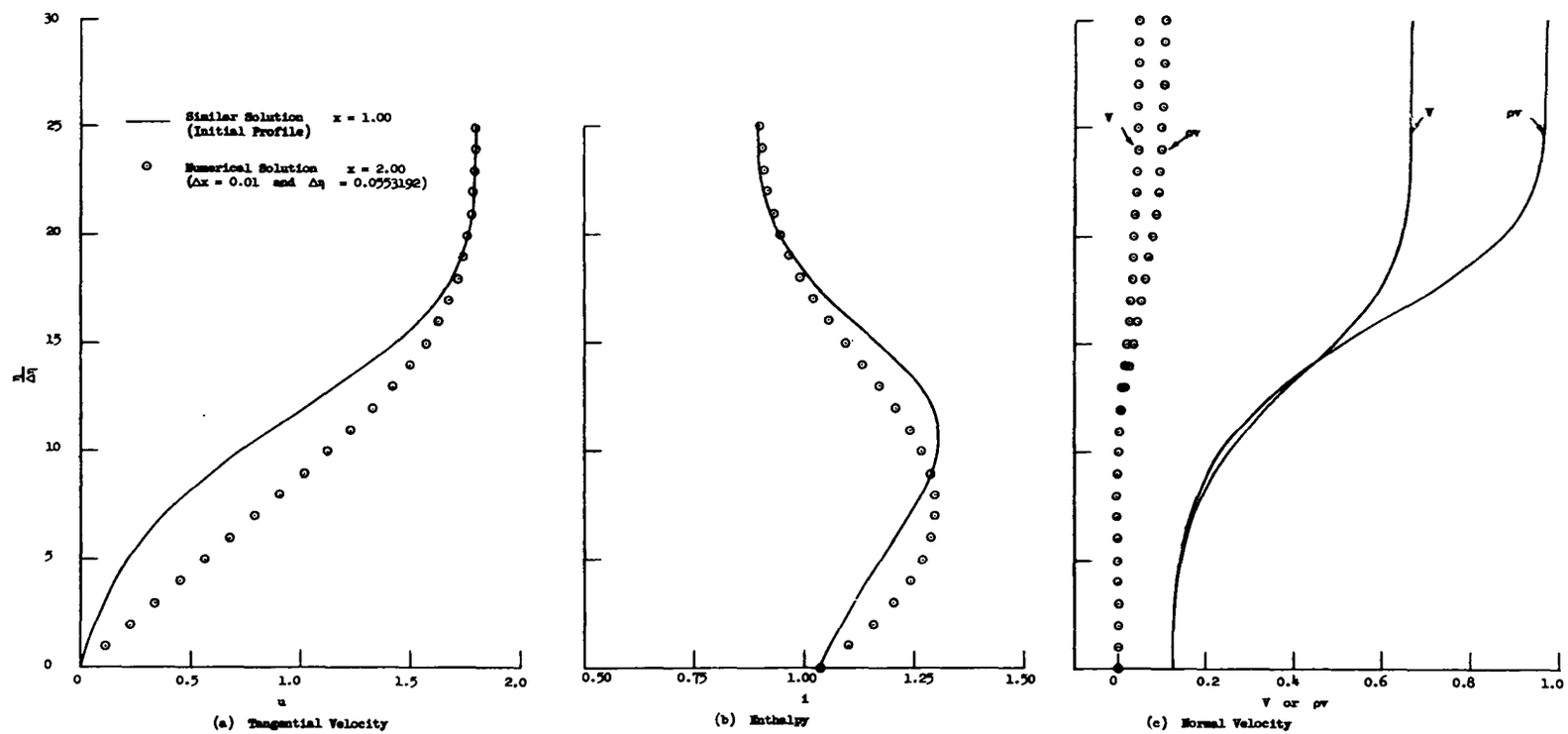

Figure 21. Boundary-Layer Profiles for Flow Downstream of Transpiration Cooled Region - Linear Viscosity Law

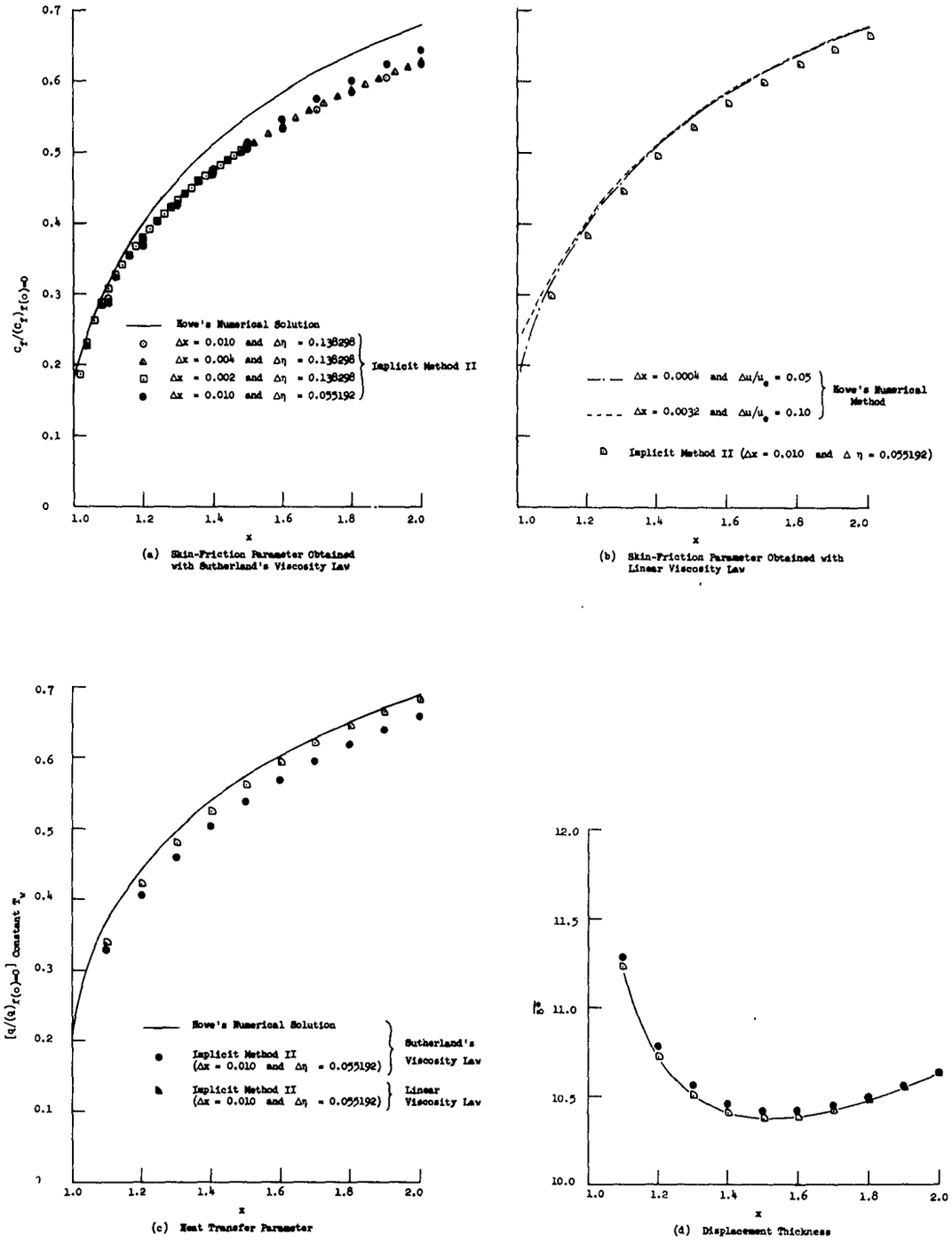

Figure 22. Boundary-Layer Characteristics for Flow Downstream of Transpiration Cooled Region

error attributed to Δx is reasonably small. The step-size across the boundary layer has been varied also. For the two values of $\Delta \eta$ there is an appreciable change in the skin-friction ratio. However, the truncation error due to $\Delta \eta$ is small for the smaller step-size across the boundary layer. It has been estimated that the result for the case when $\Delta x = 0.01$ and $\Delta \eta = 0.055192$ will change about 1 percent near $x = 2.0$ as the grid size goes to zero. In Figure 22a the numerical solution by Howe, which uses the Flügge-Lotz and Baxter method as given in Ref. 10, is presented. This result is based upon Sutherland's viscosity law and the same conditions (4.11) are used in this example. These two methods give results within 5 percent, which is very good in comparison to other approximate methods for solving this problem as discussed by Howe (Ref. 17). However, one would expect the results to be even closer as the methods should be close to the exact solution if the step-size is sufficiently small.

Since the initial profiles in this problem are determined using a linear viscosity law, this problem has been solved with the same law to eliminate any initial error. The result for the skin-friction ratio is given in Figure 22b when Implicit Method II and Howe's method are employed. The results for two grid sizes with Howe's numerical method are presented in this figure. As the grid size is reduced, the skin-friction ratio is decreased when Howe's method is used while the skin-friction ratio is increased when the implicit method is used. Since the results in Figure 22b are reasonably close, the two methods would become very close as the grid size is decreased. Since there is a discontinuity in certain quantities at the initial profiles, there are unusually large errors introduced near the start of the computations. The effect of these errors can, perhaps, contribute to any remaining difference between the two methods with a very small grid size.

When the viscosity law is changed there is no significant variation in the skin-friction ratio as obtained by Howe's method. The implicit method indicates approximately a 5 percent decrease in the skin-friction ratio when Sutherland's viscosity law is employed. Because of this discrepancy, this problem has been solved using the explicit method as described in Chapter III Section B.1. The results of the explicit method

are in agreement with the results obtained with the implicit method. It seems that the method employed by Howe is insensitive to the viscosity law employed. This peculiarity of the numerical solution of the Crocco form of the boundary-layer equations is discussed further in the next example.

In Figure 22c the heat transfer parameter for this problem is presented. It was obtained by dividing the nondimensional local heat transfer rate for this problem by the same quantity for a flat plate with a constant wall temperature. The latter quantity called $(q)_{f(0)=0}$ is the following for this problem and is based upon a linear viscosity law:

$$(q)_{f(0)=0} = \frac{1}{8.05458\sqrt{x}} \tag{4.13}$$

In Figure 22c the heat transfer parameter results obtained with the linear and Sutherland's viscosity law with Implicit Method II are presented. The result for this parameter as obtained by Howe is also shown and is computed with Sutherland's viscosity law. However, his result is in closer agreement with the implicit result obtained with the linear viscosity.

The displacement thickness is presented in Figure 22d for the implicit results when the two viscosity laws are employed. There is first a decrease in displacement thickness after the transpiration cooled region. This kind of behavior has been predicted by Pallone (Ref. 34) for this type of problem with an insulated wall.

As discussed previously, these examples provide an indirect method of comparing several of the numerical schemes. However, this comparison can be only approximate as different digital computers were used, computation time is very sensitive to the accuracy obtained, and slightly different problems were solved. A problem similar to the present example, except the wall is insulated, has been solved with a linear viscosity law by Pallone (Ref. 34). The same problem has been solved by Howe (Ref. 17) with Sutherland's viscosity law. The two methods give approximately the same result for the skin-friction ratio.

Although one would expect some differences between the two results because of the different viscosity laws, the peculiarity of the Howe method discussed earlier can account for the results being nearly the same. The computation of Pallone was performed with an IBM 704 computer in 20 minutes. Since the computations went from $x = 1.0$ to $x = 4.0$ and the IBM 704 is approximately twice as fast as the Burroughs 220, the Pallone method would probably require about 20 minutes with the Burroughs 220 for the present problem. The computation of Howe was performed with an IBM 650 computer and required 7 1/2 hours. For the present problem on the Burroughs 220 the Howe method would require about 90 minutes. When Implicit Method II is used, from 11 to 22 minutes are required for the results obtained for this problem with the Burroughs 220 computer. When Sutherland's viscosity law is employed, approximately 50 percent more computation time is required than the results obtained with a linear law. The more accurate results with the smaller grid size take the larger computation time indicated. When the same grid size is used as in the implicit scheme, the explicit method requires about 27 percent less computation time. However, the truncation error appears to be approximately the same when the grid size Δx for the explicit scheme is 2.5 times smaller. Therefore, the Implicit Method II requires less computer time than the explicit scheme with the same accuracy. From the above considerations, this problem can be solved with Implicit Method II as efficiently as any of the other methods.

3. Flat Plate Flow with "Hot Spot". To illustrate that the implicit scheme can be used to solve boundary-layer flows with a variable wall temperature, the problem solved by Baxter and Flügge-Lotz (Ref. 1) of flow along a flat plate with a "hot spot" is now considered. The same conditions are used so that a comparison of results can be made. These conditions are:

$$M_\infty = 0.5 \tag{4.14a}$$

$$T^*_\infty = 389.99^\circ R \tag{4.14b}$$

$$\gamma = 1.4 \tag{4.14c}$$

$$Pr = 0.72 \tag{4.14d}$$

$$S^* = 216^{\circ}R \tag{4.14e}$$

The following equation is used to specify the wall enthalpy for $1 \leq x \leq 1.0256$:

$$i_w = \left[2 + 0.04\left(\frac{x - 1}{0.0128}\right)^3 \left(\frac{1.0256 - x}{0.0128}\right)^3 \right] i_{ad} \tag{4.15a}$$

For $x > 1.0256$, the wall enthalpy is

$$i_w = 2\left[1 + \frac{\gamma - 1}{2} M_e^2\, 0.845\right] i_e = 2i_{ad} \tag{4.15b}$$

As this is a flat plate problem, the pressure gradient is zero. When the linear viscosity law is used, the constant C is determined using the wall temperature upstream of the "hot spot".

The boundary-layer characteristics for this problem are presented in Figure 23. The skin-friction and heat-transfer parameters have been determined with Implicit Method II with the two viscosity laws. The result of Baxter and Flügge-Lotz is presented in this figure and was computed using Sutherland's viscosity law. In Figure 23a the value of the skin-friction parameter for a flat plate without a "hot spot" is presented. This result with a linear viscosity law was obtained from Low (Ref. 26), while the result with Sutherland's viscosity law was obtained from Crocco (Ref. 9). Far downstream from the "hot spot" the boundary-layer characteristics should approach the flat plate similar solution results. The pecularity of the Crocco finite-difference scheme of numerical solution appears in this problem again. The skin-friction parameter obtained by Baxter and Flügge-Lotz, which uses the Crocco method, does not appear to approach the similar solution of Crocco. However, the implicit solution with Sutherland's viscosity law appears to be approaching the Crocco similar solution. When the linear viscosity law is employed with the implicit method, the variation of the skin-friction parameter is similar to the Baxter and Flügge-Lotz result. The

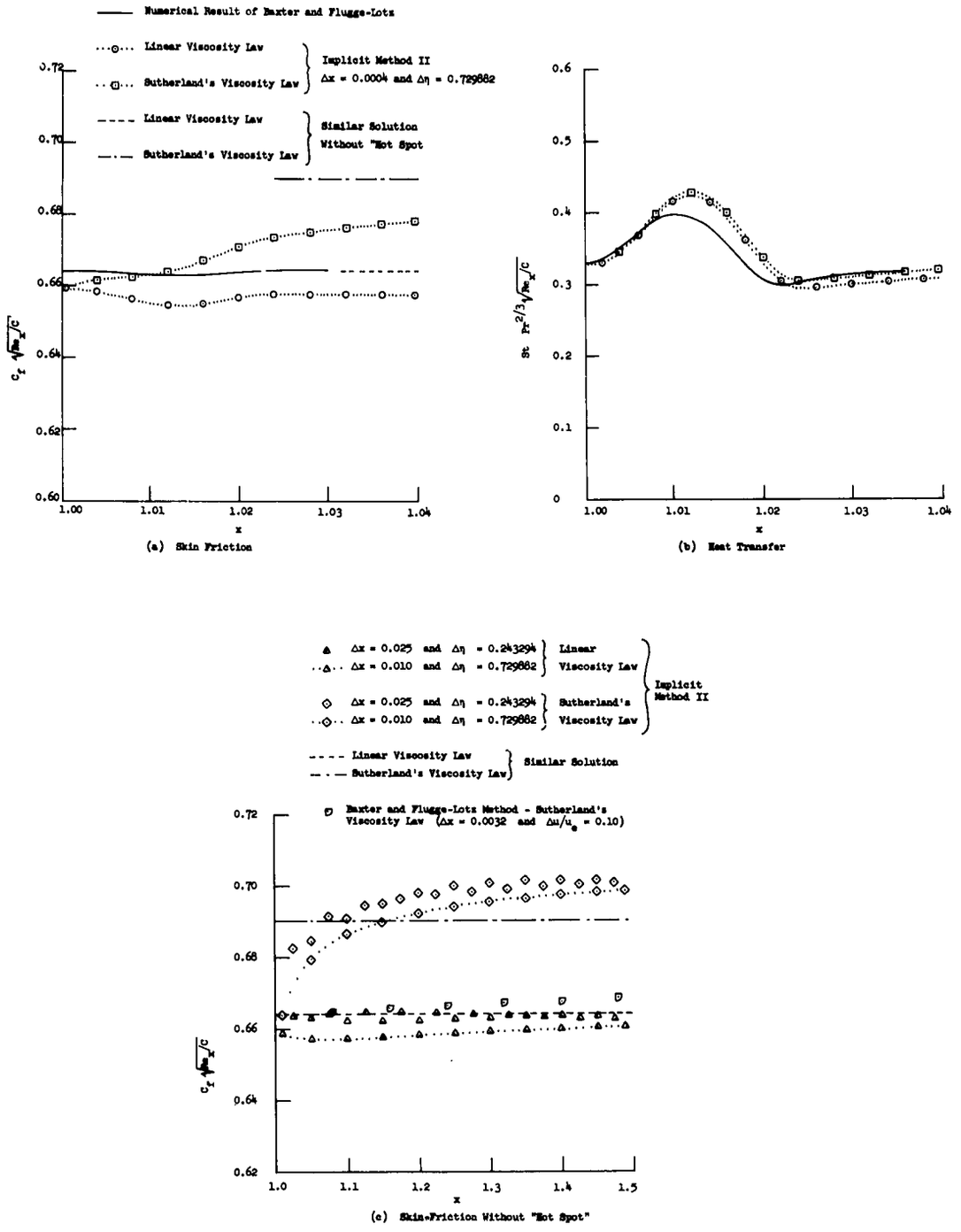

Figure 23. Boundary-Layer Characteristics for Flow Along a Flat Plate with a "Hot Spot"

shift in the skin-friction occurs because the step-size $\Delta \eta$ across the layer is not sufficiently small.

In Figure 23b the implicit results for the heat-transfer parameter are compared with the Baxter and Flügge-Lotz results. The viscosity law employed in the implicit solution has only a small effect on the results. The implicit method predicts a higher peak with a shift downstream when compared with the Baxter and Flügge-Lotz result. This difference is insignificant when compared to other methods of predicting the heat transfer, and the conclusions of Baxter and Flügge-Lotz are still valid.

In order to investigate the closeness of the numerical and Crocco similar solutions further downstream, the flow along the same flat plate without the "hot spot" has been solved. The skin-friction parameter is presented in Figure 23c. Two step-sizes have been employed and the two viscosity laws have been used with Implicit Method II. For the skin-friction parameter with the linear viscosity law, reasonable agreement is obtained with the similar solution when the step-size is sufficiently small. When Sutherland's viscosity law is employed, the implicit scheme indicates a slightly larger value of the skin-friction than the similar solution. The present problem has been solved with Sutherland's viscosity law by Baxter and Flügge-Lotz (Ref. 1), but the computations only extend a short distance downstream. This computation has been extended further downstream, and the result for the skin-friction is presented in Figure 23c.

The solution is coming closer to the Crocco similar solution, but the process is very slow. Therefore, the Baxter and Flügge-Lotz method appears to be insensitive to the viscosity law employed in the examples investigated.

For the Implicit Method II solution in Figure 23c with the larger value of Δx, an oscillation of the skin-friction parameter occurs. This is attributed to an error being introduced by the linearization of the difference equations and propagated when the continuity equation is replaced by Method B (see equation 3.20). After the two methods of replacing the continuity equation have been studied, the following statements can be made: (1) For Method A errors in V are only

propagated indirectly by the influence on u and i at the next step. (2) For Method B an isolated error in V will oscillate in sign as the computations proceed and the indirect influence will also occur. Therefore, Method B can give results with a small oscillation, but with less over-all error.

CHAPTER V

NUMERICAL SOLUTION OF THE BOUNDARY-LAYER EQUATIONS WITH DISPLACEMENT THICKNESS INTERACTION

In this chapter only the boundary-layer flow along a flat plate with a sharp leading edge will be investigated. However, the displacement thickness interaction between the boundary-layer and external flow will be included in the solution. The reasons for neglecting other parameters that contribute to the interaction between the boundary-layer and external flow were discussed in Chapter I.

In Hayes and Probstein (Ref. 14) the flat plate and wedge interaction problems have been discussed in terms of weak and strong pressure interaction. The weak interaction region $\left(\bar{\chi} = M_\infty^3 \sqrt{C/Re_{x_\infty}} < 1\right)$ occurs far downstream from the leading edge where the induced pressure has a small effect on the boundary-layer flow. The more interesting region is near the leading edge where the strong interaction occurs $(\bar{\chi} \gg 1)$. In this region the boundary-layer flow is greatly influenced by the induced pressure caused by the viscous layer near the wall changing the effective shape of the body. The strong pressure interaction theory expands quantities in an asymptotic series in terms of the interaction parameter $\bar{\chi}$. Hence, the boundary-layer equations are reduced to simultaneous nonlinear ordinary differential equations for the zeroth-order approximation while the higher approximations are linear equations. Only the zeroth-order problem has been solved exactly with a linear viscosity law and Prandtl number equal to one. For an insulated flat plate at zero angle of attack, the first-order problem has been solved approximately.

The results of the strong pressure interaction theory will be used to obtain initial profiles. Also results of this theory will be compared with examples solved numerically in this chapter. However, before these subjects are presented, the method of solving the boundary-layer equations with interaction is considered.

A. Method of Solution

The essential difference between the boundary-layer flow without and with displacement thickness interaction is that the pressure distribution is known in the first case and unknown in the other. Therefore, after the Howarth-Dorodnitsyn transformation, the boundary-layer equations (2.29 - 2.31) are applicable for this problem; except the pressure gradient p_e' is now an unknown. As the pressure along a body with interaction cannot be computed directly, an iteration scheme is employed. Two methods of iterating for the desired pressure distribution have been considered.

One method initially assumes no interaction and the boundary-layer equations are solved using the invisid pressure distribution on the body. By using the displacement thickness resulting from this solution, we know the effective shape of the body, and a new pressure distribution (induced pressure plus inviscid pressure) can be determined. Next, the boundary-layer equations are solved with the new pressure distribution and then a new effective body is determined. The above procedure is iterated until the assumed pressure distribution is sufficiently close to the pressure calculated from the effective body shape. The initial profiles for the first solution of the boundary-layer equations are readily available for the case of flow along a flat plate. For the other iteration solutions of the boundary-layer equations, there are no accurate initial profiles. Because of this fact, this type of iteration is not feasible for the numerical solution of the flat plate interaction problem near the leading edge and is not considered further.

The other method of iterating for the pressure distribution assumes that initial profiles are available for the case of interaction between the boundary-layer and external flow. This seems, perhaps, to be a severe hindrance. But for the flow near the leading edge of a flat plate or wedge, the strong pressure interaction profiles can be used when the interaction parameter, $\bar{\chi}$, is very large. (See the next section for further discussion of the initial profiles.) When the pressure at the next step downstream from the starting profile is assumed, the pressure gradient term in the boundary-layer equations for Implicit Method II can be written as:

$$p'_{e_{m+\frac{1}{2}}} = \frac{p_\infty}{\Delta\xi}\left[\left(p_e/p_\infty\right)_{m+1} - \left(p_e/p_\infty\right)_m\right] \tag{5.1}$$

The pressure ratio at $(m + 1)$ is estimated by the following:

$$\left(p_e/p_\infty\right)_{m+1} = \left(p_e/p_\infty\right)_A^{(1)} = 1.5\left(p_e/p_\infty\right)_m - 0.5\left(p_e/p_\infty\right)_{m-1} \tag{5.2}$$

This equation results from taking the average of the pressure ratio at (m) and the predicted value at $(m + 1)$ when a linear extrapolation formula is used. The superscript (1) indicates the first iteration, while the subscript A indicates the assumed pressure ratio at $(m + 1)$. When equation (5.1) is used in the boundary-layer equations (2.29-2.31), the resulting equations are solved using Implicit Method II as presented in Chapter III. From equation (3.50c) the displacement thickness is determined at the next step downstream. The slope of the effective body then can be determined. For the case of a flat plate, this slope is approximated as:

$$\theta_{m+1} = \frac{\bar{\delta}^*_{m+1} - \bar{\delta}^*_m}{\sqrt{Re_0}\ \Delta\xi} \tag{5.3}$$

In order to determine the pressure along the body, the tangent-wedge formula is used. Although the tangent-wedge formula is an approximate relation, it is a reasonable assumption for this problem and is written as:

$$\left(p_e/p_\infty\right)_C^{(i)} = 1 + \gamma M_\infty^2\,\theta^2\left(\sqrt{\frac{\gamma+1}{4}^2 + \frac{1}{M_\infty^2\,\theta^2}} + \frac{\gamma+1}{4}\right) \tag{5.4}$$

The subscript (C) indicates the quantity is calculated after the pressure at $(m + 1)$ has been assumed, while the superscript (i) indicates the iteration being performed. Using the slope θ_{m+1} with

the tangent-wedge formula gives the pressure at the edge of the boundary-layer at the next step downstream. As this calculated pressure is most likely different from the pressure assumed initially, the above procedure must be iterated until the two pressures are sufficiently close to each other.

When the boundary-layer equations are solved at (m + 1), the corresponding pressure can be calculated from the tangent-wedge formula (5.4). The result of such a procedure is given in Figure 24 for $x = 0.015$. The desired result is reached when the assumed and calculated pressures are equal, and this occurs at the intersection of the two curves. This figure shows that a rudimentary iteration procedure is unstable (the calculated pressure is further away from the correct value than the assumed pressure). Therefore, the usual iteration procedure of using the calculated pressure for the assumed pressure in the next calculation will not work. If two pressures $(p_e/p_\infty)_A^{(i-1)}$ and $(p_e/p_\infty)_A^{(i)}$ are assumed, then two pressures $(p_e/p_\infty)_C^{(i-1)}$ and $(p_e/p_\infty)_C^{(i)}$ can be calculated. A linear extrapolation or interpolation, depending upon the location of the points (i) and (i+1), is made as shown in Figure 24. The new estimate for the pressure ratio is written as

$$(p_e/p_\infty)_A^{(i+1)} = \frac{(p_e/p_\infty)_C^{(i-1)}(p_e/p_\infty)_A^{(i)} - (p_e/p_\infty)_A^{(i-1)}(p_e/p_\infty)_C^{(i)}}{(p_e/p_\infty)_A^{(i)} - (p_e/p_\infty)_A^{(i-1)} + (p_e/p_\infty)_C^{(i-1)} - (p_e/p_\infty)_C^{(i)}} \quad (5.5)$$

Once the iteration procedure has been initiated, the above equation can be used in determining increasingly accurate values for the pressure ratio at (m + 1). The iteration is completed when the following relations is satisfied:

$$\left|(p_e/p_\infty)_A^{(i)} - (p_e/p_\infty)_C^{(i)}\right| < \epsilon_1 \quad (5.6)$$

The quantity ϵ_1 is a small number determined by the desired accuracy and values will be given with the examples in Section C of this chapter. Because of the round-off errors, equation (5.5) does not work for ϵ_1

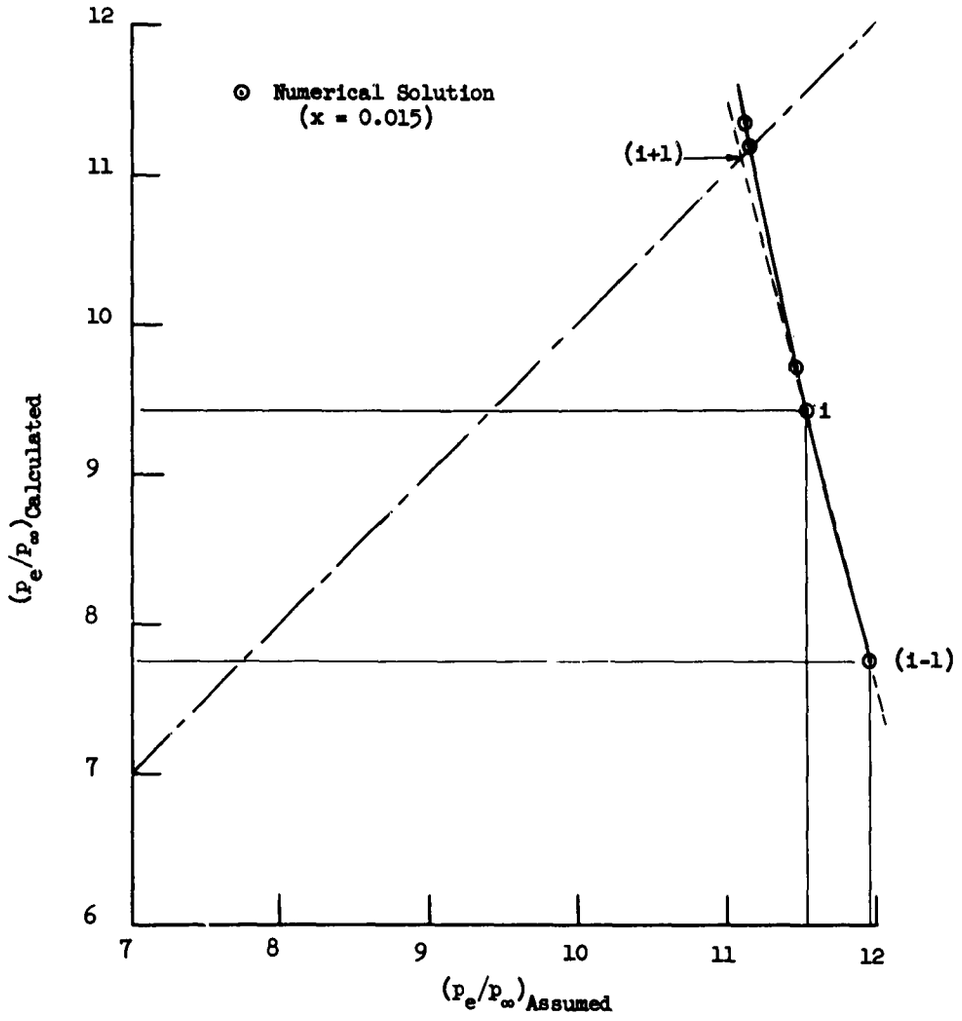

Figure 24. Variation of Assumed and Calculated Pressure Ratio

approximately 10^{-4} or smaller. However, for the examples investigated in this paper, equation (5.5) has been satisfactory.

The flow diagram for computing the boundary-layer flow with interaction is given in Figure 25. For greater details of various elements of this flow diagram, see Figure 3. The new elements in Figure 25 are discussed below and related to formulas presented in this chapter.

1. Input. The pressure ratio and displacement thickness at the initial profiles must be supplied.
2. Program Constants. See Chapter III, Section G.1.
3. Estimate $(p_e/p_\infty)_A^{(1)}$. Use equation (5.2) to determine this quantity.
4. Compute Exterior Flow Quantities. See Chapter III, Section G.3.
5. Compute $p'_{e_{m+\frac{1}{2}}}$. Use equation (5.1) to determine the pressure gradient.
6. Compute $u_{m+1,n}$ and $i_{m+1,n}$. See Chapter III, Section G.5 and G.6.
7. Compute $\bar{\delta}^*_{m+1}$. See Chapter III, Section G.10.
8. Compute θ_{m+1}. The effective slope of the body is determined from equation (5.3).
9. Compute $(p_e/p_\infty)_C^{(i)}$. Use the tangent-wedge formula (5.4) to calculate the pressure ratio at (m + 1).
10. Is $|(p_e/p_\infty)_A^{(i)} - (p_e/p_\infty)_C^{(i)}| < \epsilon_1$? This test is used to determine when the iteration process is to be terminated.
11. Estimate $(p_e/p_\infty)_A^{(i+1)}$. A more accurate value of the pressure ratio at (m + 1) is estimated using equation (5.5). In order to use this formula for the first iteration, the following relations are assumed:

$$(p_e/p_\infty)_A^{(0)} = (p_e/p_\infty)_m \tag{5.7a}$$

$$(p_e/p_\infty)_C^{(0)} = 0 \tag{5.7b}$$

12. Compute $V_{m+1,n}$. See Chapter III, Section G.8.
13. Compute Wall Quantities. See Chapter III, Section G.10.

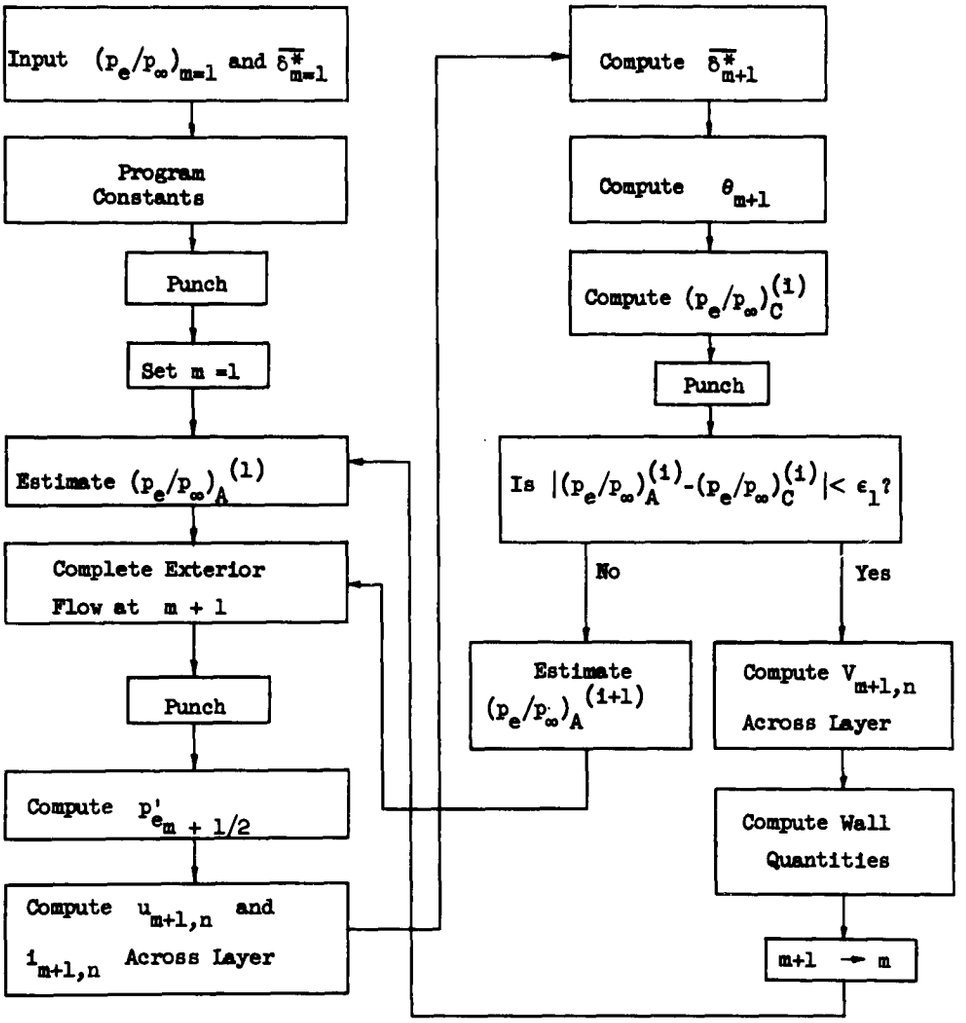

Figure 25. Flow Diagram for Computing Boundary-Layer Flow with Interaction

B. Initial Profiles

For the flow over a wedge or flat plate with $\bar{\chi} >> 1$, the initial profiles can be determined from the strong pressure interaction theory. (See page 353 of Ref. 14). However, this theory is not valid near the leading edge as the pressure goes to infinity. Oguchi (Ref. 33) gives an estimate of the upstream limit of the strong interaction theory. For the examples considered in this chapter $\bar{\chi} \approx 25$ or $x \approx 0.01$ at this limit. Therefore, the strong interaction theory should give accurate initial profiles at $x = 0.01$.

Rather than compute higher-order approximations to the available solution of the strong interaction theory, the zeroth-order solution is used to approximate the initial profiles. The zeroth-order solution with a linear viscosity law and Pr = 1.0 is obtained from Li and Nagamatsu (Ref. 25). The following relations are used to determine the initial profiles for the transformed plane in terms of quantities given by Li and Nagamatsu.

$$\eta = Q_i \, \eta_{Li} \tag{5.8a}$$

$$u = u_e \, K'(\eta_{Li}) \tag{5.8b}$$

$$i = i_e \, G(\eta_{Li}) + \frac{1}{2} u_e^2 \, [G(\eta_{Li}) - K'^2(\eta_{Li})] \tag{5.8c}$$

$$V = \frac{u_e Q_i}{4x} \, [- K(\eta_{Li}) + \eta_{Li} \, K'(\eta_{Li})] \tag{5.8d}$$

where

$$Q_i = \frac{2 \rho_e x}{M_e^2 M_\infty} \sqrt{Re_0^* \, \bar{\chi} / p_{(0)}} \tag{5.8e}$$

The above relations 5.8a to 5.8c are easily obtained from Li and Nagamatsu while relations 5.8d and 5.8e require derivation. The procedure used to determine the later relations is given in Appendix A Part 2.

C. Examples Solved

The three examples presented are for flow along a flat plate with the following conditions assumed :

$$M_\infty = 9.60 \tag{5.9a}$$

$$T^*_\infty = 82.34^\circ R \tag{5.9b}$$

$$\gamma = 1.40 \tag{5.9c}$$

$$Pr = 1.00 \text{ or } 0.72 \tag{5.9d}$$

$$S^* = 198.6^\circ R \tag{5.9d}$$

$$\sqrt{Re_0} = 2198.79 \tag{5.9f}$$

These values correspond to conditions in hypersonic wind tunnels. Either the linear or Sutherland's viscosity law is used as indicated in the examples. In the first and second examples the wall enthalpy is specified such that the wall is approximately insulated when $Pr = 0.72$ and is insulated when $Pr = 1.0$ ($i_w/i_o = 1.0$). In the first example the pressure distribution is specified, while in the second example the pressure distribution is unknown. The third example is the same as the second except the wall temperature is specified such that $i_w/i_o = 0.15$. The last two examples illustrate the iteration procedure for solving the boundary-layer and external flow interaction problem. The case of a heated wall has not been considered as initial profiles are not readily available.

The initial profiles for these examples are determined from the zeroth-order strong interaction theory as given by equations (5.8). The initial profiles are determined at $x_i = 0.010$ and are given with the examples.

The boundary-layer equations were solved using Implicit Method II on the Burroughs 220 computer. In the finite-difference scheme the

test for the edge of the boundary layer uses $\epsilon = 0.001$ in the three examples of this chapter. For the termination of the pressure iteration process in the interaction problems (See equation 5.6), $\epsilon_1 = 0.001$.

1. Flow Along a Flat Plate with Specified Strong Interaction Pressure Distribution. Before the iteration procedure is used to solve the interaction problem, the pressure distributions from the strong interaction theory are used to solve the boundary-layer equations in order to test the numerical scheme with strong pressure changes. This theory gives the pressure for an insulated flat plate ($Pr = 1.0$ and linear viscosity law) as

$$p_e/p_\infty = 0.514\,\bar{x} + 0.759 + \ldots \qquad (5.10)$$

where the first term corresponds to the zeroth-order theory and the inclusion of the next term gives the first-order theory. The same problem has been solved numerically using first the zeroth and then the first-order pressure distribution. The initial profiles for this example were determined using equations (5.8) and are shown in Figure 26. Also shown in this figure is the zeroth-order similar solution and numerical solution at $x = 0.125$ when the zeroth-order pressure distribution is specified. The numerical solution should approach the similar solution as the Mach number goes to infinity. Even with $M_\infty = 9.6$ for the numerical solution, agreement is obtained with the similar solution.

The effective slope of the body (5.3) can be determined from the displacement thickness which is obtained from the numerical solution of the boundary-layer equations. Then the tangent-wedge formula is used to calculate the pressure along the flat plate. The result for this calculated pressure, when the zeroth and first-order strong interaction pressure distribution has been specified, is given in Figure 27a. This figure shows that the first-order strong interaction theory gives a close estimate of the pressure in the region investigated. The large difference between the assumed and calculated curves near the start for the first-order results can be attributed to using the zeroth-order strong interaction profiles.

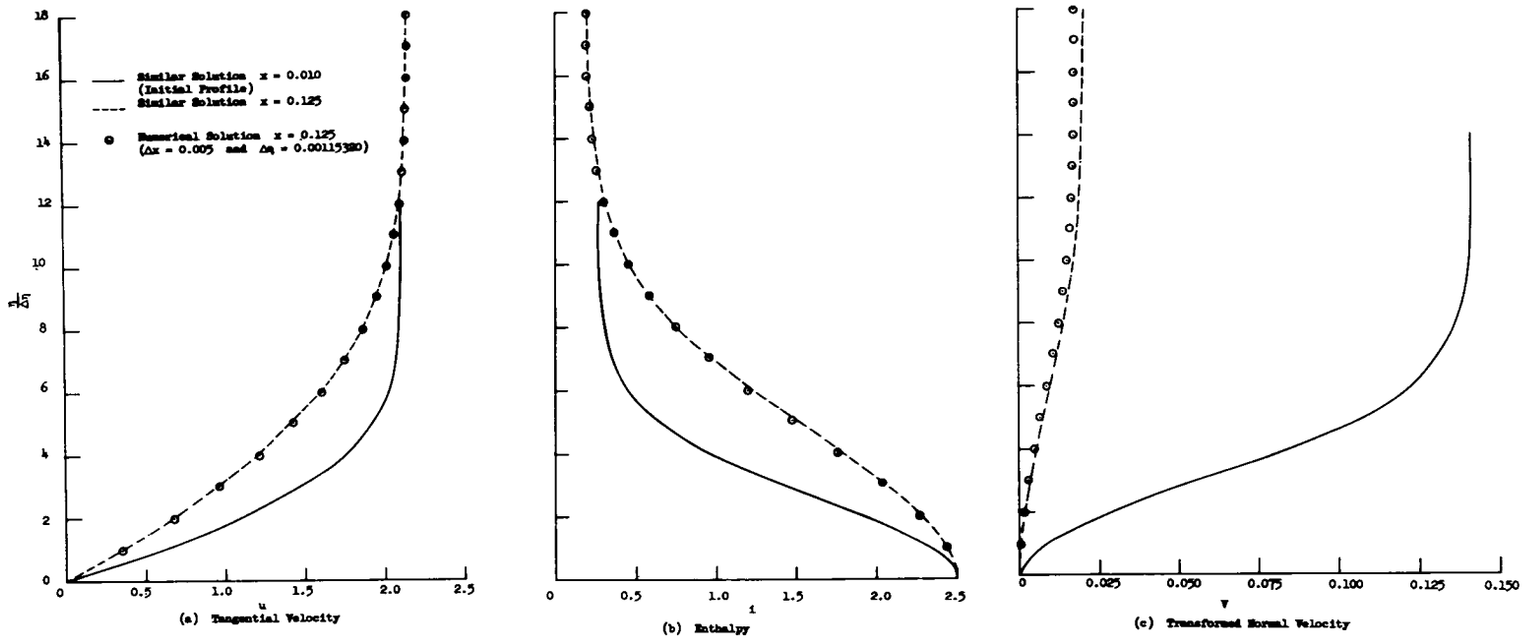

Figure 26. Boundary-Layer Profiles for Zeroth-Order Strong Interaction Theory with Insulated Wall

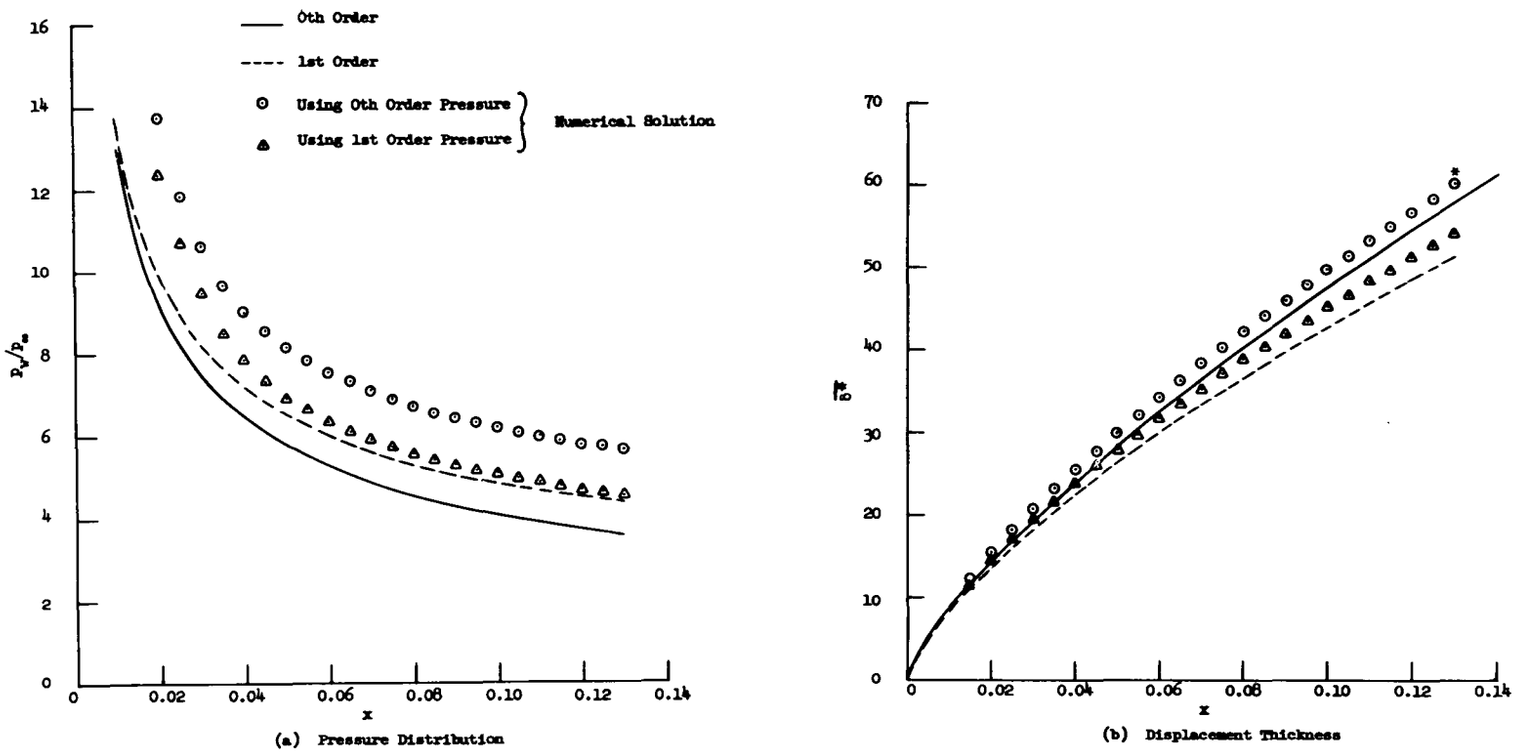

Figure 27. Pressure Distribution and Displacement Thickness for Strong Interaction Theory

The displacement thickness for the zeroth and first-order strong interaction theory is given in Figure 27b. The numerical solutions for the displacement thickness are given in this figure also. These results were obtained by assuming the pressure distribution as given by the zeroth and first-order strong interaction theory. Some of the difference between the numerical and theoretical results can be traced to the method of determining the displacement thickness in the strong interaction theory. If the displacement thickness is determined exactly from the zeroth-order profiles, the value at $x = 0.13$ is indicated by the star in Figure 27b. The remaining error can be attributed to the fact that an insufficiently large free stream Mach number was used.

2. Flat Plate with Nearly Insulated Wall. The previous problem is solved again with the pressure distribution taken as an unknown. The iteration procedure as presented in Section A of this chapter is used to determine the pressure along the flat plate. The initial profiles for this example are obtained from the zeroth-order strong interaction theory and have been presented in Figure 26. When $Pr = 1.0$ and a linear viscosity law are employed, the numerical solution for the pressure as a function of the interaction parameter is presented in Figure 28a. The zeroth and first-order strong and second-order weak interaction theories are given in this figure. All of the results in part (a) are for a linear viscosity law and $Pr = 1.00$. The pressure is reasonably close to the first-order strong interaction theory except near the start of the computations. This error is because the zeroth-order strong interaction initial profiles are employed. The problem has been solved with $Pr = 0.72$ and Sutherland's viscosity law, but the same initial profiles have been used. The results of these computations are presented in Figure 28b along with experimental data obtained from Bertram and Blackstock (Ref. 3). These data were obtained with a small wall temperature gradient and with a certain amount of heat transfer, but have been corrected to the case of an insulated flat plate. The numerical results have $i_w/i_o = 1$ while the experimental results have $i_w/i_o = 0.85$. A new correction factor has been estimated from zeroth-order strong interaction theory. From this estimate the experimental data in Figure 28b should be multiplied by 1.10. With this correction there is agreement between the numerical and experimental results.

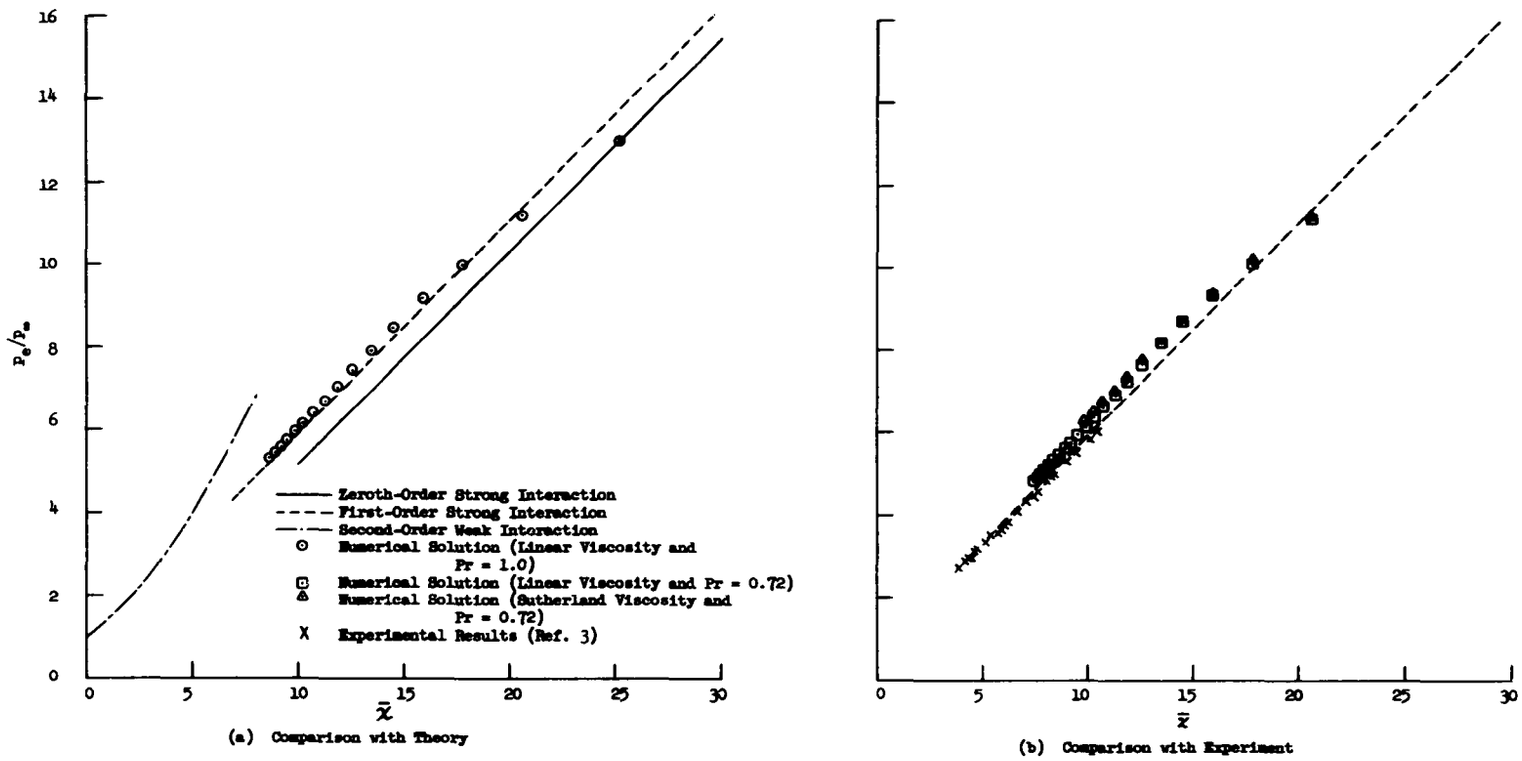

Figure 28. Induced Pressure on Nearly Insulated Flat Plate

3. Flat Plate with a Cold Wall. This example is the same as the previous problem except the flat plate has a cold wall ($i_w/i_o = 0.15$). The initial profiles have been obtained from equations (5.8) and are shown in Figure 29. The numerical profiles at $x = 0.125$ are given in this figure, and $Pr = 1.0$ and a linear viscosity law are used in the computation.

The boundary-layer characteristics for this example are presented in Figure 30. Theoretical, numerical, and experimental results are presented in this figure. All of the theoretical results are based on a linear viscosity law and $Pr = 1.0$. The experimental results are from Hall and Golian (Ref. 13) and $i_w/i_o \approx 0.14$ for these shock-tunnel studies. In part (a) of the figure the pressure along the flat plate as a function of the interaction parameter is presented. When the numerical computations use $Pr = 0.72$, the pressure ratio is in closer agreement with the experimental data. The numerical skin-friction results are compared with the theoretical predictions in part (b). The skin-friction parameter is reduced when the Prandtl number is changed from 1.00 to 0.72. The heat-transfer results are presented in part (c). Only a few of the experimental points of Hall and Golian are presented, but these indicate the average result. The experimental data indicated a higher value of the heat-transfer parameter than the other results predict. There is a damped oscillation in the numerical result with $Pr = 0.72$. This can be attributed to using the initial profiles from zeroth-order strong interaction theory with $Pr = 1.0$. There seems to be very little effect of the Prandtl number on the heat transfer in this example.

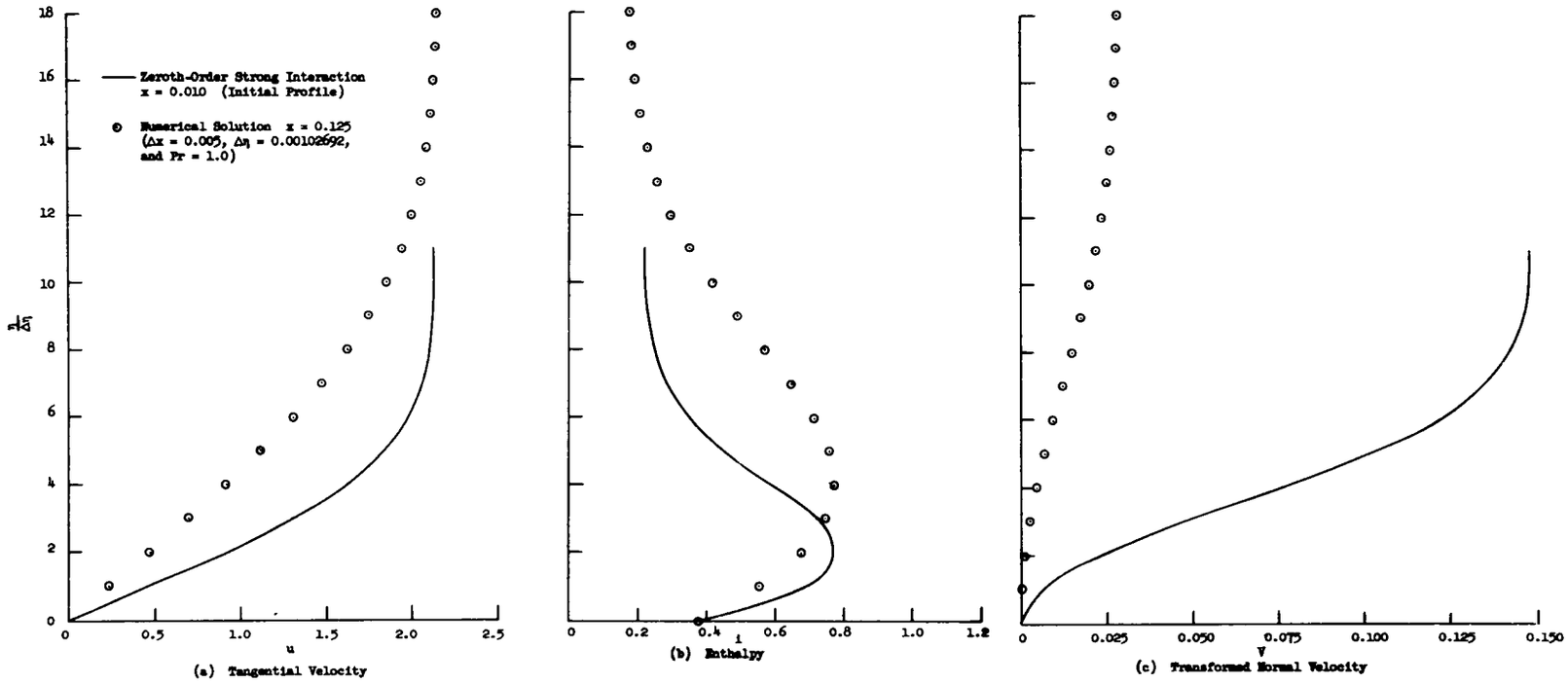

Figure 29. Boundary-Layer Profiles with Interaction for a Cold Flat Plate

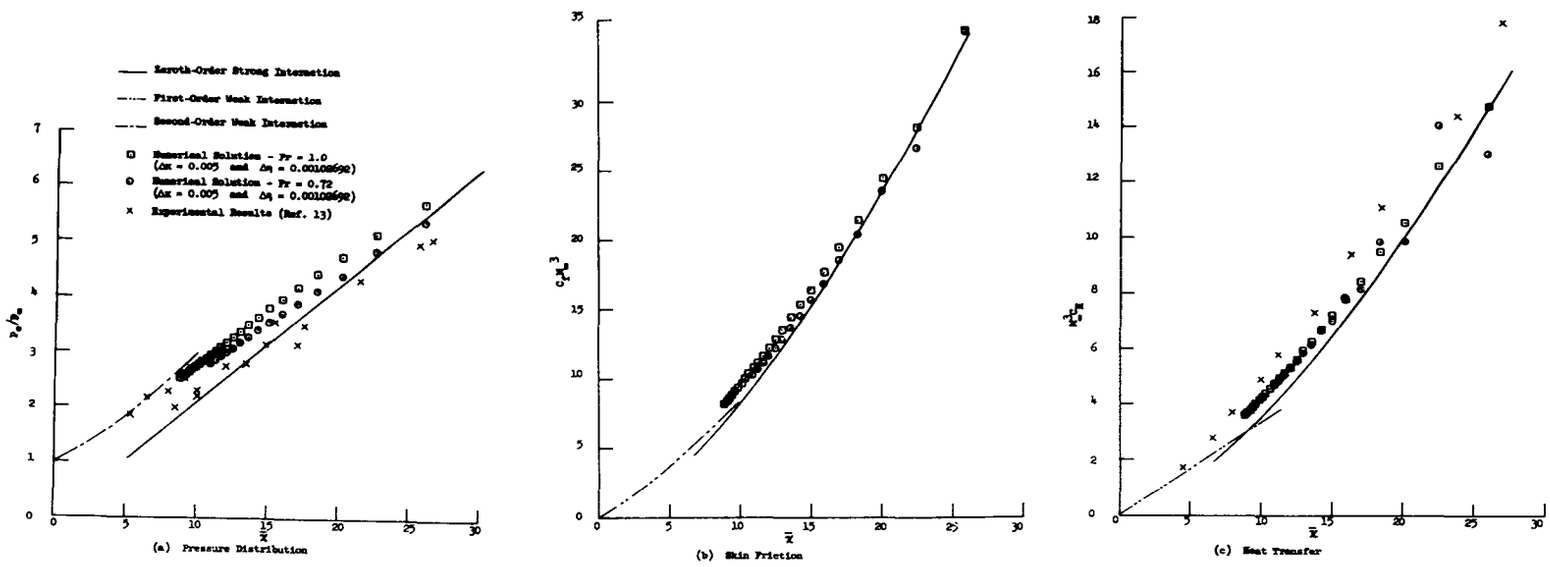

Figure 30. Boundary-Layer Characteristics with Interaction for a Cold Flat Plate

CHAPTER VI

DISCUSSION AND CONCLUSIONS

The boundary-layer equations are solved in either the physical plane or the Howarth-Dorodnitsyn transformed plane. These equations are used rather than the Crocco form as they are convenient for the interaction examples and introduce no problems when velocity profiles with "overshoot" occur. Two implicit methods have been investigated to solve the boundary-layer equations without displacement thickness interaction. Implicit Method II, which solves the Howarth-Dorodnitsyn transformed equations with the Crank-Nicolson scheme, is superior to Method I which solves the equations in the physical plane with the usual implicit scheme. The truncation error for the difference quotients of Method II is of order Δx^2 and $\Delta \eta^2$, while Method I is of order Δx and Δy^2. This allows a larger step of Δx to be used in Method II. When the transformed equations are used, the velocity and enthalpy profiles across the hypersonic boundary layer are readily approximated by equally spaced points. For the same problem with the boundary-layer equations in the physical plane, either a larger number of grid points are required or unequally spaced points must be used to approximate the profiles. For the transformed equations, similar solution results are in a form such that initial profiles are readily obtained. When the equations are used in the physical plane, interpolation between unequally spaced points is required.

Wu's procedure of using freestream quantities except at the wall for the initial profiles has been investigated (see Chapter III, Section D). This would be advantageous for the present implicit scheme. Reasonable results can be obtained if the proper grid size is used and the proper value of the normal velocity is chosen. The Wu type initial profiles must be used with care as the appropriate values of these quantities are difficult to ascertain.

A simplified analysis has been employed to show that Implicit Method II is stable without any restrictions on the grid size. The results obtained in this investigation corroborate this conclusion.

However, oscillations can occur in the transformed normal velocity, V, when Method B is used to replace the continuity equation. The over-all error is still less with Method B than with Method A. This oscillation in V appears to be introduced by the error produced in the linearization procedure. When small Δx steps are used, the oscillation is not detectable. The truncation error due to linearization can be reduced by iterating at each step downstream rather than reducing the step-size Δx.

With the implicit methods the following type of first-order compressible boundary-layer problems have been solved: wall with varying temperature, specified heat transfer along the wall, pressure gradient along the wall, and flow downstream of a transpiration cooled wall. The implicit method should be a useful method to solve more involved boundary-layer problems where several of the above events are occuring simultaneously.

In solving these problems the step-sizes across and along the wall have remained fixed. Since the number of points across the boundary layer usually increase as the computations proceed, the computer program can be written such that the points can be reduced when the number becomes excessive. Generally, one wants the number of points to remain constant so that the truncation error remains approximately the same throughout the computations. Also, the step-size along the wall should vary depending upon the rapidity with which the profiles are changing. Possibly by observing the rate of change of the shearing stress at the wall, the step-size Δx could be varied to keep this quantity within certain bounds.

In Chapter I several numerical schemes for solving the compressible boundary-layer equations without interaction were discussed. Some of the methods are: (1) Pallone's method of reducing the boundary-layer equations to ordinary differential equations, (2) Wu's explicit finite-difference scheme in the transformed plane, and (3) Baxter and Flügge-Lotz's explicit, and Kramer and Lieberstein's implicit finite-difference schemes with the Crocco boundary-layer equations. Results of this investigation indicate that Implicit Method II requires less computation time than the other schemes, except possibly Pallone's method where the

time is nearly the same (See example B.2 in Chapter IV for comparison of computation times). Pallone's method is probably not exact in any limit as discussed in Chapter I. However, Implicit Method II becomes closer to the exact solution as the grid size is reduced. Recently a rapid and precise procedure has been developed and studied by Smith and Clutter (Ref. 44) for solving the incompressible boundary-layer equations. This procedure is similar to the method proposed by Manohar which is discussed in Chapter I. The boundary-layer equations are reduced to an ordinary differential equation that is solved across the layer at succeeding steps downstream. Smith and Clutter are extending the method to the more complex case of compressible flow. It is impossible to predict at present how this procedure will compare with Implicit Method II.

The boundary-layer equations with displacement thickness interaction, which occurs when second-order boundary-layer theory is considered, have been solved by an iterative procedure with Implicit Method II. The zeroth-order strong interaction profiles are used to start the numerical computations of the boundary-layer flow near the leading edge of a flat plate. After a transition from the initial profiles, the numerical results are in agreement with weak and strong interaction theory. For the insulated wall, the first-order strong interaction theory is slightly different from the numerical result. The numerical and experimental results are in reasonable agreement. When $Pr = 0.72$, there is closer agreement between the numerical and experimental results for the pressure distribution on the cold flat plate. Even closer agreement with experimental results should be obtained when Sutherland's viscosity law is used. Before such computations are performed, it would be desirable to obtain better initial profiles. Initial profiles from first-order strong interaction theory should be sufficient and these profiles can be obtained. Then the problem of displacement thickness interaction on wedges and flat plates at angle of attack can be solved.

If the methods developed in this report are employed or extended, several interesting boundary-layer problems can be solved. Two-dimensional flows starting with stagnation-point profiles can be solved. Also, boundary-layer flows near the stagnation point of axisymmetric bodies

can be studied. For these flows the finite-difference approach becomes even more important as similar solutions are only valid at the stagnation point. When the methods developed in this investigation are employed, binary or chemical boundary-layer flows can be studied. Also, the results of this report can be utilized in studying the other interaction effects (vorticity, curvature, etc.) between the boundary-layer and external flow.

APPENDIX A

DERIVATION OF FORMULAS USED TO CALCULATE INITIAL VELOCITY AND ENTHALPY PROFILES

1. Flat Plate Without Interaction

a. Physical Plane. The profiles for a flat plate in the physical plane were obtained from Low (Ref. 26). The distance y, velocity u, and enthalpy i are easily obtained from Low by appropriate notation changes. To obtain the formula for the velocity v, certain mathematical operations have to be performed and these are presented below. From Low the following relations are obtained:

$$v = - \sqrt{Re_o^*} \frac{\rho_e u_e}{\rho L^*} \frac{\partial \psi}{\partial x} \bigg|_{y = \text{constant}} \tag{1A}$$

$$\psi = \frac{1}{2} \frac{L^*}{\sqrt{Re_o^*}} Q(x) f(\eta_{Low}) = \psi(x, \eta_{Low}) \tag{2A}$$

where

$$\eta_{Low} = \eta_{Low}(x,y) \qquad \text{and} \quad Q = 2 \frac{\mu_e Cx}{\rho_e u_e}$$

Therefore the following relation exists :

$$\frac{\partial \psi}{\partial x}\bigg|_y = \frac{\partial \psi}{\partial x}\bigg|_{\eta_{Low}} + \frac{\partial \psi}{\partial \eta_{Low}}\bigg|_x \frac{\partial \eta_{Low}}{\partial x}\bigg|_y \tag{3A}$$

where

$$\frac{\partial \psi}{\partial x}\bigg|_{\eta_{Low}} = \frac{1}{4} \frac{L^*}{\sqrt{Re_o^*}} \frac{Q}{x} f(\eta_{Low}) \tag{4A}$$

$$\left.\frac{\partial \psi}{\partial \eta_{Low}}\right|_x = \frac{1}{2} \frac{L^*}{\sqrt{Re_o^*}} Q\, f'(\eta_{Low}) \tag{5A}$$

Now $\left.\frac{\partial \eta}{\partial x}\right|_y$ must be determined and the relation for $y(\eta_{Low}, x)$ is used

$$y = Q(x)\, g(\eta_{Low}) \tag{6A}$$

The total derivative of y gives

$$dy = \frac{\partial y}{\partial x} dx + \frac{\partial y}{\partial \eta_{Low}} d\eta_{Low}$$

and for constant y, $dy = 0$. The above relation is solved for the desired derivative

$$\left.\frac{d\,\eta_{Low}}{dx}\right|_y = -\frac{\frac{\partial y}{\partial x}}{\frac{\partial y}{\partial \eta_{Low}}} = -\frac{1}{2x} \frac{g(\eta_{Low})}{g'(\eta_{Low})} \tag{7A}$$

Using relations (3A), (4A), (5A), and (7A) with (1A) results in

$$v = \frac{\rho_e u_e Q}{4x\rho} \left[\frac{f'(\eta_{Low})\, g(\eta_{Low})}{g'(\eta_{Low})} - f\,(\eta_{Low}) \right] \tag{8A}$$

Since ρ can be written as

$$\rho = \frac{\rho_e i_e}{i} = \rho_e / g'(\eta_{Low})$$

equation (8A) becomes

$$v = \frac{u_e Q}{4x} \left[f'(\eta_{Low})\, g(\eta_{Low}) - f(\eta_{Low}) g'(\eta_{Low}) \right] \tag{9A}$$

b. Transformed Plane. The profiles for a flat plate in the transformed plane were also obtained from Low (Ref. 26). The formulas for the velocity u and enthalpy i are the same as those for the

physical plane. However, the relation between the coordinates normal to the wall has changed. In Low the similarity variable is given as

$$\eta_{Low} = \frac{1}{Q}\int_0^y (\rho/\rho_e)dy \tag{10A}$$

When the above relation (10A) and the transformation (2.26) are used, the following is obtained:

$$\eta = \rho_e Q \eta_{Low} \tag{11A}$$

The transformed velocity V can be written as

$$V = \rho v + \eta_x u = \rho v + \rho_e u Q \frac{\partial}{\partial x}(\eta_{Low}) + \rho_e u \eta_{Low} \frac{\partial Q}{\partial x} \tag{12A}$$

where $d\rho_e/dx = 0$, since only a flat plate is being considered. The use of equations (7A) and (8A) in equation (12A) gives

$$V = \frac{\rho_e u_e Q}{4\xi}\left[f'(\eta_{Low})\,\eta_{Low} - f(\eta_{Low})\right] \tag{13A}$$

2. Flat Plate With Interaction. The zeroth-order strong interaction initial profiles for flow along a flat plate were obtained from Li and Nagamatsu (Ref. 25). In the zeroth-order strong interaction theory $M_e \gg 1$ and $u_e \approx u_\infty$. Although these velocities are approximately equal, the velocity at the edge of the boundary layer as determined from the pressure distribution is used in computing the initial profiles. This is done because u_e varies in the numerical computations. The pressure for this case is given as

$$p_e/p_\infty = p_{(o)}\,\bar{\chi}$$

or

$$\frac{1}{p_e}\frac{dp_e}{dx} = -1/2x \tag{14A}$$

Again the velocity u and enthalpy i are easily obtained for the initial profiles from Li and Nagamatsu and are not considered here. There is however more work required to express the coordinate η and the velocity V. The coordinate related to the distance normal to the wall is given by Li and Nagamatsu as

$$\eta_{Li} = \frac{u_e \, c^*_{p_o} \, L^*}{T_e \, \rho_e \, N \, c^*_o \sqrt{Re^*_o}} \int_0^y \rho \, dy \qquad (15A)$$

The transformed coordinate η, as given by equation (2.26), becomes the following when (15A) is used.

$$\eta = \frac{T_e \, \rho_e \, N \, c^*_o \sqrt{Re^*_o}}{u_e \, c^*_{p_o} \, L^*} \eta_{Li} = Q_i \, \eta_{Li} \qquad (16A)$$

A more convenient form of the expression for Q_i will now be obtained. When the definition of N from Li and Nagamatsu and the fact that $M_e \gg 1$ are used, equation (16A) yields

$$Q_i = 2 \, T_e \, \rho_e \sqrt{\frac{R \, C \, \mu_\infty \, x}{p_\infty \, T_\infty \, u_e \, p_e/p_\infty}} \qquad (17A)$$

With the equation of state $p_\infty = R \, \rho_\infty \, T_\infty$, the relation

$$T_e/T_\infty = \frac{1 + \frac{\gamma-1}{2} M_\infty^2}{1 + \frac{\gamma-1}{2} M_e^2} \approx M_\infty^2/M_e^2$$

and equation (14A), equation (17A) simplifies to

$$Q = \frac{2 \, \rho_e \, x}{M_e^2 \, M_\infty} \sqrt{Re^*_o \, \bar{\chi}/p_{(o)}} \qquad (18A)$$

Now the transformed velocity V as defined by equation (2.28) is

related to quantities of Li and Nagamatsu. The following expression for ρv is easily obtained from this reference.

$$\rho v = - u_e Q_i \left[\frac{1}{p_e} \frac{dp_e}{dx} K(\eta_{Li}) + \frac{1}{N} \frac{dN}{dx} K(\eta_{Li}) + K'(\eta_{Li}) \frac{\partial \eta_{Li}}{\partial x} \right] \qquad (19A)$$

From equation (16A) the derivative $\partial\eta/\partial x$ can be determined

$$\frac{\partial \eta}{\partial x} = Q_i \frac{\partial \eta_{Li}}{\partial x} + \eta_{Li} Q_i \left(\frac{1}{N} \frac{dN}{dx} + \frac{1}{\rho_e} \frac{d\rho_e}{dx} + \frac{1}{T_e} \frac{dT_e}{dx} - \frac{1}{u_e} \frac{du_e}{dx} \right) \qquad (20A)$$

From Li and Nagamatsu we obtain the following when the zeroth-order strong interaction assumptions are employed.

$$\frac{1}{N} \frac{dN}{dx} = 3/4x$$

$$\frac{1}{\rho_e} \frac{d\rho_e}{dx} = - 1/2\gamma x$$

$$\frac{1}{T_e} \frac{dT_e}{dx} = - (\gamma - 1)/2\gamma x$$

$$\frac{1}{u_e} \frac{du_e}{dx} = 0 \qquad (21A)$$

When equations (19A), (20A), and (5.8b) are used in equation (2.28) for V and the resulting expression simplified with equations (21A), the transformed velocity becomes

$$V = \frac{u_e Q_i}{4x} \left[-K(\eta_{Li}) + \eta_{Li} K'(\eta_{Li}) \right] \qquad (22A)$$

APPENDIX B

Verification of Method of Solving Difference Equations

The method of solving the difference equations (3.7 and 3.8) is presented in Chapter III, Section C.2. However, certain relations were stated to exist without proof and these will now be considered further. The following discussion is essentially an elaboration of pages 178 to 180 of Richtmyer (Ref. 38) in order to clarify certain questions.

Consider the following linear algebraic equations (equivalent to difference equations 3.7 and 3.8):

$$A_{1_n}\, u_{n-1} + B_{1_n}\, u_n + C_{1_n}\, u_{n+1} + D_{1_n}\, i_{n-1} + E_{1_n}\, i_n + F_{1_n}\, i_{n+1} = G_{1_n} \qquad (2 \leq n \leq N-1) \tag{1B}$$

$$A_{2_n}\, u_{n-1} + B_{2_n}\, u_n + C_{2_n}\, u_{n+1} + D_{2_n}\, i_{n-1} + E_{2_n}\, i_n + F_{2_n}\, i_{n+1} = G_{2_n} \tag{2B}$$

Let $w_n = \begin{bmatrix} u_n \\ i_n \end{bmatrix}$, then equations 1B and 2B become

$$X_n\, w_{n-1} + Y_n\, w_n + Z_n\, w_{n+1} = g_n \tag{3B}$$

where

$$X_n = \begin{bmatrix} A_{1_n} & D_{1_n} \\ A_{2_n} & D_{2_n} \end{bmatrix} \qquad Z_n = \begin{bmatrix} C_{1_n} & F_{1_n} \\ C_{2_n} & F_{2_n} \end{bmatrix}$$

$$Y_n = \begin{bmatrix} B_{1_n} & E_{1_n} \\ B_{2_n} & E_{2_n} \end{bmatrix} \qquad g_n = \begin{bmatrix} G_{1_n} \\ G_{2_n} \end{bmatrix}$$

The boundary conditions for a very general case can be written as

$$Y_1 w_1 + Z_1 w_2 = g_1 \tag{4B}$$

$$X_N w_{N-1} + Y_N w_N = g_N \tag{5B}$$

where

$$Y_1 = \begin{bmatrix} Y_1^{(11)} & Y_1^{(12)} \\ Y_1^{(21)} & Y_1^{(22)} \end{bmatrix} \qquad X_N = \begin{bmatrix} X_N^{(11)} & X_N^{(12)} \\ X_N^{(21)} & X_N^{(22)} \end{bmatrix}$$

$$Z_1 = \begin{bmatrix} Z_1^{(11)} & Z_1^{(12)} \\ Z_1^{(21)} & Z_1^{(22)} \end{bmatrix} \qquad Y_N = \begin{bmatrix} Y_N^{(11)} & Y_N^{(12)} \\ Y_N^{(21)} & Y_N^{(22)} \end{bmatrix}$$

$$g_1 = \begin{bmatrix} g_1^{(1)} \\ g_1^{(2)} \end{bmatrix} \qquad g_N = \begin{bmatrix} g_N^{(1)} \\ g_N^{(2)} \end{bmatrix}$$

For the case of a specified wall temperature distribution the boundary conditions (3.22a and 3.22c) give the following for the above matrices:

$$Y_1 = I \qquad X_N = \emptyset$$

$$Z_1 = \emptyset \qquad Y_N = I$$

$$g_1 = \begin{bmatrix} 0 \\ i_w \end{bmatrix} \qquad g_N = \begin{bmatrix} u_e \\ i_e \end{bmatrix}$$

where I is unit matrix and $\emptyset$ is zero matrix. The boundary conditions (4B and 5B) and the system of equations (3B) can be written as

$$Y_1 w_1 + Z_1 w_2 = g_1$$

$$X_n w_{n-1} + Y_n w_n + Z_n w_{n+1} = g_n \quad (2 \leq n \leq N-1) \qquad (6B)$$

$$X_N + Y_N w_N = g_N$$

The above can be written in matrix notation as

$$PW = R \qquad (7B)$$

where

$$P = \begin{bmatrix} Y_1 & Z_1 & & & & \\ X_2 & Y_2 & Z_2 & & & \\ & X_3 & Y_3 & Z_3 & & \\ & & - & - & - & \\ & & & - & - & - \\ & & & & X_{N-1} & Y_{N-1} & Z_{N-1} \\ & & & & & X_N & Y_N \end{bmatrix}$$

$$W = \begin{bmatrix} w_1 \\ w_2 \\ w_3 \\ . \\ . \\ . \\ w_N \end{bmatrix} \qquad R = \begin{bmatrix} g_1 \\ g_2 \\ g_3 \\ . \\ . \\ . \\ g_N \end{bmatrix}$$

Now P may be decomposed into two triangular matrices

$$P = MN \tag{8B}$$

where

$$M = \begin{bmatrix} M_1 & & & & \\ X_2 & M_2 & & & \\ & X_3 & M_3 & & \\ & & - & - & \\ & & & X_N & M_N \end{bmatrix}, \quad M_n = \begin{bmatrix} M_n^{(11)} & M_n^{(12)} \\ M_n^{(21)} & M_n^{(22)} \end{bmatrix}$$

$$N = \begin{bmatrix} I & N_1 & & & \\ & I & N_2 & & \\ & & I & N_3 & \\ & & & - & - \\ & & & I & N_{N-1} \\ & & & & I \end{bmatrix}, \quad N_n = \begin{bmatrix} N_n^{(11)} & N_n^{(12)} \\ N_n^{(21)} & N_n^{(22)} \end{bmatrix}$$

Therefore, the following relations exist:

$$\begin{aligned} M_1 &= Y_1 \\ M_n &= Y_n - X_n N_{n-1} \qquad 2 \leq n \leq N \\ N_n &= M_n^{-1} Z_n \qquad 1 \leq n \leq N-1 \end{aligned} \tag{9B}$$

Define a new column matrix, U, such that

$$MU = R \tag{10B}$$

where

$$U = \begin{bmatrix} U_1 \\ U_2 \\ \vdots \\ U_N \end{bmatrix} \quad , \quad U_n = \begin{bmatrix} U_n^{(1)} \\ U_n^{(2)} \end{bmatrix}$$

and the following relations exist:

$$U_1 = M_1^{-1} g_1$$

$$U_n = M_n^{-1}[g_n - U_{n-1} X_n] \tag{11B}$$

Substitute equations (8B) and (10B) into equation (7B) and the following is obtained:

$$NW = U \tag{12B}$$

When the above matrix equation is written out, the following relations result:

$$w_N = U_N$$

$$w_n = U_n - N_n w_{n+1} \qquad 1 \leq n \leq N-1 \tag{13B}$$

where $U_1 = Y_1^{-1} g_1$

$$N_1 = Y_1^{-1} Z_1$$

$$U_n = [Y_n - X_n N_{n-1}]^{-1} [g_n - U_{n-1} X_n]$$

$$N_n = [Y_n - X_n N_{n-1}]^{-1} Z_n$$

If the matrix equation (13B) is written out, the resulting relations are

$$u_n = U_n^{(1)} - N_n^{(11)} u_{n+1} - N_n^{(12)} i_{n+1}$$

$$i_n = U_n^{(2)} - N_n^{(21)} u_{n+1} - N_n^{(22)} i_{n+1} \tag{14B}$$

which shows that relations (3.23a and 3.23b) are valid. The following relations are obtained by using (13B) with the wall boundary conditions (4B):

$$U_1^{(1)} = \Delta_2 \left(Y_1^{(22)}\, g_1^{(1)} - Y_1^{(12)}\, g_1^{(2)}\right) = K_{m,1}^{(1)}$$

$$U_1^{(2)} = \Delta_2 \left(- Y_1^{(21)}\, g_1^{(1)} + Y_1^{(22)}\, g_1^{(2)}\right) = L_{m,1}^{(1)}$$

$$N_1^{(11)} = \Delta_2 \left(Y_1^{(22)}\, Z_1^{(11)} - Y_1^{(12)}\, Z_1^{(21)}\right) = - K_{m,1}^{(2)} \qquad (15B)$$

$$N_1^{(12)} = \Delta_2 \left(Y_1^{(22)}\, Z_1^{(12)} - Y_1^{(12)}\, Z_1^{(22)}\right) = - K_{m,1}^{(3)}$$

$$N_1^{(21)} = \Delta_2 \left(- Y_1^{(21)}\, Z_1^{(11)} + Y_1^{(22)}\, Z_1^{(21)}\right) = - L_{m,1}^{(2)}$$

$$N_1^{(22)} = \Delta_2 \left(- Y_1^{(21)}\, Z_1^{(21)} + Y_1^{(22)}\, Z_1^{(22)}\right) = - L_{m,1}^{(3)}$$

where $\Delta_2 = 1/\left(Y_1^{(11)}\, Y_1^{(22)} - Y_1^{(12)}\, Y_1^{(21)}\right)$.

REFERENCES

1. Baxter, D. C. and I. Flügge-Lotz, "The Solution of Compressible Laminar Boundary Layer Problems by a Finite Difference Method, Part II. Further Discussion of the Method and Computation of Examples." Tech. Rep. No. 110, Division of Eng. Mech., Stanford Univ., Stanford, Calif., Oct., 1957.

2. Bertram, Mitchel H. "Boundary-Layer Displacement Effects in Air at Mach Numbers of 6.8 and 9.6." NASA Technical Report R-22, 1959.

3. Bertram, Mitchel H. and Blackstock, Thomas A., "Some Simple Solutions to the Problem of Predicting Boundary-Layer Self-Induced Pressures", NASA TN D-798, April, 1961.

4. Bertram, Mitchel H. and Feller, William V., "A Simple Method for Determining Heat Transfer, Skin Friction, and Boundary-Layer Thickness for Hypersonic Laminar Boundary-Layer Flows in a Pressure Gradient." NASA Memorandum 5-24-59L, June, 1959.

5. Bertram, Mitchel H. and Henderson, Arthur., "Effects of Boundary-Layer Displacement and Leading-Edge Bluntness on Pressure Distribution, Skin Friction, and Heat Transfer of Bodies at Hypersonic Speeds." NACA TN 4301, July, 1958.

6. Cheng, H. K.; Hall, J. Gordon; Golian, T. C., and Hertzberg, A., "Boundary-Layer Displacement and Leading-Edge Bluntness Effects in High-Temperature Hypersonic Flow." Journal of the Aerospace Sciences, Vol. 28, May, 1961, p. 353.

7. Cohen, C. B. and Reshotko, E., "Similar Solutions for the Compressible Laminar Boundary Layer with Heat Transfer and Pressure Gradient." NACA TN 3325, Feb., 1955.

8. Crank, J. and Nicolson, P., "A Practical Method for Numerical Evaluation of Solutions of Partial Differential Equations of the Heat Conduction Type." Proc. Camb. Phil. Soc., vol. 43, 1947, p. 50.

9. Crocco, L., "Lo Strato Limite Laminare Nei Gas." Monografie Scientifiche di aeronautica no. 3., Associazione Culturale Aeronautica, Roma, Dic., 1946. (Translation in North American Aviation Aerophysics Lab. Rep. AL-684, July, 1948.)

10. Flügge-Lotz, I. and Baxter, D.C., "The Solution of Compressible Laminar Boundary Layer Problems by a Finite Method." Tech. Rep. No. 103, Div. of Eng. Mech., Stanford Univ., Stanford, California., Sept. 1956.

REFERENCES (Continued)

11. Flügge-Lotz, I. and Yu, Er-Yung, "Development of a Finite-Difference Method for Computing a Compressible Laminar Boundary-Layer with Interaction." Division of Engineering Mechanics, Stanford University, Technical Report No. 127, (AFOSR TN 60-577), May 15, 1960.

12. Forsythe, G. E. and W. Wasow, "Finite Difference Methods for Partial Differential Equations." John Wiley and Sons, Inc., New York, 1960.

13. Hall, J. Gordon, and Golian, T.C., "Shock-Tunnel Studies of Hypersonic Flat-Plate Airflows." Cornell Aeronautical Laboratory, Inc., Report No. AD-1052-A-10, December, 1960.

14. Hayes, W. D. and R. F. Probstein, "Hypersonic Flow Theory", Academic Press, New York, 1959.

15. Hildebrand, F. B., "Methods of Applied Mathematics." Prentice-Hall, 1952.

16. Howarth, L., "Concerning the Effect of Compressibility on Laminar Boundary Layers and Their Separation." Proc. Roy. Soc. (London), Ser. A., vol. 194, 1948, p. 16.

17. Howe, John T., "Some Finite Difference Solutions of the Laminar Compressible Boundary Layer Showing the Effects of Upstream Transpiration Cooling." NASA Memo 2-26-59A, February, 1959.

18. Kendall, James M., "An Experimental Investigation of Leading-Edge Shock-Wave-Boundary-Layer Interation at Mach 5.8". Journal of the Aeronautical Sciences, Vol. 24, January, 1957, p. 47.

19. Kennard, Earle H., "Kinetic Theory of Gases." McGraw-Hill Co., New York, 1938.

20. Klunker, E. B. and McLean, F.E., "Effect of Thermal Properties on Laminar-Boundary-Layer Characteristics." NACA TN 2916, March, 1953.

21. Kramer, R. F. and Lieberstein, H. M., "Numerical Solution of the Boundary-Layer Equations Without Similarity Assumptions." Journal of the Aerospace Sciences, Vol. 26, August 1959, p. 508.

22. Lees, Lester, "Influence of the Leading Edge Shock Wave on the Laminar Boundary Layer at Hypersonic Speeds." Journal of the Aeronautical Sciences, Vol. 23, June, 1956, p. 594.

23. Lees, Lester, "On the Boundary-Layer Equations in Hypersonic Flow and Their Approximate Solutions." Journal of the Aeronautical Sciences, Vol. 20, 1953, p. 143.

24. Lees, Lester and Probstein, Ronald F., "Hypersonic Viscous Flow Over a Flat Plate." Report No. 195, Aeronautical Engineering Laboratory, Princeton University, April, 1952.

25. Li, T-Y and Nagamatsu, H. T., "Similar Solutions of Compressible Boundary-Layer Equations." Journal of the Aeronautical Sciences, Vol. 22, 1955, p. 607.

26. Low, G. M., "The Compressible Laminar Boundary Layer with Heat Transfer and Small Pressure Gradient." NACA TN 3028, Oct., 1953.

27. Low, G. M., "The Compressible Laminar Boundary Layer with Fluid Injection." NACA TN 3404, March, 1955.

28. Makofski, Robert A., "On the Use of the Boundary-Layer Equations in the Hypersonic Viscous-Layer Regime." Journal of the Aerospace Sciences, Vol. 27, June, 1960, p. 468.

29. Manohar, R., "A Characteristic Difference Method for the Calculation of Steady Boundary-Layer Flow." Proc. 4th Congress Theoret. Appl. Mech. 1958, pp. 135-144, Indian Soc. Theoret Appl. Mech. Kharagpur.

30. Mirels, Harold, "Estimate of Slip Effect on Compressible Laminar Boundary-Layer Skin Friction." NACA TN 2609, January, 1952.

31. Moron, J. P. and Scott, P. B., "A Mass-Transfer Finite-Difference Formulation Employing Crocco Variables." Journal of the Aerospace Sciences, Vol. 28, September 1961, p. 737.

32. O'Brien, G. G.; Hyman, M. A.; and Kaplan, S., "A Study of the Numerical Solution of Partial Differential Equations." Jour. of Math. and Phys., Vol. 29, 1950, p. 223.

33. Oguchi, Hakuro, "The Sharp Leading Edge Problem in Hypersonic Flow." Brown University, ARL TN 60-133, August, 1960.

34. Pallone, Adrian, "Nonsimilar Solutions of the Compressible-Laminar-Boundary-Layer Equations with Applications to the Upstream-Transpiration Cooling Problem." Journal of the Aerospace Sciences, Vol. 28, June, 1961, p. 449.

35. Prandtl, L., "Uber Flüssigkeitsbewegung bei sehr kleiner reibung." Verhandlgndes III. Internat. Math-Kongr., Heidelberg, 1904.

36. Raetz, G. S., "A Method of Calculating Three-Dimensional Laminar Boundary Layers of Steady Compressible Flows." Northrop Aircraft, Inc., Report No. NAI-58-73, December, 1957.

37. Reshotko, Eli and Beckwith, Ivan E., "Compressible Laminar Boundary Layer over a Yawed Infinite Cylinder with Heat Transfer and Arbitrary Prandtl Number." NACA Report 1379, 1958.

38. Richtmyer, R. D., "Difference Methods for Initial-Value Problems." Interscience Publishers, Inc., New York, 1957.

39. Rouleau, W. T. and Osterle, J. F., "Application of Finite Difference Methods to Boundary Layer Type Flows." Journal of the Aeronautical Sciences, Vol. 22, 1955, p. 249.

40. Van Driest, E. R., "Investigation of Laminar Boundary Layer in Compressible Fluids Using the Crocco Method." NACA TN 2597, January, 1952.

41. Van Dyke, M., "Second-Order Compressible Boundary-Layer Theory with Application to Blunt Bodies in Hypersonic Flow." Department of Aeronautical Engineering, Stanford University, SUDAER No. 112, (AFOSR-TN-61-1270), July, 1961.

42. Wu, J. C., "The Solution of Laminar Boundary-Layer Equations by the Finite Difference Method." Douglas Aircraft Company, Inc., Report No. SM-37484, June 1, 1960.

43. Young, G. B. W. and Janssen, E., "The Compressible Laminar Boundary Layer." Journal of the Aeronautical Sciences, Vol. 19, 1952, p. 229.

44. Smith, A.M.O. and Clutter, Dorwin W., "Solution of the Incompressible Laminar Boundary Layer Equations." Douglas Aircraft Company, Inc., Report No. ES 40446, July 29, 1961.

(10) ASTIA
Arlington Hall Station
Arlington 12, Virginia
Attn: TIPCR

AFOSR
Washington 25, D. C.
(2) Attn: SREM
(2) Attn: SMOL

(2) HOOAR
Shell Building
47 Rue Cantersteen
Brussels, Belgium

AEDC
Arnold Air Force Station
Tennessee
Attn: AEOIM

AFFTC
Edwards Air Force Base, California
Attn: FTOTL

AFMDC
Holloman Air Force Base
New Mexico
Attn: MDOI

AFMTC
Patrick Air Force Base, Florida
Attn: AFMTC Tech Library-MU-135

AFOSR (SRLTL)
Holloman Air Force Base
New Mexico

Aeronautical Systems Division
Wright-Patterson Air Force Base
Ohio
(2) Attn: WWAD
(1) Attn: WWRMDN
(1) Attn: ASRMOC

(2) ARL (OAR)
Wright-Patterson Air Force Base
Ohio

Institute of Technology Library (AU)
MCLI-LIB, Bldg. 125, Area B
Wright-Patterson Air Force Base, Ohio

AFOC (FGAPI)
Eglin Air Force Base, Florida

AFCRL
L. G. Hanscomb Field
Bedford, Massachusetts
(2) Attn: CRRELA

AFSWC (SWOI)
Kirtland Air Force Base, New Mexico

Director BRL
Aberdeen Proving Ground, Maryland
Attn: Library

Office of Ordnance Research
Box CM
Duke Station
Durham, North Carolina

Army Rocket and Guided Missile Agency
Redstone Arsenal, Alabama
Attn: Technical Library

Signal Corps Engineering Laboratory
Fort Monmouth, New Jersey
Attn: SIGFM/EL-RPO

Office of the Chief of R and D
Department of the Army
Washington 25, D. C.
Attn: Scientific Information

(2) Office of Naval Research
Washington 25, D. C.
Attn: Mechanics Branch
Airbranch

Naval Research Laboratory
Washington 25, D. C.
Attn: Documents Library

Naval Ordnance Laboratory
White Oak, Maryland
Attn: Library

David Taylor Model Basin
Aerodynamics Laboratory
Washington 7, D. C.
Attn: Library

Chief, Bureau of Ordnance
Department of the Navy
Washington 25, D. C.
Attn: Special Projects Office,
SP-2722

NASA
1502 H Street, N. W.
Washington 25, D. C.
Attn: Document Library

Ames Research Center (NASA)
Moffett Field, California
Attn: Technical Library

High Speed Flight Station(NASA)
Edwards Air Force Base, California
Attn: Technical Library

Langley Research Center (NASA)
Langley Air Force Base, Virginia
Attn: Technical Library

Lewis Research Center (NASA)
21000 Brookpark Road
Cleveland 35, Ohio
Attn: Technical Library

National Bureau of Standards
U.S. Department of Commerce
Washington 25, D. C.
Attn: Technical Reports Section

Office of Technical Services
U.S. Department of Commerce
Washington 25, D. C.
Attn: Technical Reports Section

National Science Foundation
1951 Constitution Avenue, N.W.
Washington 25, D. C.
Attn: Engineering Sciences Division

U.S. Atomic Energy Commission
Technical Information Extension
P. O. Box 62
Oak Ridge, Tennessee

U.S. Atomic Energy Commission
Technical Information Service
1901 Constitution Avenue, N.W.
Washington 25, D. C.

(2) Southwest Research Institute
8500 Culebra Road
San Antonio 6, Texas
Attn: Applied Mechanics Reviews

Aeronautical Engineering Review
2 East 64th Street
New York 21, New York

Institute of Aeronautical Sciences
2 East 64th Street
New York 21, New York
Attn: Library

Chairman
Canadian Joint Staff (DRB/DSIS)
2450 Massachusetts Avenue, N.W.
Washington 25, D. C.

Director
National Aeronautical Establishment
Ottawa, Ontario
Canada

University of Toronto
Institute of Aerophysics
Toronto 5, Canada
Attn: Library

Training Center for Experimental
Aerodynamics
Rhode-Saint-Genese (Belgique)
72, Chaussee de Waterloo
Brussels, Belgium
Attn: Library

Library (Route to Dr. W. P. Jones)
Aeronautical Research Council
National Physical Laboratory
Teddington, England

Aeronautical Research Associates
of Princeton
50 Washington Road
Princeton, New Jersey

Auburn University
Dept. of Mechanical Engineering
Auburn, Alabama

Brown University
Gifts and Exchanges Library
Providence 12, Rhode Island

University of California
Institute of Engineering Research
Low Pressures Research Project
Berkeley 4, California

University of California
Engineering Department
Los Angeles 24, California
Attn: Library

California Institute of Technology
2800 Oak Grove Drive
Pasadena 4, California
Attn: JPL Library

California Institute of Technology
Guggenheim Aeronautical Laboratory
Pasadena 4, California
Attn: Aeronautics Library (Route to
Prof. Liepmann)

Colorado State University
Department of Civil Engineering
Fort Collins, Colorado
Attn: Prof. J. E. Cermak, ASCE

Columbia University
Department of Civil Engineering and
Engineering Mechanics
New York 27, New York
Attn: Library (Route to Prof.
G. Herrmann)

Cornell University
Graduate School of Aeronautical
Engineering
Ithaca, New York
Attn: Library (Route to Prof. W. R. Sears)

Harvard University
Department of Engineering Sciences
Cambridge 38, Massachusetts
Attn: Library

John Crerar Library
86 E. Randolph Street
Chicago 1, Illinois

The Johns Hopkins University
Applied Physics Laboratory Library
8621 Georgia Avenue
Silver Spring, Maryland

The Johns Hopkins University
Department of Mechanics
Baltimore 18, Maryland
Attn: Library (Route to Profs.
Clauser and Corrsin)